นางสาวปาริสา ดำรงค์ศักดิ์

ศูนย์วิทยทรัพยากร
จุฬาลงกรณ์มหาวิทยาลัย

วิทยานิพนธ์นี้เป็นส่วนหนึ่งของการศึกษาตามหลักสูตรปริญญาวิทยาศาสตรมหาบัณฑิต
สาขาวิชาปิโตรเคมีและวิทยาศาสตร์พอลิเมอร์
คณะวิทยาศาสตร์ จุฬาลงกรณ์มหาวิทยาลัย
ปีการศึกษา 2553

THEORETICAL STUDY OF CONVERSION OF ETHANOL TO
LIGHT OLEFINS OVER ZSM-5

Miss Parisa Dumrongsak

ศูนย์วิทยทรัพยากร
จุฬาลงกรณ์มหาวิทยาลัย

A Thesis Submitted in Partial Fulfillment of the Requirements

for the Degree of Master of Science Program in Petrochemistry and Polymer Science

Faculty of Science

Chulalongkorn University

Academic Year 2010
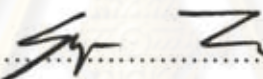
530595
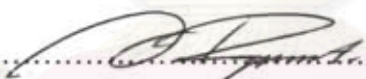
Thesis Title   THEORETICAL STUDY OF CONVERSION OF
                      ETHANOL TO LIGHT OLEFINS OVER ZSM-5
By   Miss Parisa Dumrongsak
Field of Study   Petrochemistry and Polymer Science
Thesis Advisor   Associate Professor Vithaya Ruangpornvisuti, Dr.rer.nat.

Accepted by the Graduate School, Chulalongkorn University in Partial
Fulfillment of the Requirements for the Master's Degree
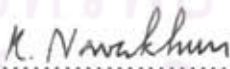
……………………………………………. Dean of the Graduate School

(Professor Supot Hannongbua, Dr.rer.nat.)

THESIS COMMITTEE

………………………………………….. Chairman

(Associate Professor Supawan Tantayanon, Ph.D.)

……………………………………….……. Thesis Advisor

(Associate Professor Vithaya Ruangpornvisuti, Dr.rer.nat.)

………………………………………….. Examiner

(Assistant Professor Somsak Pianwanit, Ph.D.)

…………………………………………….. External Examiner

(Assistant Professor Korakot Navakhun, Ph.D.)

ปาริสา ดำรงค์ศักดิ์ : การศึกษาเชิงทฤษฎีของการเปลี่ยนเอทานอลเป็นโอเลฟินเบา บนแซดเอสเอ็ม–5. (THEORETICAL STUDY OF CONVERSION OF ETHANOL TO LIGHT OLEFINS OVER ZSM-5) อ.ที่ปรึกษาวิทยานิพนธ์หลัก: รศ.ดร.วิทยา เรืองพรวิสุทธิ์, 89 หน้า.

ปฏิกิริยาการเปลี่ยนเอทานอลเป็นเอทิลีนและ 1–บิวทีน โดยใช้ซีโอไลต์ชนิด H–ZSM–5 และ M–ZSM–5 เมื่อ M = Cu^+, Ag^+, Au^+, Ni^{2+}, Pd^{2+} และ Pt^{2+} โดยการคำนวณด้วยวิธีทฤษฎีเดนซิตี ฟังก์ชัน การหาโครงสร้างการเกิดปฏิกิริยาระหว่างสารประกอบต่างๆ ที่เป็นตัวถูกดูดซับกับตัวเร่ง ปฏิกิริยาโดยคลัสเตอร์แบบต่างๆ โดยวิธี B3LYP/LanL2DZ และหาค่าพลังงาน สมบัติทางเทอร์โม ไดนามิกส์ ค่าคงที่อัตราเร็วที่อุณหภูมิ 25 องศาเซลเซียส เปรียบเทียบกับระบบที่ไม่มีตัวเร่ง ปฏิกิริยา พบว่าค่าคงที่ของปฏิกิริยาการเปลี่ยนเอทานอลเป็นเอทิลีนบนตัวเร่ง H–ZSM–5 และ M–ZSM–5 ลดลงตามลำดับดังนี้ Pt–ZSM–5 > Pd–ZSM–5 ≈ Au–ZSM–5 > Ag–ZSM–5 > H–ZSM–5 > Cu–ZSM–5 >> Ni–ZSM–5 ค่าคงที่ของปฏิกิริยาการเปลี่ยนเอทานอลเป็น 1–บิวทีน บนตัวเร่ง H–ZSM–5 และ M–ZSM–5 ลดลงตามลำดับคือ H–ZSM–5 >> Ni–ZSM–5 > Pd–ZSM–5 ≈ Pt–ZSM–5 ≈ Au–ZSM–5 > Ag–ZSM–5 > Cu–ZSM–5

สาขาวิชา ปิโตรเคมีและวิทยาศาสตร์พอลิเมอร์ ลายมือชื่อนิสิต ปาริสา ดำรงค์ศักดิ์

ปีการศึกษา 2553 ลายมือชื่อ อ.ที่ปรึกษาวิทยานิพนธ์หลัก

#5172363123: PETROCHEMISTRY AND POLYMER SCIENCE PROGRAM

KEYWORDS: ZEOLITE/ H–ZSM–5/ M–ZSM–5/ ETHANOL/ CONVERSION/ ETHYLENE/ BUTENE/ DFT

PARISA DUMRONGSAK: THEORETICAL STUDY OF CONVERSION OF ETHANOL TO LIGHT OLEFINS OVER ZSM–5. THESIS ADVISOR: ASSOC. PROF. VITHAYA RUANGPORNVISUTI, Dr.rer.nat. , 89 pp.

The conversion of ethanol to ethylene and 1–butene on the H–ZSM–5, M–ZSM–5, M = Cu^+, Ag^+, Au^+, Ni^{2+}, Pd^{2+} and Pt^{2+} has theoretically been investigated using density functional theory (DFT) calculations. The configurations of interaction between adsorbate and catalysts at various cluster models were obtained using the B3LYP/LanL2DZ computations. The energetics, thermodynamic properties, rate and equilibrium constants for all the reaction steps were determined at 298.15 K compared to its reaction without catalyst. The rate constants for the ethanol conversion to ethylene over H–ZSM–5 and M–ZSM–5 catalysts are in decreasing order: Pt–ZSM–5 > Pd–ZSM–5 ≈ Au–ZSM–5 > Ag–ZSM–5 > H–ZSM–5 > Cu–ZSM–5 >> Ni–ZSM–5. The rate constants for the ethanol conversion to 1–butene over the M–ZSM–5 catalysts are in decreasing order: H–ZSM–5 >> Ni–ZSM–5 > Pd–ZSM–5 ≈ Pt–ZSM–5 ≈ Au–ZSM–5 > Ag–ZSM–5 > Cu–ZSM–5.

Field of study: <u>Petrochemistry and Polymer Science</u> Student's signature: Parisa Dumrongsak

Academic year: <u>2010</u> Advisor's signature

ACKNOWLEDGEMENTS

I would like to take this opportunity to thank all those who have contributed to this work. Firstly, I especially thank Associate Professor Dr. Vithaya Ruangpornvisuti; my advisor for his valuable guidance and advice in this thesis, for allowing time for discussion and his continuous encouragement and patience over the years. His dedication is appreciated so much.

I would like to acknowledge the committee, Associate Professor Dr. Supawan Tantayanon, Assistant Professor Dr. Somsak Pianwanit and Assistant Professor Dr. Korakot Navakhun for their valuable suggestions and comments as committee and thesis examiners.

Special thanks to all members in Supramolecular Chemistry Research Unit for their kind help. I also would like thank all teaching staff and my friends for all their good suggestions, friendship and continuous encouragement.

Finally, I would like to thank my beloved family; my father and mother, my aunt, my grandmother, my sisters and my brother for their endless love and for always supporting and trusting in my decisions. I am very proud to be a part of this beloved family.

CONTENTS

ศูนย์วิทยทรัพยากร

จุฬาลงกรณ์มหาวิทยาลัย

LIST OF FIGURES

ศูนย์วิทยทรัพยากร
จุฬาลงกรณ์มหาวิทยาลัย

LIST OF TABLES

LIST OF ABBREVIATIONS AND SYMBOLS

Å	Angstrom
B3LYP	Becke 3-Parameter, Lee, Yang and Parr
ECP	Effective core potential
DFT	Density functional theory
E	Energy
G	Gibbs free energy
H	Enthalpy
HF	Hartree–Fock
h	Plank's constant
IRC	Intrinsic reaction coordinate
k	Rate constant
k_B	Boltzman's constant
K	Equilibrium constant
LanL2DZ	Los alamos national laboratory 2-double-zeta
MFI	Mobil-five
MO	Molecular orbital
q	Partition function
q_{rot}	Rotational partition function
q_{trans}	Translational partition function
q_{vib}	Vibrational partition function
q_{elect}	Electronic partition function
R	Gas constant
RDS	Rate determining step
S	Entropy
SCF	Self-consistent field
STO	Slater type orbital
T	Absolute temperature
TS	Transition state
TST	Transition state theory
ZPVE	Zero point vibrational energy
ψ	Wave function

κ	Kappa
σ	Rotational symmetry number of the molecule
v_i	Imaginary frequency
ZSM-5	Zeolite Socony Mobil Number 5

CHAPTER I

INTRODUCTION

1.1. Background

Light olefins such as ethylene, propylene and butylenes are important intermediates and building blocks in the petrochemical industry which the most produced by stream cracking of naphtha. However, the amount of petroleum resource is limited and cannot be obtained everywhere. Moreover, production of light olefins from ethanol has many advantages. The ethanol can be produced from natural gas, many different raw materials and derived from many crop as called bio–ethanol. The bio–ethanol can be produced with low emission of greenhouse gases (GHGs) and renewable resource. Because of the increasing demands for light olefins, the transformation of ethanol into hydrocarbons on solid acid catalyst is an interesting route for upgrading renewable resource and to obtain petrochemical raw materials.

Zeolites play a very important role in the petroleum and petrochemical industries because of their high catalytic activity and good selectivity. The H–ZSM–5 zeolite is used as catalyst for conversion of methanol and ethanol to gasoline and other hydrocarbon [1–3] also a catalyst for solid acid alkylation, interconversion and isomerization of alkenes, alkylation of phenol and production of oxygenates [4]. On the other hand, under extreme condition (> 450°C) the presence of stream caused deactivation due to it dealuminates zeolite [5]. The H–ZSM–5 zeolite exchanged with different metal ions has drawn a lot of attention because of their chemical and electronic properties, especially for their catalytic activity in many important chemical processes. However, its poor hydrothermal stability and resistance to coke formation are modified by different metal transition ions for enhancing hydrothermal stability and acid structure performance [6].

1.2. Zeolites

1.2.1. Fundamentals of the zeolite structure

Zeolites are well–defined class of crystalline alumino–hydro–silicates. Silica may be thought of as being built up from $[SiO_4]^{4-}$ tetrahedral, each oxygen being share by two tetrahedral as shown in Figure 1.1 [7]. Substitution of aluminium into silicon gives the $[AlO_4]^{5-}$ ion so for each aluminium atom introduced there is one excess negative is strongly acidic.
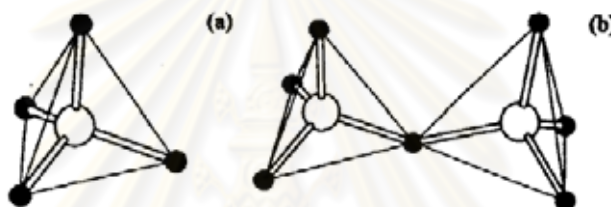
Figure 1.1 (a) SiO_4 or AlO_4 tetrahedral, (b) SiO_4 or AlO_4 tetrahedral sharing a common oxygen vertex.

Such aluminosilicates are amorphous and much interest has been shown in recent years in crystalline aluminosilicates having the general formula as shown below these are known as zeolites.

$$M_v(AlO_2)_x(siO_2)_y \cdot zH_2O$$
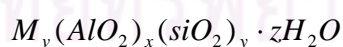
When M is monopositive cation (e.g. sodium or ammonium), v equals x; for divalent cations, v is $x/2$; and so on. The useful catalytic properties of zeolites hinge on three factors: (i) the regular crystalline structure and uniform pore size, which allow only molecules below certain size to react; (ii) the presence of strongly acidic hydroxyl groups, which can initiate carbonium–ion reactions and (iii) the presence of very large electrostatic field in the neighborhood of the cations, which can thus induce reactivity in

reactant molecules. Catalytic activity therefore depends heavily on the nature of cation, which also seem able to affect the acidity of hydroxyl groups [8].

The framework of a zeolite can be thought of as being made of finite component units such as secondary building units (SBUs) was introduced by Meier and Smith. The 18 kinds of SBUs, that have been found to occur in tetrahedral framework. These SBUs, which contain up to 16 tetrahedrally coordinated atoms, are derived by assuming that the entire framework is made up of one type of SBU only. It should be noted that SBUs are invariably nonchiral. A unit cell always contains an integral number of SBUs.

1.2.2 ZSM–5 zeolite

ZSM-5 (Zeolite Socony Mobil Number 5 is discovered by Mobil Oil Company) is a commercial name of MFI zeolite with high silica to alumina ratio. The dimensions of the pores and channels are of the order of a nanometer. Type material ZSM–5, $[Na_n^+(H_2O)_{16}][Al_nSi_{96-n}O_{192}]$–MFI ($n < 27$), orthorhombic, P_{nma}, $a = 20.07$ Å, $b = 19.92$ Å, $c = 13.42$ Å [9]. Its framework density is $17.9T/1000$ Å^3. The number of Al atoms in the unit cell varies from 0 to 27, so the ratios of Si/Al can be changed within a wide range.

The ZSM–5 structure is built up by 5–1 secondary SBU which are link together to form chains and inter connection of these chains leads to the formation of the channel in structure. Adjacent sheets that are related by an inversion center are linked by oxygen bridges to the next, forming a 3–dimensional framework. This produces an intersecting channel with straight 10–ring channels $(5.3 \times 5.6$ Å$)^2$ parallel to corrugation, and sinusoidal 10–ring channels $(5.5 \times 5.1$ Å$)^2$ perpendicular to the sheet with an angle of 150° Figure 1.2.
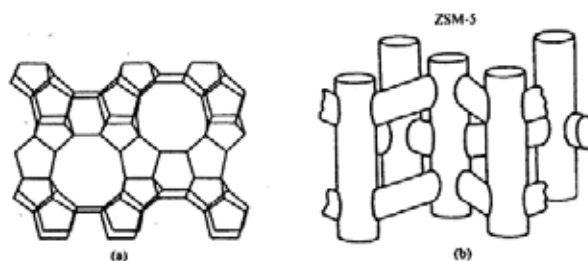
Figure 1.2 (a) Porous sheet parallel to the (100) plane in ZSM–5; (b) the channel structure in ZSM–5.

1.2.3 Acidity

The substitution of an Al^{3+} for a Si^{4+} requires the additional presence of a positive charge i.e. H^+ to balance the negative charge of the framework. This additional proton gives the zeolite a high level of acidity (H–ZSM–5), which causes its acidity. The acidic catalytic activity of H–ZSM–5 strongly depends on the Al component in the framework.

A solid acid is capable of converting an adsorbed basic molecule into its conjugate acid form. Therefore, the acids site is able to either transfer a proton from the solid to the adsorbed molecule which this type of acid center is called a Brønsted site or transfer an electron pair from the adsorbed molecule to the solid surface this type of acid site are known as Lewis acidity. The proton can then catalyze hydrocarbon reactions that proceed by a carbonium ion mechanism. Many other mixed oxides containing atom having different valencies show acidity for the same reason. Generally, both types of acid sites are simultaneously present in zeolites. Schematically, this would be represented as in Figure 1.3.
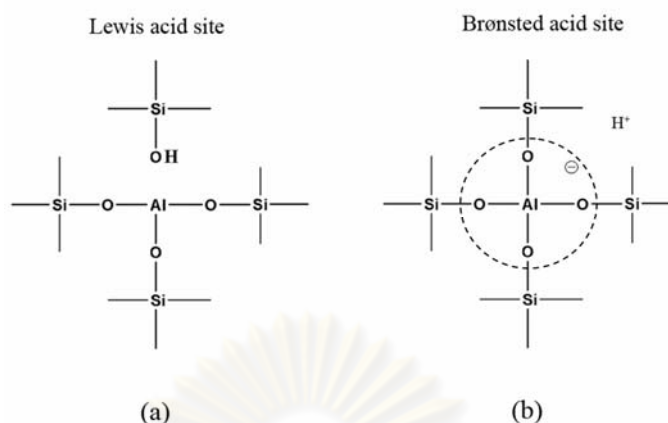
Figure 1.3 Representation of an acidic site in silica–alumina [10].

As already mentioned protonated zeolites have acidic properties. The protons which balance the negative charge of a zeolite framework are not strongly bound to the framework and are able to move within the pores and react with molecules which penetrate into the zeolite pore system. A protonated zeolite thus can act as a Brønsted acid. Furthermore, Lewis acidity can be caused by cations within the pores. The cations balancing the negative charge of the framework locate in the channels and cages of a zeolite structure. The number and sites of cations are of interest due to their effects on the performance of a zeolite such as ion–exchange and catalytic properties.

1.2.4 Ion exchange

The ion exchange behavior of zeolites depends upon the nature of the cation species, the cation size, both anhydrous and hydrated, and cation charge. Zeolites structures have unique features that lead to unusual type of cation selectivity and sieving. The ion exchange process may be represented by the following equation:

$$Z_A B_{(Z)}^{Z_B^+} + Z_B A_{(s)}^{Z_A^+} \leftrightarrow Z_A B_{(s)}^{Z_B^+} + Z_A A_{(z)}^{Z_A^+} \tag{1.1}$$
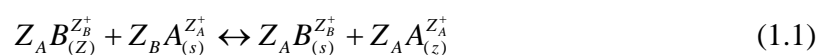
where Z_A and Z_B are the charges of the exchange cations A and B and the subscripts z and s refer to the zeolites and solutions, respectively.

The ion exchange model originally proposed by Eiseman has been extended to account for the variation in ion specificity exhibited by zeolites. Interaction of the ion with the zeolites and solution phases is considered. For the uni–univalent ion exchange reaction:

$$A_s^+ + B_z^+ \leftrightarrow A_z^+ + B_s^+ \tag{1.2}$$

where s and z represent the solution and zeolites phase. The free energy of the reaction is considered to consist of two terms:

$$\Delta G^\circ = \left(\Delta G_z^A - \Delta G_z^B\right) - \left(\Delta G_s^A - \Delta G_z^B\right) \tag{1.3}$$

The first term in this expression represent the difference between the free energy of A^+ and B^+ in solution. The first term is more important if the force fields in the zeolites are very strong that zeolites with a high framework charge and correspondingly low Si/Al ratio and small ions are preferred. If the fields are weak and large, weakly hydrated cations are preferred [11].

1.3 Alcohol dehydration

Dehydration of an alcohol is a common method of introducing unsaturation into an organic compound. This type of reaction belongs to the important class of organic reactions called elimination reactions. Converting an alcohol to alkenes requires removal of the hydroxyl group and a hydrogen atom on the neighboring carbon atom. Dehydrations are most commonly carried out by warming the alcohol in the presence of a strong dehydrating acid. The reaction generally obeys Zaitsev's Rule [12], which states that the most stable (usually the most substituted) alkenes are formed.

Ethanol for use as an industrial feedstock or is often made from petrochemical feed stocks, primarily by the acid–catalyzed hydration of ethylene, represented by the chemical equation as shown in Figure 1.4.
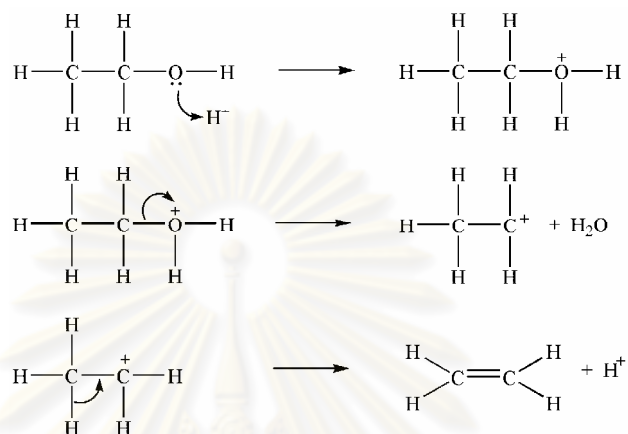
Figure 1.4 Mechanism of ethanol dehydration to ethylene.

1.4 Literature reviews

1.4.1 Experimental studies

In 1987, Mao *et al.* [13] presented the conversion of ethanol or its mixture with light alcohols and optionally water into hydrocarbons with specific and unusual selectivity toward ethylene at 400 ℃. The characterization and the use in the process of the present invention of three calalyst sample: the pure ZSM–5 zeolite based; the ZSM–5/Zn and the ZSM–5/Zn–Mn. The selectivity to ethylene increases as follows: ZSM–5 ≤ ZSM–5/Zn ≤ ZSM–5/Zn–Mn. Furthermore, the data of conversion and product selectivities over ZSM–5/Zn–Mn of pure alcohol (methanol, ethanol, propanol, *n*–butanol and *iso*–butanol) revealed only ethanol among the light alcohols tested gave very high yield in light olefins and in ethylene.

In 1997, Talukdar *et al.* [14] described the reaction temperature was extended up to 773 K with aqueous ethanol to converse to hydrocarbons, over HZSM–5 of silica–

alumina ratio Si/Al = 206 and Si/Al = 40. It was found that the higher reaction temperature (673–773 K) favored the formation of gaseous olefins from ethanol. The H–ZSM–5 with Si/Al = 206 gave high yield of $C_{2=}$, while the HZSM–5 with Si/Al = 40 catalysts obtained higher yield of $C_{3=}$ and $C_{4=}$ than $C_{2=}$ olefins. In addition a good yield of high olefins could also be obtained with dilute ethanol.

In 2008, Zhang et al. [3] investigated the activity and stability of γ–Al_2O_3, HZSM–5, silicoaluminophosphate (SAPO–34) and Ni–substituted SAPO–34 (NiAPSO–34) as catalysts in the dehydration of ethanol to ethylene. The FT–IR, framework vibration frequencies shifted to position of lower wavenumber indicated that Ni^{2+} is probably combined into the SAPO–34 framework also proved by XRD and TPR techniques. NH_3–TPD profiles of H–ZSM–5 sample exhibited highest desorption temperature of both weak and strong acid site and most weak acid sites. The conversion and selectivity of ethanol dehydration to ethylene decreased in the order H–ZSM–5 > NiAPSO–34 > SAPO–34 > Al_2O_3. In contrast, NiAPSO–34 demonstrated better stability than other catalysts.

In 2009, Song et al. [15] studied the direct conversion of ethanol to propylene over unmodified H–ZSM–5 and metal–modified ZSM–5. The catalytic results from NH_3–TPD profiles of H–ZSM–5 (Si/Al = 30, 80 and 280) suggested that low surface acidity favored ethane production, whereas the moderate and high surface acidity are optimum for the conversion of ethanol to propylene and C_{5+} aliphatics and aromatics respectively. Modification with Cr, Ce, Pd, Ti, Zr, Mo and W enhanced both the ethylene yield and propylene yield also Zr–ZSM–5 (Si/Al = 80) exhibited better stability than H–ZSM–5 (Si/Al = 80) for catalytic conversion of ethanol to propylene.

1.4.2 Computational studies

In 1991, Redondo et al. [16, 17] investigated ab initio quantum mechanical calculation in monomeric cluster modeling the 12 different T (tetrahedral) sites of zeolite ZSM–5. The two main basis sets used in these calculations were the STO–3G minimum basis set and the valence double–ζ (VDZ) set. The total energies for the minimum basis and the valence double–ζ showed that the main deficit of the minimum basis set rests in

their lack of flexibility for the proper description of variations in the bond angles then this basis set is unreliable for predicting trends with the replacement aluminum atom in different T sites zeolite. The calculations using valence double–ζ basis sets exhibited that the most preferable sites for Al substitution are T_6, T_9, and T_{12} all within 0.6 kcal/mol while Friplat et al. [18] found the T_{12} site to be most stable.

In 2008, Barone *et al.* [19] studied the isomerization of *cis*–2– butene to *trans*–2– butene within a 22T of H–ZSM–5 zeolite model, also in the presence of two adsorbed Pd atoms by optimizing the different geometries at the DFT/ B3LYP level. The low level basis sets (LLBS) procedure make use of the 6–31G(d,p) basis set atom of 2–butene derivatives and the LanL2DZ basis set Pd atoms. The *cis/trans*–2–butene isomerization also occurs within the 22T of H–ZSM–5 fragment in the presence of adsorbed palladium atoms inside the zeolite cavity. The strong H–Pd interactions seem to cause higher activation energy along the formation of the involved intermediates and transition states.

In 2008, Huang *et al.* [20] elucidated the effect of Ag^+ cation over H–ZSM–5 on activation of methane using B3LYP/6–31+G(d,p) method. The core electrons potential and its valence electrons were described by LanL2DZ basis set. The calculated activation barrier of alkyl pathway compared with carbenium pathway showed the alkyl pathway preferential pathway of the initial step for methane activation over Ag–ZSM–5. The catalytic cycle of ethane react with the $Ag^+CH_3^-$ group to form propene was investigated.

In 2009, Sierraalta *et al*. [21] presented the understanding of active site of the Au(I) ion–exchanged ZSM–5 catalysts using the DFT approach (B3LYP) with the LanL2DZ basis set for H, Si, Al and O atoms belonging to the zeolite model and the full–electron 6–31+G* basis set for CO, NO, NO_2, SO_2, H_2O NH_3, CH_3NH_2 and CH_3SH molecules. The gold atom substitutes the H^+ proton that corresponds to the Brønsted acid site which adsorption at 298.15 K. The ΔH is larger and the reaction ΔG is more negative for CH_3SCH_3 than for CH_3OCH_3 thus the Au/ZSM–5 active site behaving as a soft acid. Therefore, the adsorption of soft bases such as CO, R_2P, C_2H_4, and R_2S preferred hard bases such as H_2O, R_2O and ROH. At soft acid site, Au can transfer more electrons than at hard acid sites. The but–2–ene adsorption on the considered systems and the mutual influence occurring between the metal atoms and the hydrogen acidic sites at different multiplicity states have also been taken into consideration.

In 2009, Jiang *et al*. [22] studied the interaction of CO molecules with Ag–ZSM–5 by using the B3LYP and the core electrons of the Ag atom are described by LanL2DZ basis set, while the other atoms by normally used 6–31+G* basis set. The NBO charge on Ag^+ cation of isolated Ag–ZSM–5 cluster is 0.946 |e|. So Ag^+ from Ag–ZSM–5 can accept electrons from probe molecules. The electron transfers from CO to the Ag^+ cation to form an σ–bond and accompanies the week π–back donation by the d–electrons from Ag^+ cation to the CO ($π^*$) orbital. CO and H_2O molecules co–adsorption on Ag^+ ion is stable at room temperature are explained by the Gibbs free energy change (ΔG) value. The $ΔG_{CO}$ is –5.55 kcal/mol when one CO molecule is adsorbed, while $ΔG_{H2O}$ is –6.58 kcal/mol when H_2O molecule is adsorbed on CO–Ag–ZSM–5.

1.5 Objectives

To rationalize and get more understanding on the experiments of conversion reaction of ethanol to light olefins such as ethylene and 1–butene, the aim of this work is therefore to theoretically study the reaction mechanisms of the conversion of ethanol to ethylene and 1–butene using the H–ZSM–5 and M–ZSM–5, M = Cu(I), Ag(I), Au(I), Ni(II), Pd(II) and Pt(II) catalysts. These conversion reactions on the 5T cluster models for Cu–ZSM–5, Ag–ZSM–5 and Au–ZSM–5 and 8T cluster models for Ni–ZSM–5, Pd–ZSM–5 and Pt–ZSM–5 as catalysts have theoretically been investigated employing the calculations at the B3LYP/LanL2DZ level of theory. Furthermore, 28T cluster models for the conversion of ethanol to ethylene compared with 5T and 8T cluster model have been presented. The energetic and thermodynamic quantities of catalytic reactions for each model have been determined. Due to get new efficient M–ZSM–5 catalysts for the conversions of ethanol to ethylene and ethanol to 1–butene, this rate constant catalyzed by the M–ZSM–5 catalysts have been also determined.

CHAPTER II

THEORETICAL BACKGROUND

Computational chemistry, alternatively sometimes called theoretical chemistry or molecular modeling is the application of chemical problems. It allows one to calculate molecular geometries, reactivities, spectra and other properties. However, computational chemistry has become a good way to investigate materials which are difficult to find. It also helps chemists make prediction before running the actual experiments in order that it can be better prepared for making observations.

2.1 Quantum mechanics in computational chemistry

In quantum mechanics (QM), it mentions to describe a unit that quantum theory assigns to certain physical quantities, such as the energy of an atom at rest. The bases of QM were established during the first half of twentieth century by Waner Heisenberg, Max Planck, Louise de Broglie, Niels Bohr, Erwin Schrödinger and other. Some fundamental perspectives of the theory are still studied. The key features of assumption of QM is so-called wave function, Ψ, exist for any chemical system, and that appropriate functions which act upon Ψ return the observable properties of the system. Two equivalent formulations of QM were devised by Schrödinger and Heisenberg. The Schrödinger equation is

$$\hat{H}\psi = E\psi \tag{2.1}$$

where $\hat{H}$ is the Hamiltonian operator, ψ is a wave function, and E is the energy [23].

2.2 Ab initio method

Ab initio methods are procedures that do not included any empirical parameters in their equations being acquired from theoretical principles, with no inclusion of experiment data. The simplest type of ab initio electronic structure calculation is Hartree-Fock (HF). The HF associated with an extension of molecular orbital theory which related electron-electron repulsion referred to electronic correlation. Thus, HF was adopted as useful in ab initio philosophy because it provides a very well described stepping stone on the way to more sophisticated theories that come closer to accurate solution of the Schrödinger equation.

The Hartree-Fock equation determines the set of spin orbitals which minimize the energy and gives us this best single determinant. So, we need to minimize the Hartree-Fock energy expression with respect to changes in the orbitals:

$$\chi_i \rightarrow \chi_i + {}^{\delta}\chi_i \qquad (2.2)$$

We have also been assuming that the orbitals are orthonormal, and we want to ensure that our variation procedure leaves them orthonormal. The Hartree-Fock equation can be solved numerically, or they can be solved in the space spanned by a set of basis set functions (Hartree-Fock-Roothaan equation). In either case, note that the solution depends on the orbitals. Hence, we need to guess some initial orbitals and then refine our guess iteratively. For this reason, HF is called self-consistent-field (SCF) approach.

2.3 Density functional theory (DFT) method

The basis for density functional theory (DFT) is the proof by Hohenberg and Kohn that the ground-state electronic energy is determined completely by the electron density (ρ) [24]. In other words, there exists a one-to-one correspondence between the electron density of a system and the energy. The significance of this is perhaps best illustrated by comparing to the wave function approach. A wave function for an *N*-electron system contains *3N* coordinates, three for each electron (four if spin is included).

The electron density is the square of the wave function, integrated over N-1 electron coordinates, this only depends on three coordinates, independently of the number of electrons. While the complexity of a wave function increases with the number of electrons, the electron density has the same number of variables, independently of the system size. The "only" problem is that although it has been proven that each different density yields different ground-state energy, the functional connection these two quantities are not known. The goal of DFT methods is to design functionals connecting the electron density with the energy.

The foundation for the use of DFT methods in computational chemistry was the introduction of orbitals by Kohn and Sham. The basic idea in the Kohn and Sham (KS) formalism is splitting the kinetic energy functional into two parts, one of which can be calculated exactly, and a small correction term.

2.3.1 The Kohn-Sham energy

The ideal energy is that of an ideal system, a fictitious non-interacting reference system, defined as one in which the electrons do not interact and in which the ground state electron density ρ_r is exactly the same as in our real ground state system, $\rho_r = \rho_0$. The electronic energy of the molecule is the total internal "frozen-nuclei" energy can be found by adding the internuclear repulsions and the 0 K total internal energy by further adding the zero-point energy.

The ground state electronic energy of our real molecule is the sum of the electron kinetic energy, the nucleus-electron attraction potential energies, and the electron-electron repulsion potential energies and each is a functional of the ground-state electron density.

$$E_0 = \langle T[\rho_0] \rangle + \langle V_{ne}[\rho_0] \rangle + \langle V_{ee}[\rho_0] \rangle \tag{2.3}$$

Focusing on the middle term, the nucleus-electron potential energy is the sum over all *2n* electrons of the potential corresponding to attraction of an electron for all the nuclei A.

$$\langle V_{ne} \rangle = \sum_{i=1}^{2n} \sum_{nucleiA} -\frac{Z_A}{r_{iA}} = \sum_{i=1}^{2n} v(r_i) \qquad (2.4)$$

where $v(r_i)$ is the external potential for the attraction of electron i to the nuclei. The density function ρ can be introduce into $\langle V_{ne} \rangle$ by using that

$$\int \psi \sum_{i=1}^{2n} f(r_i) \psi \, dt = \int \rho(r) f(r) dr \qquad (2.5)$$

where $f(r_i)$ is a function of the coordinates of the $2n$ electrons of a system and ψ is the total wavefunction from equations (2.4) and (2.5), invoking the concept of expectation value $\langle V_{ne} \rangle = \langle \psi | \hat{V}_{ne} | \rangle \psi$, and since $\hat{V} = V_x$, and get,

$$E_0 = \int \rho_0(r) v(r) dr + \langle T[\rho_0] \rangle + \langle V_{ee}[\rho_0] \rangle \qquad (2.6)$$

that cannot known the function in $\langle T[\rho_0] \rangle$ and $\langle V_{ee}[\rho_0] \rangle$. The Kohn and Sham introduced the idea of a reference system of non-interacting electrons. Let us to define the quantity $\Delta \langle T[\rho_0] \rangle$ as the deviation of the real kinetic energy from that of the reference system.

$$\Delta \langle T[\rho_0] \rangle \equiv \langle T[\rho_0] \rangle - \langle T_r[\rho_0] \rangle \qquad (2.7)$$

Let us next define $\Delta \langle V_{ee} \rangle$ as the deviation of the real electron-electron repulsion energy from classical charged-cloud coulomb repulsion energy. This classical electrostatic repulsion energy is the summation of the repulsion energies for pairs of infinitesimal volume elements $\rho(r_1)dr_1$ and $\rho(r_2)dr_2$ separated by distance r_{12}, multiplied by one-half. The sum infinitesimals is an integral and so

$$\Delta\langle V_{ee}[\rho_0]\rangle = \langle V_{ee}[\rho_0]\rangle - \frac{1}{2}\iint\frac{\rho_0(r_1)\rho_0(r_2)}{r_{12}}dr_1dr_2 \qquad (2.8)$$

Actually, the classical charged-cloud repulsion is somewhat inappropriate foe electrons in that smearing an electron out into a cloud forces it to repel itself, as any two regions of the cloud interact repulsively. This physically incorrect electro self-interacting will be compensated for by a good exchange-correlation functional can be written as

$$E_0 = \int\rho_0(r)v(r)dr + \langle T_r[\rho_0]\rangle + \frac{1}{2}\iint\frac{\rho_0(r_1)\rho_0(r_2)}{r_{12}} + \Delta\langle T[\rho_0]\rangle + \Delta\langle V_{ee}[\rho_0]\rangle \qquad (2.9)$$

The sum of the kinetic energy deviation from the reference system and the electron-electron repulsion energy deviation from the classical system is called the exchange-correlation energy, E_{xc}

$$E_{xc}[\rho_0] \equiv \Delta\langle T[\rho_0]\rangle + \Delta\langle V_{ee}[\rho_0]\rangle \qquad (2.10)$$

The $\Delta\langle T\rangle$ term represents the kinetic correlation energy of the electrons and the $\langle\Delta V_{ee}\rangle$ term the potential correlation energy and the exchange energy, although exchange and correlation energy in DFT do have exactly.

2.3.2 The Kohn-Sham equations

The Kohn-Sham (KS) equations are theorem obtained by utilizing the variation principle, which the second Hohenberg-Kohn theorem assures applies to DFT. We use the fact that the electron density of the reference system, which is the same as that of our real system, is given by

$$\rho_0 = \rho_r = \sum_{i=1}^{2n}\left|\psi_i^{KS}(1)\right|^2 \qquad (2.11)$$

where ψ_i^{KS} is the KS spatial orbital. Substituting the above expression for the orbitals into the energy and varying E_0 with respect to the ψ_i^{KS} subject to the constraint that these remain orthonormal lead to the KS equations, procedure is similar to that used in deriving the HF equations,

$$\left[-\frac{1}{2}\nabla_i^2 - \sum_{nucleiA} \frac{Z_A}{r_{iA}} + \int \frac{\rho(r_2)}{r_{12}} dr_2 + v_{xc}(1) \right] \psi_i^{KS}(1) = \varepsilon_i^{KS} \psi_i^{KS}(1) \qquad (2.12)$$

where $\in_i^{KS}$ are the KS energy levels and v_{xc} (*1*) is the exchange correlation potential, arbitrarily designated here for electron number 1, since the KS equations are a set of one-electron equations with the subscript *i* running from 1 to *n*, over all the *2n* electron in the system. The exchange correlation potential is defined as the functional derivative of $E_{xc}[\rho_0(r)]$ with respect to $\rho(r)$

$$v_{xc}(r) = \frac{\delta E_{xc}[\rho(r)]}{\delta\rho(r)} \qquad (2.13)$$

We need the derivative v_{xc} for the KS equations, and the exchange-correlation function itself for the energy equation. The KS equations can be written as

$$\hat{h}^{KS}(1)\psi_i^{KS}(1) = \varepsilon_i^{KS}\psi_i^{KS}(1) \qquad (2.14)$$

The KS operator $\hat{h}^{KS}$ is defined by equation (2.14). The difference between DFT method is the choice of the functional from of the exchange-correlation energy. Functional forms are often designed to have a certain limiting behavior, and fitting parameters to known accurate data. Which functional is the better will have to be settled by comparing the performance with experiments or high-level wave mechanics calculations.

2.3.3 DFT exchange and correlations

The form of E_{XC} is generally unknown and its exact value has been calculated only for a few very simple systems. In the density functional theory, the exchange energy is defined as

$$E_X[\rho] = \left\langle \phi[\rho] \middle| \hat{V}_{ee} \middle| \phi[\rho] \right\rangle - U[\rho] \tag{2.15}$$

when $U[\rho]$ is the Hartree piece of the columbic potential. The correlation term is defined as the remaining unknown piece of the energy:

$$E_C[\rho] = F[\rho] - T_S[\rho] - U[\rho] - E_X[\rho] \tag{2.16}$$

Due to the definition of $F[\rho]$, the correlation energy consists of two separate contributions:

$$E_C[\rho] = T_C[\rho] + U[\rho] \tag{2.17}$$

when $T_C[\rho]$ and $U_C[\rho]$ are respectively the kinetic contribution and the potential contribution of the correlation energy.

In electronic structure calculations, E_{XC} is the most commonly approximation within the local density approximation or generalized–gradient approximation. In the local density approximation (LDA), the value of $E_{XC}[\rho(\mathrm{r})]$ is approximated by exchange–correlation energy of an electron in homogeneous electron gas of the same density $\rho(r)$, *i.e.*

$$E_{XC}^{LDA}[\rho(r)] = \int \in_{XC} (\rho(r)) \rho(r) dr \tag{2.18}$$

The most accurate data for $\in_{XC}(\rho(r))$ is calculated from Quantum Monte Carlo calculation. For the systems with slowly varying charge densities, this approximation generally gives very good results. An obvious approach to improve the LDA, so called generalized gradient approximation (GGA), is to include gradient corrections by making E_{XC} a function of the density and its gradient as shown below

$$E_{XC}^{GGA}[\rho(r)] = \int \in_{XC}(\rho(r))\rho(r)dr + \int F_{XC}[\rho(r),|\nabla\rho(r)|]dr \qquad (2.19)$$

where F_{XC} is a correction chosen to satisfy one or several known limits for E_{XC}. Clearly, there is no unique equation for the F_{XC}, and several functions have been proposed. The development of the improved functions is currently a very active area of research although incremental improvements are likely. It is ambiguous whether the research will be successful in providing the substantial increase in accuracy that is desired.

2.3.4 Hybrid functions

Hybrid functional augment the DFT exchange-correlation energy with a term calculated from Hartree-Fock theory. The Kohn-Sham orbitals are quite similar to the HF orbitals, give an expression, based on Kohn-Sham orbitals, for the HF exchange energy.

$$E_x^{HF} = -\sum_{i=1}^{n}\sum_{j=1}^{n}\left\langle \psi_i^{KS}(1)\psi_i^{KS}(2)\left|\frac{1}{r_{ij}}\right|\psi_j^{KS}(2)\psi_j^{KS}(1)\right\rangle \qquad (2.20)$$

Since the KS Slater determinant is an exact representation of the wavefunction of the noninteracting electron reference system, E_x^{HF} is the exact exchange energy for a system of noninteracting electron with electron density equal to real system.

Including in a LSDA gradient-corrected DFT expression for E_{xc} ($E_{xc} = E_x + E_c$) a weighted contribution of the expression for E_x^{HF} give a FH/DFT exchange-correlation functional, commonly called a hybrid DFT functional. The most popular hybrid functional at present is based on an exchange-energy functional developed by Becke, and

modified Steven *et al.* which is the introduction of the LYP correlation-energy functional. This exchange-correlation functional, called the Becke3 LYP or B3LYP functional is

$$E_{xc}^{B3LYP} = (1 - a_0 - a_x)E_x^{LSDA} + a_0 E_x^{HF} + a_x E_x^{B88} + (1 - a_c)E_x^{VWN} + a_c E_c^{LYP} \qquad (2.21)$$

Here E_x^{LSDA} is the kind accurate pure DFT LSDA non-gradient-corrected exchange functional, E_x^{HF} is the Kohn-Sham orbitals based HF exchange energy functional, E_x^{B88} is the Becke 88 exchange functional

$$\begin{aligned}
E_x^{B88} &= E_x^{LDA} + \Delta E_x^{B88} \\
\Delta E_x^{B88} &= -\beta \rho^{1/3} \frac{x^2}{1 + 6\beta x \sinh^{-1} x}
\end{aligned} \qquad (2.22)$$

The β parameter is determined by fitting to known atomic data and x is a dimension gradient variable. The E_x^{VWN} is the Vosko, Wilk, Nusair function (VWN) can be written

$$\begin{aligned}
E_x^{VWN} &= E_x^{LDA}(1 + ax^2 + bx^4 + cx^6)^{1/5} \\
x &= \frac{|\nabla \rho|}{\rho^{4/3}}
\end{aligned} \qquad (2.23)$$

which forms part of the accurate functional for the homogeneous electron gas of the LDA and LSDA, and E_c^{LYP} is the LYP correlation functional. The parameters a_0, a_x and a_c are those that give the best fit of the calculated energy to molecular atomization energies. This is thus gradient-corrected hybrid functional.

2.4 Basis sets

Basis sets are the mathematical functions used in ab initio and DFT calculations to describe the electron distribution and hence model the shape of the electron density

and the molecular orbitals. Large basis sets more accurately approximation the orbitals of the by imposing fewer restrictions on the locations of the electrons in space. Standard basis sets for electronic structure calculations use linear combinations of Gaussian function to form the orbitals. Gaussian offers a wide range of pre-defined basis sets, which may be classified by the number and types of basis functions they contain. Basis sets assign a group of basis function to each atom within a molecule to approximate its orbital. These basis functions themselves are composed of a linear combination of gaussian functions, such basis functions are referred to as *contracted functions* and the component gaussian functions are referred to as *primitives*. A basis function consisting of a single gaussian function is *termed uncontracted*.

2.4.1 Slater type orbital (STO)

STOs use a function that correctly models the form of the vibration of the electron density with distance from the nucleus. The first intuition in the choice of a mathematical function for performing an atomic calculation is to use similar functions to those of a hydrogen atomic orbital. For this reason, Roothaan and Bagus wrote and SCF code for atoms under the linear combination of atomic orbitals (LCAO) approximation, which is expressed by

$$f^{STO}(r) = \left(\frac{\xi^3}{\pi} \right)^{0.5} \exp(-\xi r) \tag{2.24}$$

where ξ is the orbital exponent optimized variationally with respect to each total atomic energy. Unfortunately, these STOs do not lend themselves well to calculations as the two electron integrals are difficult to evaluate. To overcome these problems, Gaussian Type Orbitals (GTOs) are commonly used instead.

2.4.2 Gaussian type orbitals (GTO)

Gaussian type orbitals (GTO) are the usual alternative functions to the STOs in the molecular calculations. GTOs have the advantage that the two electron integrals may be quickly and easily evaluated. The functions are defined by

$$f^{GTO}(r) = \left(\frac{2\alpha}{\pi}\right)^{0.75} \exp(-\alpha r^2) \qquad (2.25)$$

where α is the GTO exponent. The first derivative of GTO with respect to r, when r tends to zero, is null, in contrast to the non null value achieved by some STO.

2.4.3 Minimal basis sets

Minimal basis sets contain the minimum number of basis functions needed for each atom to explain atomic orbitals. For examples, the minimum basis set for the methane molecule includes *1s* orbital of 4 hydrogen atoms and the set of carbon atom consists of *1s*, *2s*, and the full set of three *2p* orbitals then total set comprises 9 basis functions. Actually, a single Gaussian is a poor approximation to the nearly ideal description of an atomic wavefunction that Slater function provides. The most popular minimal basis sets are the STO-*n*G, where n denotes number of primitives in the contraction. These set were obtained by the least square fit of the combination of *n* Gaussian function to a Slater type orbital of the same type with $\xi = 1$. Then, these exponents are multiplied by the square of zeta in Slater orbitals. This type basis is known as STO-3G its uses three GTOs to approximate to STO. This lead to a great improvement over the single GTO it is also a minimal basis set as there is only one basis function per electron.

2.4.4 Split-valence basis sets

A major problem with minimal basis sets that they treat all electrons as equal. The solution to use is Split valence basis sets which are applied to describe valence orbitals

than core orbitals. In these, we partition electrons into core and valence types. For each of a core electrons are used a single contracted GTO but for the valence electron are used more than one contracted GTO. The first way that a basis set can be made larger is to increase the number of basis function per atom, such as 3-21G and 6-31G have two (or more) sizes of the basis function for each valence orbitals. For example, hydrogen and carbon are represented as:

H: 1s, 1s'

C: 1s, 2s, 2s', $2p_x$, $2p_y$, $2p_z$, $2p_x$', $2p_y$', $2p_z$'

where the primed and unprimed orbitals differ in size. The 3-21G basis sets are known as double-ξ (zeta), referring to the fact that like have two contracted GTOs for each electron in the valence space. Similarly, triple split valence basis sets, like 6-31G, use three size of contracted functions for each orbitals-type.

2.4.5 Polarization functions

Despite split valence basis sets allow orbitals change, but not change shape. Polarization functions can be added to basis sets to try to model the polarization effect as two atoms are brought close together. The electron cloud on one atom introduces a distortion in the shape of the electron cloud in the neighboring atom. Polarization functions basically consist of adding functions of a higher quantum number than are usually present for the atom. For example, polarized basis sets add *d* functions to carbon atoms and *f* functions to transition metals, and more of them add *p* function to hydrogen atom. So far, the only polarized basis set is applied for 6-31G(d) that it means the 6-31G basis set with *d* function added to heavy atom. This basis is also known as 6-31G* and is very common for calculations involving up to medium-sized systems. Another popular polarized basis set is 6-31G(d,p), also known as 6-31G**, which add *p* functions to hydrogen atoms in addition to the *d* function on heavy atoms.

2.4.6 Diffuse functions

Diffuse functions are basis functions with a larger spatial extent than the normal ones. These functions are particularly important in the modeling of anions or exited states in which the electrons may be further removed from the nucleus than in ground state, neutral molecules. The 6-31G* basis set is the 6-31+G* basis set with diffuse functions added to heavy atoms. The double plus version, 6-31++G*, added diffuse functions to the hydrogen atoms as well. Diffuse functions on hydrogen atom seldom make a significant difference in accuracy.

2.4.7 Effective core potentials

Basis sets for atoms beyond the third row of the periodic table calculations using atomic orbital based basis sets become very time consuming due to the number of electrons and hence number of basis functions involved in the calculation. For these very large nuclei, electrons near the nucleus are treated in approximate way, via effective core potentials (ECPs or pseudo potentials). These functions replace the inner core electron in the calculation leading to an increase in speed with a very small loss in accuracy. This treatment includes some relativistic effects, which are important in these atoms. The LanL2DZ (Los Alamos National Laboratory 2 double ζ) basis set for transition metals, while using all-electron basis sets for all other non-transition-metal atoms, has become more and more popular in computations on transition-metal-containing systems [25].

2.5 Transition state theory and rate constant

Transition state theory (TST) or activated complex theory provides a simple formalism for obtaining thermal rate constant by mixing the important features of the potential energy surface with a statistical representation of the dynamics. In addition to the Born-Oppenheimer approximation, TST is based on three assumptions:

- Classically there exists a surface in phase space that divides it into a reactant region and a product region. It is assumed that this dividing surface is located at the

transition state, which is defined as the maximum value on the minimum energy path (MEP) of the potential energy surface that connects the reactant(s) and product(s). Any trajectory passing through the dividing surface from the reactant side is assumed to eventually form products. This is often referred to as the nonrecrossing rule.

- The reactant equilibrium is assumed to maintain a Boltzmann energy distribution.

- Activated complexes are assumed to have Boltzmann energy distributions corresponding to the temperature of the reacting system. These activated complexes are defined as super-molecules having configurations located in the vicinity of the transition state.

In chemistry, transition state theory is a conception of chemical reactions or other processes involving rearrangement of matter as proceeding through a continuous change or "transition state" in the relative positions and potential energies of the constituent atoms and molecules. The theory was first developed by Marcelin in 1915, then continued by Eyring and Polanyi (Eyring equation) in 1931, with their construction of a potential energy surface for a chemical reaction, and later, in 1935, by Pelzer and Wigner [26]. Evans, working in coordination with Polanyi, also contributed significantly to this theory.

TST assumes that a reaction proceeded from one energy minimum to another via an intermediate maximum. The Transition state is the configuration which divides the reactant and product parts of surface. For example, a molecule which has reached the transition state will continue on to product. The geometrical configuration of the energy maximum is called the transition–state structure. Within standard TST, the transition state and transition structure are identical, but this is not necessarily for more refined models. The direction of reaction coordinate is started from the reactant to product along a path where the energies are as low as possible and the TS is the point where the energy has a maximum, shown in Figure 2.1.
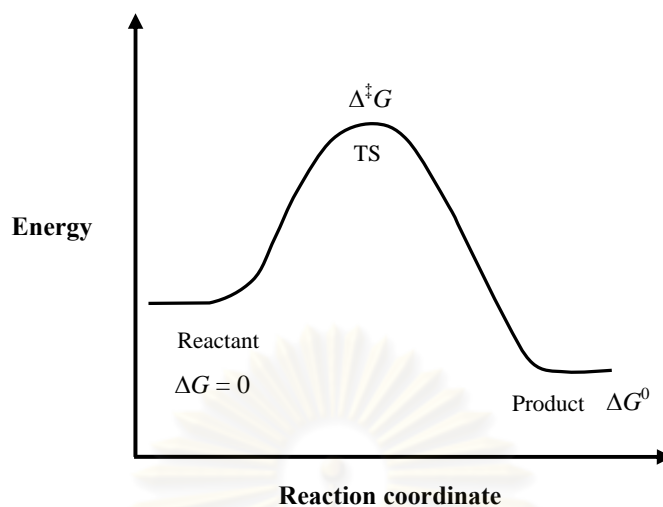
Figure 2.1 Schematic illustration of reaction path.

2.5.1 Rate constant and Boltzman distribution

TST assumes equilibrium energy distribution among all possible quantum states at all points along the reaction coordinates. The probability of finding a molecule in a given quantum state is proportional to $e^{-\Delta E^{\ddagger}/k_B T}$, which is Boltzman distribution. Assuming that the molecule at the TS is in equilibrium with the reactant, the macroscopic rate constant can be expressed as

$$k = \frac{k_B T}{hc^0} e^{-\Delta^{\ddagger} G /RT} \tag{2.26}$$

$\Delta^{\ddagger}G$ is the Gibbs free energy difference between the TS and reactant, T is absolute temperature and k_B is Boltzmann's constant and c° is concentration factor. From the TST expression (2.26) it is clear that if the free energy of the reactant and TS can be calculated, the reaction rate follows trivially. The equilibrium constant for a reaction can be calculated from the free energy difference between the reactant(s) and product(s).

$$K_{eq} = e^{-\Delta G_0 / RT}$$ (2.27)

The Gibbs free energy is given in terms of the enthalpy and entropy, $G = H - TS$.

2.5.2 Rate constant with tunneling corrections

Tunneling corrections were calculated using the Wigner, Eckart [27], the multi-dimensional zero-curvature (ZCT) [28] and centrifugal-dominant small-curvature (SCT) [29] methods. The Wigner method is a simple, zeroth-order tunneling approximation and only depends on the curvature at transition state. The Eckart method is believed to be one of the more accurate approximate one dimensional tunneling corrections. The Eckart tunneling factor is calculated by fitting an Eckart potential to the MEP using the curvature at the transition state, the zero-point energy inclusive energy barrier, and the reaction energy. The ZCT method is a minimum-energy-path, semiclassical adiabatic ground-state (MEPSAG) method which takes into account tunneling along the MEP. Reaction path curvature and coupling to modes orthogonal to the MEP are neglected. The SCT method is a centrifugal-dominant small-curvature semi-classical adiabatic ground-state (CD-SCSAG) method which accounts for the curvature of the reaction path and approximately incorporates tunneling paths other than the MEP.
Reaction rate coefficients were calculated using the

$$k = \kappa \left[\frac{k_B T}{h} \right] \left[\frac{Q_{TS}}{Q_{complex}} \right] e^{-\Delta E^{\ddagger} / RT}$$ (2.28)

where tunneling factor, $\kappa = 1 + (1/24)(h v_i c / k_B T)^2$, k_B is Boltzman constant, T is absolute temperature, Q_{TS} and $Q_{Complex}$ are the partition functions of transition state and complex, respectively, h is Plank constant, c is speed of light and v_i is imaginary frequency of transition state.

2.5.3 Partition functions

The first step in determining the thermal contributions to the enthalpies and entropies of a molecule is to determine its partition function, q which is a measure of the number of accessible to the molecule (translational, rotational, vibrational and electronic states) at a particular temperature.

It is assumed that the translational (T), rotational (R), vibrational (V) and electronic (E) modes of the system can be separated, thus allowing the energy of each level, E_i, to be separated into T, R, V and E contributions as

$$E = E_i^T + E_i^R + E_i^V + E_i^E \qquad (2.29)$$

While the translational modes are truly independent from the rest, the separations of other modes are based on an approximation, in particular the Bohn–Oppenheimer approximation for electronic and vibrational motion and the rigid rotor approximation which assumes (that the geometry of the molecule does not change as it rotates) for vibrational and rotational modes. Within these approximations, the total molecular partition function can therefore be factorized into translational, rotational, vibrational and electronic contributions:

$$q = q_{trans}q_{vib}q_{rot}q_{elect} \qquad (2.30)$$

2.5.3.1 Translational partition function

For bimolecular reactions, the ratio of the translational partition functions may be simplified to yield the relative translational partition in per unit volume as

$$q_{trans} = \frac{V}{\Lambda^3} \qquad (2.31)$$

$$\Lambda = h\left(\frac{\beta}{2\pi m}\right)^{1/2} \qquad (2.32)$$

where h is Planck's constants, m is the mass of the molecule and V is the available volume to it. For a gas phase system this is the molar volume (usually determined by the ideal gas equation) at the specific temperature and pressure.

2.5.3.2 Vibrational partition function

The vibrational partition functions are calculated quantum mechanically within the framework of the harmonic approximation. The harmonic oscillator partition function is given by:

$$q_{trans} = \prod_i \frac{1}{1 - e^{-\beta hc\tilde{v}}} \tag{2.33}$$

where $\tilde{v}_i$ is the vibrational frequency in cm^{-1} for mode i. The product is over all vibrational modes.

2.5.3.3 Rotational partition function

The formulation for rotational partition functions depends on whether or not the molecule is linear. For linear molecules

$$q_{rot} = \frac{k_B T}{\sigma hcB} \tag{2.34}$$

and for non linear

$$q_{rot} = \frac{1}{\sigma} \left(\frac{k_B T}{hc} \right)^{3/2} \left(\frac{\pi}{ABC} \right)^{1/2} \tag{2.35}$$

where σ is the rotational symmetry number of the molecule, c is the speed of light and A, B, C are the rotational constants.

2.5.3.4 Electronic partition function

For the electronic partition function, an adiabatic potential energy surface is assumed. The electronic degeneracies along the MEP are assumed to be the same as at the transition state. The formula employed is

$$q_{elect} = \omega_{e1} + \omega_{e1} \exp(-\beta \Delta \varepsilon_{12}) + ... \tag{2.36}$$

where $\Delta \varepsilon_{1j}$ is the energy of the jth electronic level relative to the ground state and ω_{ej} is the corresponding degeneracy.

2.6 Molecular vibrational frequencies

The total molecular energy E is approximately the sum of translation, rotational, vibrational, and electronic energies. In the harmonic oscillator approximation, the vibrational energy of an N-atom molecule is the sum of 3N-6 normal mode vibrational energies (3N-5 for a linear molecule) [30]:

$$E_{vib} \approx \sum_{k=1}^{3N-6} (\upsilon_k + \frac{1}{2})h\nu_k \tag{2.37}$$

where ν_k is the harmonic vibrational frequency for the kth normal mode and each vibrational quantum number υ_k has the possible values 0, 1, 2,..., independent of the value of the order vibrational quantum numbers.

The harmonic vibrational frequencies of a molecule are calculated as follows: (1) Solve the electronic Schrödinger equation $(\hat{H}_{el} + V_{NN})\psi_{el} = U\psi_{el}$ for several molecular geometries to find the equilibrium geometry of the molecule, (2) Calculate the set of second derivatives $(\partial^2 U / \partial X_i \partial X_j)_e$ of the molecular electronic energy U with respect to the 3N nuclear Cartesian coordinates of a coordinate system with origin at the center of mass, (3) Form the mass-weighted force-constant matrix elements.

$$F_{ij} = \frac{1}{(m_i m_j)^{1/2}} \left(\frac{\partial^2 U}{\partial X_i \partial X_j} \right)_e \tag{2.38}$$

where i and j each go from 1 to 3N and m_i is the mass of the atom corresponding to coordinate X_i. (4) Solve the following set of 3N linear equations in 3N unknowns

$$\sum_{j=1}^{3N} (F_{ij} - \delta_{ij} \lambda_k) l_{jk} = 0 \qquad i = 1, 2, ..., 3N \tag{2.39}$$

In this set of equations, δ_{ij} is the Kronecker delta, and λ_k and the l_{jk}'s are as-yet unknown parameters whose significance will be seen shortly. In order that this set of homogeneous equations has a nontrivial solution, the coefficient determinant must vanish

$$\det(F_{ij} - \delta_{ij} \lambda_k) = 0 \tag{2.40}$$

This determinant is of order 3N and when expanded gives a polynomial whose highest power of λ_k is λ_k^{3N}. The molecular harmonic vibrational frequencies are then calculated from

$$v_k = \lambda_k^{1/2} / 2\pi \tag{2.41}$$

Six of the λ_k values found by solving will be zero, yielding six frequencies with value zero, corresponding to the three translational and three rotational degrees of freedom of the molecule. The remaining 3N-6 vibrational frequencies are the molecular harmonic vibrational frequencies.

2.7 Thermochemistry

The usual way to calculate enthalpies of reaction is to calculate heats of formation, and take the appropriate sums and difference [31].

$$\Delta_r H^{\circ}(298.15\,K) = \sum_{products} \Delta_f H^{\circ}_{prod}(298.15\,K) - \sum_{reactants} \Delta_f H^{\circ}_{react}(298.15\,K) \qquad (2.42)$$

However, since Gaussian provides the sum of electronic and thermal enthalpies, there is a short cut: namely, to simply take the difference of the sums of these values for the reactants and the products.

Calculating enthalpies of formation is a straight–forward, albeit somewhat tedious task, which can be split into a couple of steps. The first step is to calculate the enthalpies of formation $(\Delta_f H^{o}(0\,K))$ of the species involved in the reaction. The second step is to calculate the enthalpies of formation of the species at 298.15 K. Calculating the Gibbs free energy of reaction is similar, except we have to add in the entropy term:

$$\Delta_f G^{\circ}(298.15\,K) = \Delta_f H^{\circ}(298.15\,K) - T(S^{\circ}(M,298.15\,K)$$
$$- \sum S^{\circ}(X,298.15\,K)) \qquad (2.43)$$

To calculate these quantities, we need a few component pieces first. In the descriptions below, I will use M to stand for the molecule, and X to represent each element which makes up M, and x will be the number of atoms of X in M.

- Atomization energy of the molecule, $\sum D_0(M)$:

  These are readily calculated from the total energies of the molecule $\sum \varepsilon_0(M)$, the zero-point energy of the molecule $(\varepsilon_{ZPE}(M))$ and the constituent atoms:

$$\sum D_0(M) = \sum_{atoms} x\varepsilon_0(X) - \varepsilon_0(M) - \varepsilon_{ZPE}(M) \qquad (2.44)$$

- Heats of formation of the atoms at 0 K, $(\Delta_f H^{\circ}(X,0\,K))$ [32]
- Enthalpy corrections of the atomic elements, $H_x^{\circ}(298\,K.15) - H_x^{\circ}(0\,K)$
- Enthalpy correction for the molecule, $H_M^{\circ}(298.15\,K) - H_M^{\circ}(0\,K)$

- Entropy for the atoms, $S_x^\circ(298.15\,K)$

- Entropy for the molecule, $S_M^\circ(298.15\,K)$

Putting all these pieces together, we can finally take the steps necessary to calculate

$\Delta_f H^\circ(298.15\,K)$ and $\Delta_f G^\circ(298.15\,K)$:

1. Calculate $\Delta_f H^\circ(M, 0\,K)$ for each molecule:

$$
\begin{aligned}
\Delta_f H^\circ(M, 0\,K) &= \sum_{atoms} x\Delta_f H^\circ(X, 0\,K) - \sum D_0(M) \\
&= \sum_{atoms} x\Delta_f H^\circ(X, 0\,K) - (\sum_{atoms} x\varepsilon_0(X) - \varepsilon_0(M))
\end{aligned}
\tag{2.45}
$$

2. Calculate $\Delta_f H^\circ(M, 298.15\,K)$ for each molecule:

$$
\begin{aligned}
\Delta_f H^\circ(M, 298.15\,K) &= \Delta H_f^\circ(M, 0\,K) + (H_M^\circ(298.15\,K) - H_M^\circ(0\,K)) \\
&\quad - \sum_{atoms} x(H_X^\circ(298.15\,K) - H_X^\circ(0\,K))
\end{aligned}
\tag{2.46}
$$

3. Calculate $\Delta_f G^\circ(M, 298.15\,K)$ for each molecule:

$$
\begin{aligned}
\Delta_f G^\circ(M, 298.15\,K) &= \Delta_r H^\circ(298.15\,K) + 298.15(S^\circ(M, 298.15\,K) \\
&\quad - \sum S^\circ(X, 298.15\,K))
\end{aligned}
\tag{2.47}
$$

CHAPTER III

COMPUTATIONAL DETAILS

3.1 Cluster models for the H–ZSM–5 and M–ZSM–5

3.1.1 Strategic models I and II

H–ZSM–5 and M(I)–ZSM–5, M(I) = Cu(I), Ag(I) and Au(I) are modeled as 5T cluster $AlH_{13}O_4Si_4$ and $M(I)AlH_{12}O_4S_{i4}$, respectively. The 5T cluster models for H–ZSM–5 and M(I)–ZSM–5 are denoted as strategic model I as shown in Figure 3.1(a) and 3.1(b), respectively. M(II)–ZSM–5, M(II) = Ni(II), Pd(II), and Pt(II) are modeled as 8T cluster $Al_2H_{18}M(II)O_7Si_6$ which is denoted as strategic model II as shown in Figure 3.1(c).
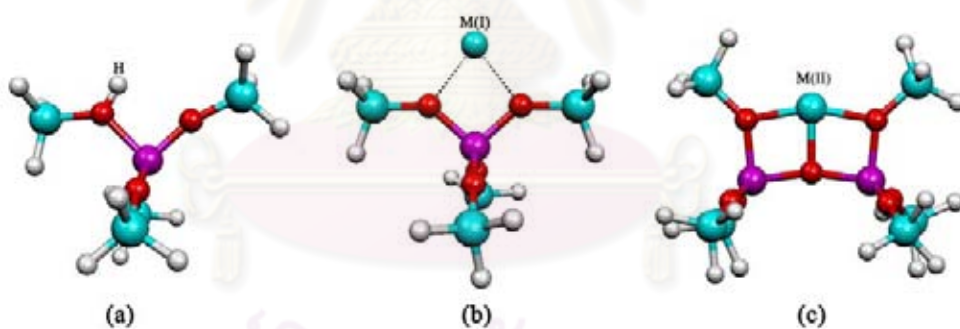
Figure 3.1 Cluster models defined for (a) H–ZSM–5, (b) M(I)–ZSM–5 as strategic model I and (c) M(II)–ZSM–5, as strategic model II.

3.1.2 Strategic models III and IV

The 28T cluster for H–ZSM–5 was obtained by the B3LYP/LanL2DZ–optimized structure. The 28T cluster cut from the ZSM–5 crystal lattice structure which dangling bonds were saturated with hydrogen atoms and T12–silica was replaced with aluminum

atom [32]. The 28T cluster for H–ZSM–5 and M(I)–ZSM–5 are modeled as $H_{35}Si_{27}AlO_{39}$ and $H_{34}Si_{27}M(I)AlO_{39}$, respectively. The 28T cluster models for H–ZSM –5 and M(I)–ZSM–5 are defined as 5T/28T–optimization model, denoted as strategic model III. The strategic model III allows 5T cluster, H^+ in H–ZSM–5 and M(I) ion in M(I)–ZSM–5 to be optimized but constrains the remaining atoms being frozen as described in Figure 3.2(a) and Figure 3.2(b), respectively. The 28T cluster model for M(II)–ZSM–5 modeled as $H_{34}Si_{26}M(II)Al_2O_{39}$ is defined as 8T/28T–optimization model, deno ted as str ategic model IV. The strategic model IV allows 8T cluster and M(II) ion to be optim ized but constrains the remaining atoms being frozen, as shown in Figure 3.2(c). The model I and model III are composed of one aluminum atom but two aluminum atoms for the model II and model IV.
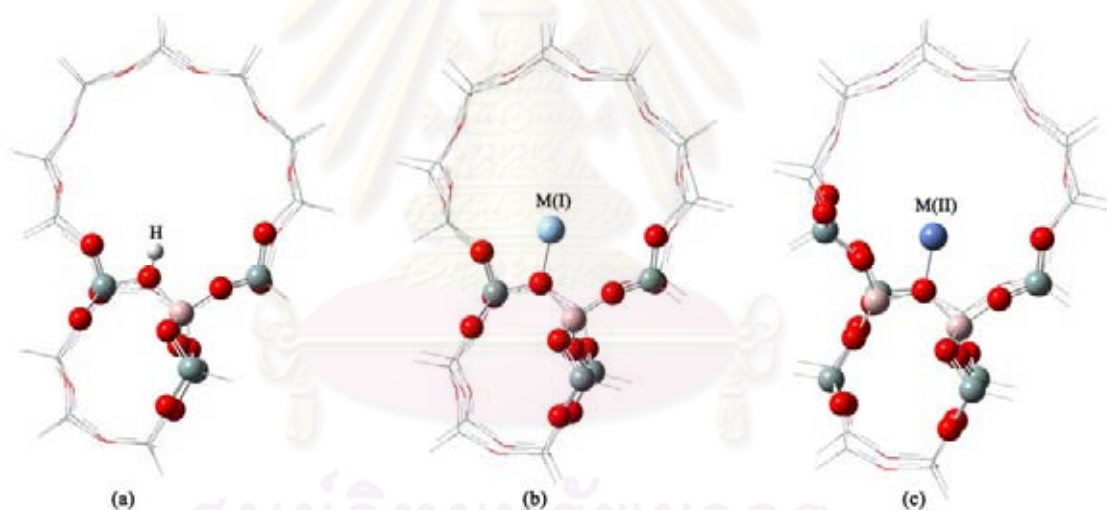
Figure 3.2 Cluster models defined for (a) H–ZSM–5, (b) M(I)–ZSM–5 as strategic model III and (c) M(II)–ZSM–5, as strategic model IV.

3.2 Structure optimization and potential energy surface

The calculations have been performed with hybrid density functional B3LYP, the Becke's three–parameter exchange functional [34] with the Lee–Yang–Parr correlation functional [35], using the Los Alamos LanL2DZ split–valence basis set [36–38]. The full

optimizations for the H–ZSM–5, M(I)–ZSM–5 and M(II)–ZSM–5 catalysts and configurations of t heir interactions with all related adsorbates were carried out a t the B3LYP/LanL2DZ level. The zero point vibrational energy (ZPVE) corrections were obtained from frequency calculations at the B3LYP/LanL2DZ level.

The transition–state structures for all conversions of ethanol to ethylene and to butenes over the selected cl uster models of H–ZSM–5 and M–ZSM–5 obtained at the B3LYP/LanL2DZ level of theory have been located using the reaction coordinate method referred to the synchro nous transit–guided quasi–newton (STQN) ca lculation [39]. The transition states for the conversion of ethanol to ethylene and to 1–butene over the H–ZSM–5 and M–ZSM–5 u sing strategic models I–IV were confi rmed by their single imaginary frequencies. The 28T cluster m odels, the intrinsic reaction coordinate (IRC) method [40] was used to tr ack minimum energy paths from transition state structures to the corresponding minimum. All calculations were performed using GAUSSIAN 03 program [41].

3.3 Calculation of thermodynamic properties, rate and equilibrium constants

Thermodynamic properties of reaction steps for all reaction systems were derived from their corresponding vibrational frequency calculations. Rate const ants for each reaction step were comput ed using equation (2.26) and (2.28) and the equilibrium constants were derived from Gibbs free energy changes.

CHAPTER IV

RESULTS AND DISCUSSION

4.1 Optimized structures for catalysts and involved compounds

The B3LYP/LanL2DZ–optimized structures of reactants and products are shown in Figure 4.1. The B3LYP/LanL2DZ–optimized structures for all catalysts H–ZSM–5, Cu–ZSM–5, Ag–ZSM–5, and Au–ZSM–5 modeled as 5T cluster (strategic model I) and Ni–ZSM–5, Pd–ZSM–5, and Pt–ZSM–5 modeled as 8T cluster (strategic model II) are shown in Figure 4.2. The selected geometrical parameters for the 5T–cluster–modeled H–ZSM–5 and M(I)–ZSM–5 and 8T–cluster–modeled catalysts are listed in Table A–1. The B3LYP/LanL2DZ–optimized structures of catalysts modeled as the 28T cluster H–ZSM–5, Cu–ZSM–5, Ag–ZSM–5, Au–ZSM–5, Ni–ZSM–5, Pd–ZSM–5, and Pt–ZSM–5 are shown in Figure 4.3. The selected geometrical parameters for the 28T–cluster–modeled H–ZSM–5, M(I)–ZSM–5 and M(II)–ZSM–5 catalysts are listed in Table A–2.
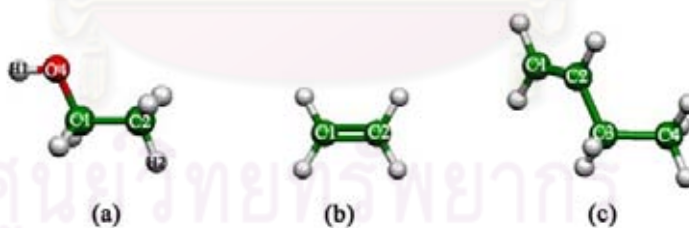
Figure 4.1 The B3LYP/LanL2DZ–optimized structures of reactant (a) C_2H_5OH and products (b) C_2H_4 and (c) $1–C_4H_8$.
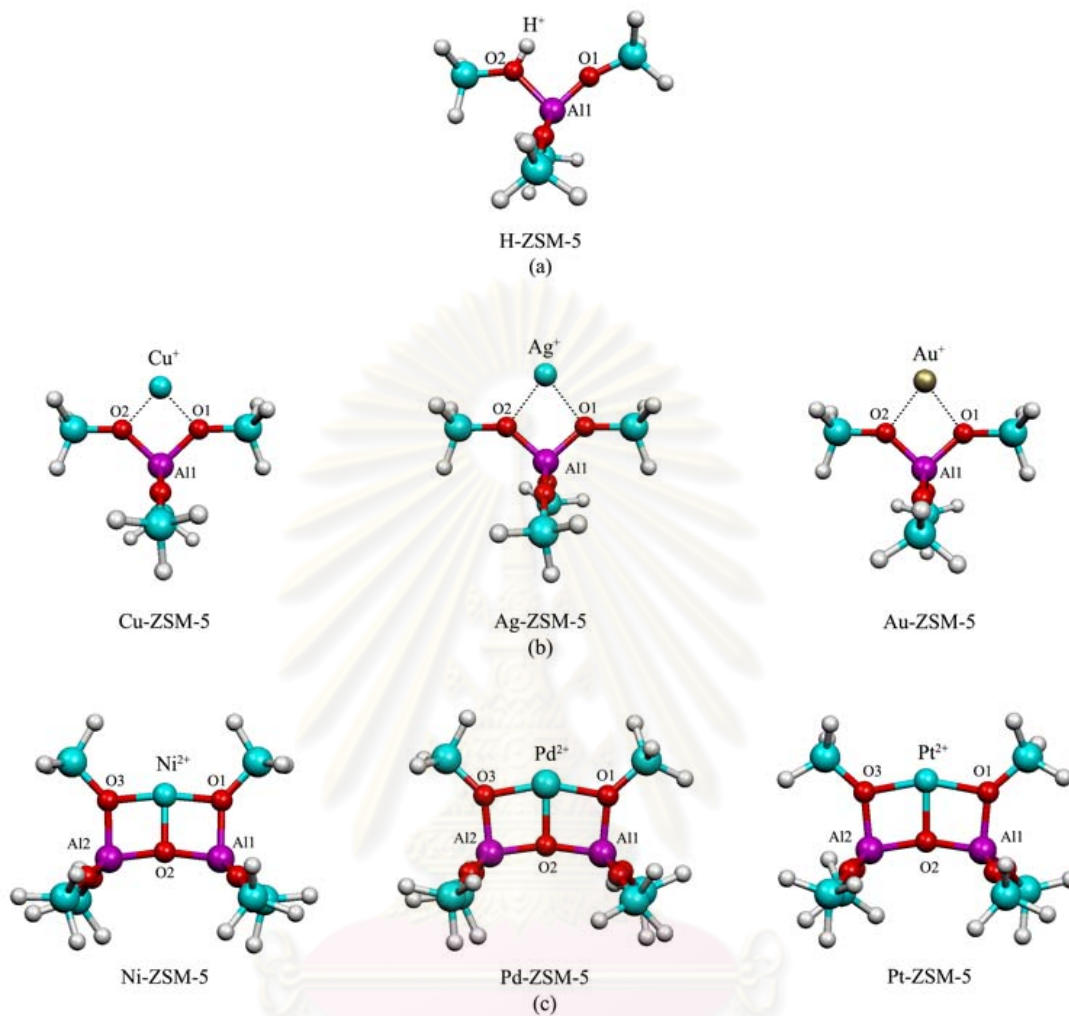
Figure 4.2 The B3LYP/LanL2DZ–optimized structures of the 5T cluster (strategic model I) (a) H–ZSM–5, (b) M(I)–ZSM–5 and the 8T cluster (strategic model II) (c) M(II)–ZSM–5.
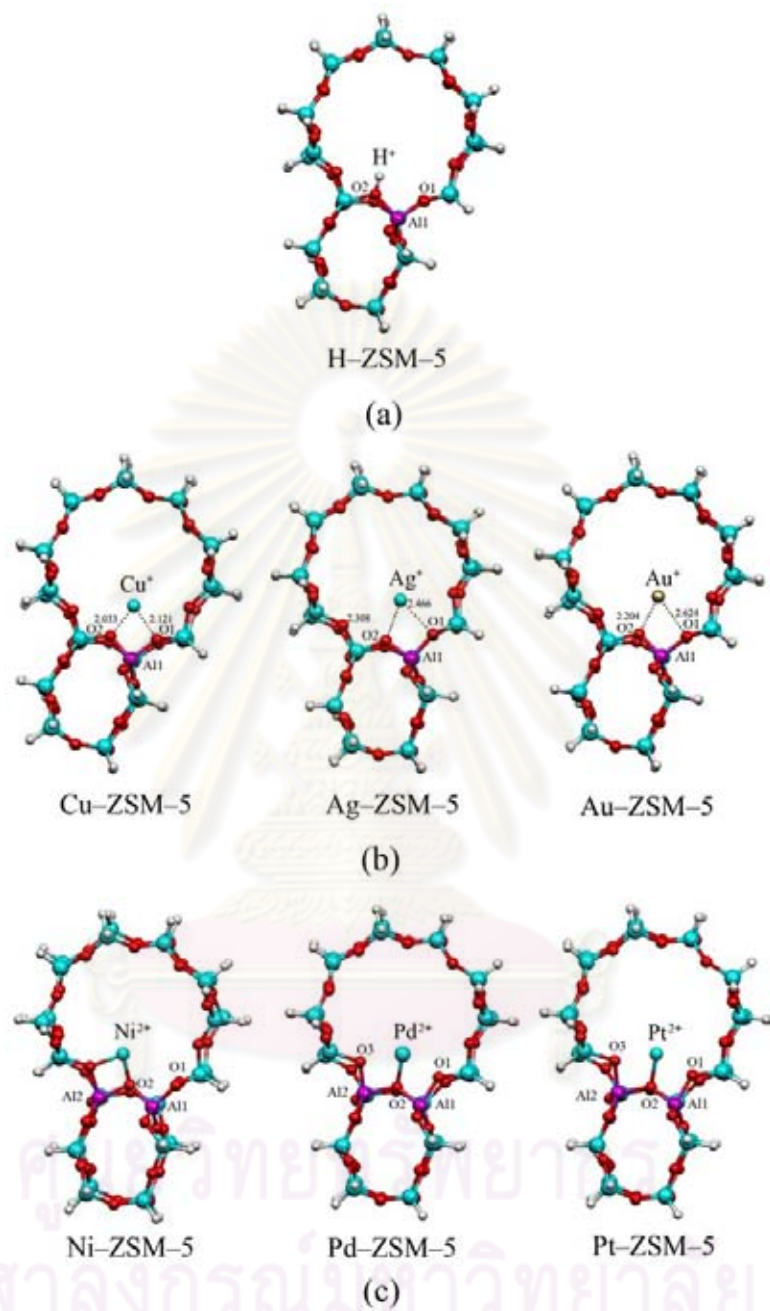
Figure 4.3 The B3LYP/LanL2DZ–optimized structures of catalysts modeled as the 28T–cluster modeled as the (a) H–ZSM–5, (b) M(I)–ZSM–5 as strategic model III and (c) M(II)–ZSM–5 catalysts as strategic model IV.

The bond distances between monovalent metal ion or proton and the nearest–neighbor oxygen atoms of 5T–cluster–modeled H–ZSM–5 and M(I)–ZSM–5 catalysts are in order: Au–O2 > Ag–O2 > Cu–O2 > H–O2. The bond distances between divalent metal ions and oxygen atoms of 8T–cluster–modeled M(II)–ZSM–5 catalysts are in different orders and they are shorter than the M–O2 bond distances of 5T–cluster–modeled H–ZSM–5 and M(I)–ZSM–5 catalysts.

The bond distances between monovalent metal ion or proton and the nearest–neighbor oxygen atoms of 28T–cluster–modeled H–ZSM–5 and M(I)–ZSM–5 catalysts are in order: Au–O2 > Ag–O2 > Cu–O2 > H–O2. The bond distances between monovalent metal ion or proton and the nearest–neighbor oxygen atoms of 28T–cluster–modeled M(II)–ZSM–5 catalysts are in order: Pt–O2 > Pd–O2 > Ni–O2. The M–O2 bond distances of M(II)–ZSM–5 catalysts are shorter than the M–O2 bond distances of H–ZSM–5 and M(I)–ZSM–5 catalysts.

4.2 Reaction mechanism of ethanol conversion to ethylene over the 5T/ZSM–5 and 8T/ZSM–5–type catalyst

4.2.1 Ethanol conversion to ethylene in non–catalytic system

The potential energy profile for the conversion of ethanol to ethylene in system without catalyst is shown in Figure 4.4. The energetics, thermodynamic properties, rate constant and equilibrium constant for the conversion of ethanol to ethylene in system without catalyst are shown in Table 4.1. All parameters for calculations of the rate constant of the reaction are listed in Table A–3. The first step of the reaction is the rate determining step (RDS) of which the activation energy is 56.59 kcal/mol. The last step is isolation of product intermediate to afford the ethylene and endothermic reaction. The rate constant of the reaction is $3.21 \times 10^{-29}\,s^{-1}$.
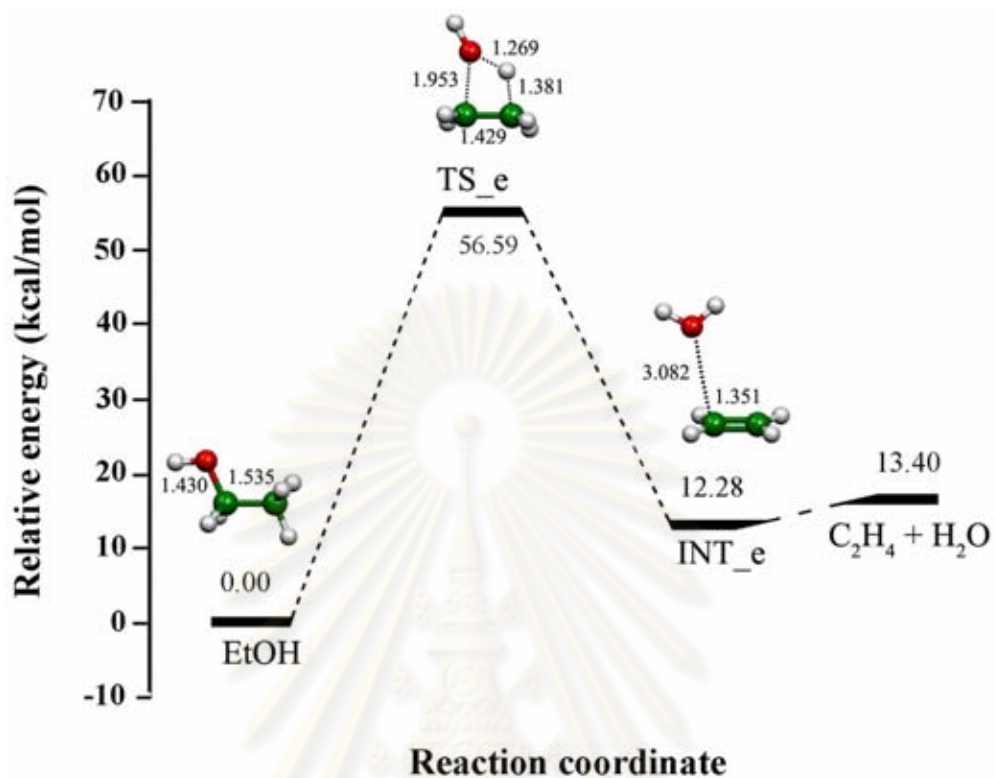
Figure 4.4 Potential energy profile for the ethanol conversion to ethylene in non–catalytic system.

Table 4.1 Energetics, thermodynamic properties, rate constants and equilibrium constants for conversion reactions of ethanol to ethylene by H–ZSM–5 and M(I)–ZSM–5 catalysts as strategic model I, compared to non–catalytic system

Catalysts/Reactions [a]	$\Delta^{\ddagger}E$ [a,b]	$\Delta^{\ddagger}G$ [a,b]	k_{298} [c]	ΔE [a]	ΔH_{298} [a]	ΔG_{298} [a]	K_{298}
Non–catalytic :							
EtOH → TS_e → INT1	56.59	56.32	3.21×10^{-29}	12.28	14.28	7.99	1.39×10^{-6}
INT1 → C_2H_4 + H_2O	–	–	–	1.12	0.68	–3.22	2.29×10^{2}
H–ZSM–5:							
EtOH + HZ→ INT1$_{H\_e}$	–	–	–	–23.73	–23.08	–13.63	9.76×10^{9}
INT1$_{H\_e}$ → TS$_{H\_e}$ → INT2$_{H\_e}$	41.33	42.83	2.48×10^{-19}	21.22	21.93	21.66	1.32×10^{-16}
INT2$_{H\_}$ e → ZH + C_2H_4 + H_2O	–	–	–	15.91	16.11	–3.27	2.50×10^{2}
Cu–ZSM–5:							
EtOH + CuZ→ INT1$_{Cu\_e}$	–	–	–	–9.45	–8.98	0.31	5.94×10^{-1}
INT1$_{Cu\_e}$ → TS$_{Cu\_e}$ → INT2$_{Cu\_e}$	45.09	44.07	3.08×10^{-20}	–12.43	–11.77	–11.47	2.56×10^{8}
INT2$_{Cu\_e}$ → CuZ + C_2H_4 + H_2O	–	–	–	35.27	35.71	15.93	2.11×10^{-12}
Ag–ZSM–5:							
EtOH + AgZ→ INT1$_{Ag\_e}$	–	–	–	–4.74	–3.94	2.63	1.19×10^{-2}
INT1$_{Ag\_e}$ → TS$_{Ag\_e}$ → INT2$_{Ag\_e}$	45.52	47.65	7.24×10^{-23}	–8.23	–8.23	–5.83	1.88×10^{4}
INT2$_{Ag\_e}$ → AgZ + C_2H_4 + H_2O	–	–	–	26.37	27.13	7.97	1.44×10^{-6}
Au–ZSM–5:							
EtOH + AuZ→ INT1$_{Au\_e}$	–	–	–	–10.68	–9.76	–3.00	1.57×10^{2}
INT1$_{Au\_e}$ → TS$_{Au\_e}$ → INT2$_{Au\_e}$	34.41	36.05	2.32×10^{-14}	–22.87	–22.30	–21.05	2.70×10^{15}
INT2$_{Au\_e}$ → AuZ + C_2H_4 + H_2O	–	–	–	46.94	47.02	28.81	7.60×10^{-22}

[a] For 5T cluster models of ZSM–5, computed at B3LYP/LanL2DZ level of theory.
[b] Activation state.
[c] In s^{-1}.

4.2.2 Ethanol conversion to ethylene catalyzed by H–ZSM–5

The potential energy profile for the ethanol conversion to ethylene on the the H–ZSM–5 catalyst is shown in Figure 4.5. The energetics, thermodynamic properties, rate constant and equilibrium constant for the conversion of ethanol to ethylene on the H–ZSM–5 catalyst are shown in Table 4.1. All parameters for calculation of the rate constant of the reaction are listed in Table A–3.

Figure 4.5 Potential energy profile for the ethanol conversion to ethylene on the H–ZSM–5 catalyst as 5T–cluster model.

The reaction steps for the conversion of ethanol to ethylene on the H–ZSM–5 are composed of three steps. The reaction is initiated by the adsorption of ethanol on the active acidic site of H–ZSM–5 catalyst. This adsorption occurs through the formation of a strong hydrogen bond between the alcoholic oxygen atom of ethanol and the OH group of zeolites which is the spontaneous reaction. The second step (RDS) is conversion of reactant intermediate to product intermediate via transition state TS_{H_e} and the rate constant of 2.48×10^{-19} s^{-1} was obtained. The activation energy for this transition state is 41.33 kcal/mol. The last step is the isolation of product intermediate to obtain the final product and endothermic reaction.

4.2.3 Ethanol conversion to ethylene catalyzed by M(I)–ZSM–5–type catalyst

Reactions for the ethanol conversion to ethylene on the Cu–ZSM–5, Ag–ZSM–5 and Au–ZSM–5 catalysts are shown in Figure 4.6. The potential energy profiles for the ethanol conversion on M(I)–ZSM–5−type catalysts are shown in Figure 4.7. The energetics, thermodynamic properties, rate constant and equilibrium constant for the conversion of ethanol to ethylene on the M(I)–ZSM–5–type catalysts are shown in Table 4.1. All parameters for calculations of the rate constant of the reaction catalyzed by M(I)–ZSM–5–type catalysts are listed in Table A–3.

The reaction is also initialized by the adsorption of the ethanol molecule on M(I)–ZSM–5–type catalysts. At the second step (RDS) of the reaction were catalyzed by M(I)–ZSM–5–type catalysts via transition–state $TS_{Cu\_}e$, $TS_{Ag\_}e$ and $TS_{Au\_}e$. The activation energies for these steps are 45.09, 45.52 and 34.41 kcal/mol, respectively. It was found that the activation energy of the conversion of ethanol to ethylene is obviously reduced by the Cu^+, Ag^+ and Au^+ metal–ion–exchanged H–ZSM–5 catalysts rather than the non–catalyst system. Rate constants (k) of the reactions are in order: Au–ZSM–5 (2.32×10^{-14} s^{-1}) > Cu–ZSM–5 (3.08×10^{-20} s^{-1}) > Ag–ZSM–5 (7.24×10^{-23} s^{-1}). Magnitudes of equilibrium constants (K) of the reactions are in order: Au–ZSM–5 (2.70×10^{15}) > Cu–ZSM–5 (2.56×10^8) > Ag–ZSM–5 (1.88×10^4). The third steps for the reactions either catalyzed by Cu–ZSM–5 or Ag–ZSM–5 or Au–ZSM–5 are the endothermic reaction.

Figure 4.6 Reactions for the ethanol conversion to ethylene on (a) Cu–ZSM–5, (b) Ag–ZSM–5 and (c) Au–ZSM–5 catalysts as 5T–cluster model. Bond distances are in Å.

Figure 4.7 Potential energy profiles for the ethanol conversion to ethylene on the H–ZSM–5, Cu–ZSM–5, Ag–ZSM–5 and Au–ZSM–5 catalysts of 5T–cluster model compared to non–catalytic reaction.

4.2.4 Ethanol conversion to ethylene catalyzed by M(II)–ZSM–5–type catalyst

Reactions for the ethanol conversion to ethylene on the Ni–ZSM–5, Pd–ZSM–5 and Pt–ZSM–5 catalysts are shown in Figure 4.8. The potential energy profiles for the ethanol conversion on M(II)–ZSM–5−type catalysts are shown in Figure 4.9. The energetics, thermodynamic properties, rate constant and equilibrium constant for the conversion of ethanol to ethylene on the M(II)–ZSM–5–type catalysts are shown in Table 4.2. All parameters for calculations of the rate constant of the reaction catalyzed by M(II)–ZSM–5–type catalysts are listed in Table A–4.
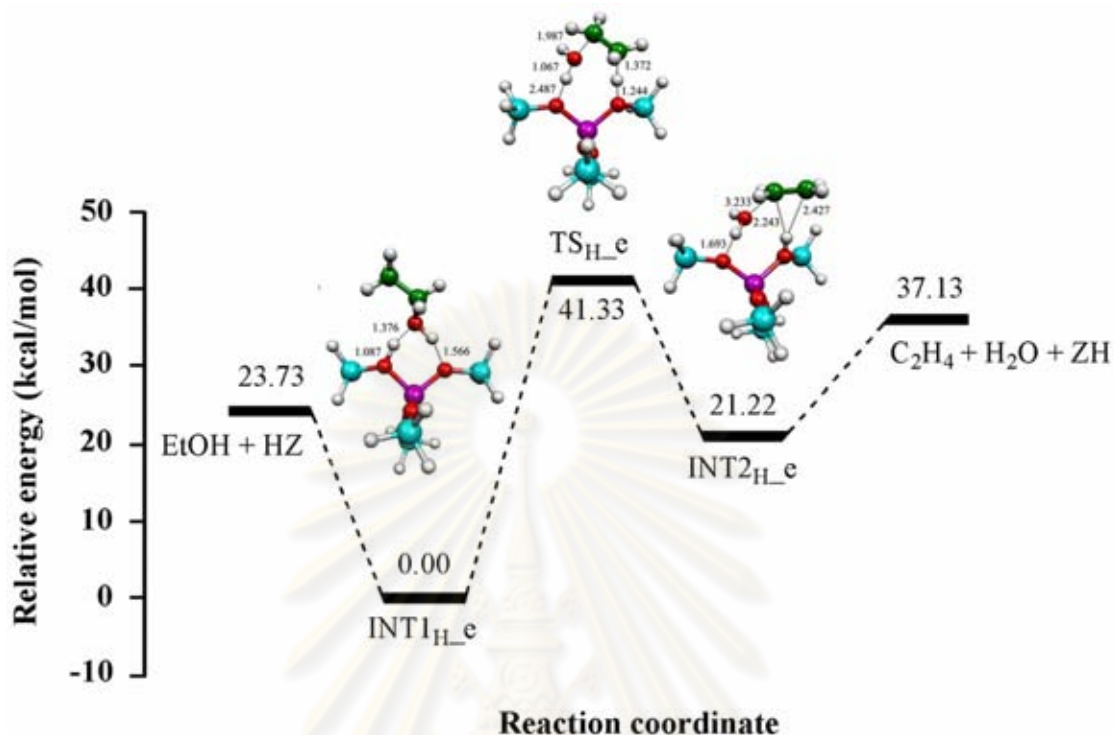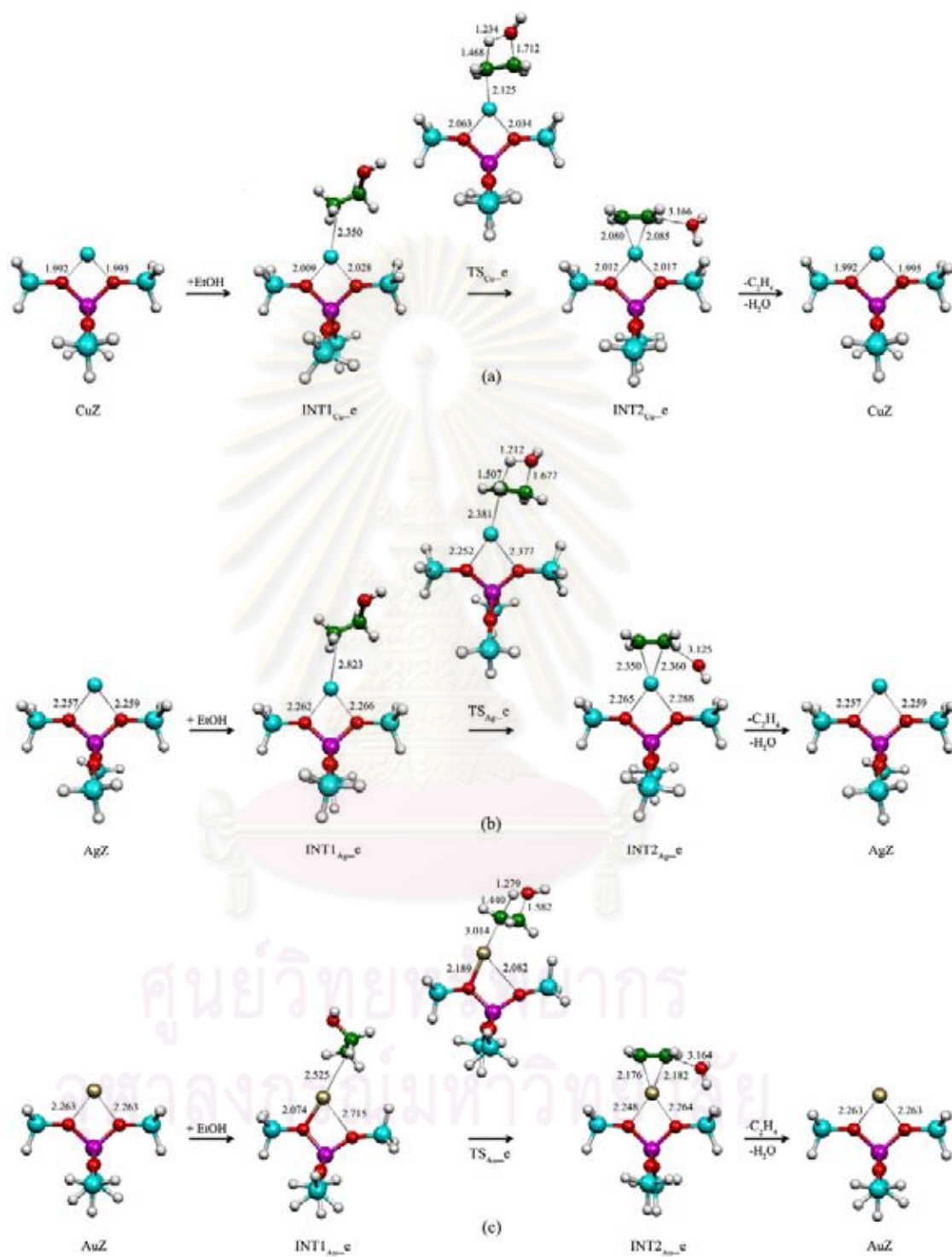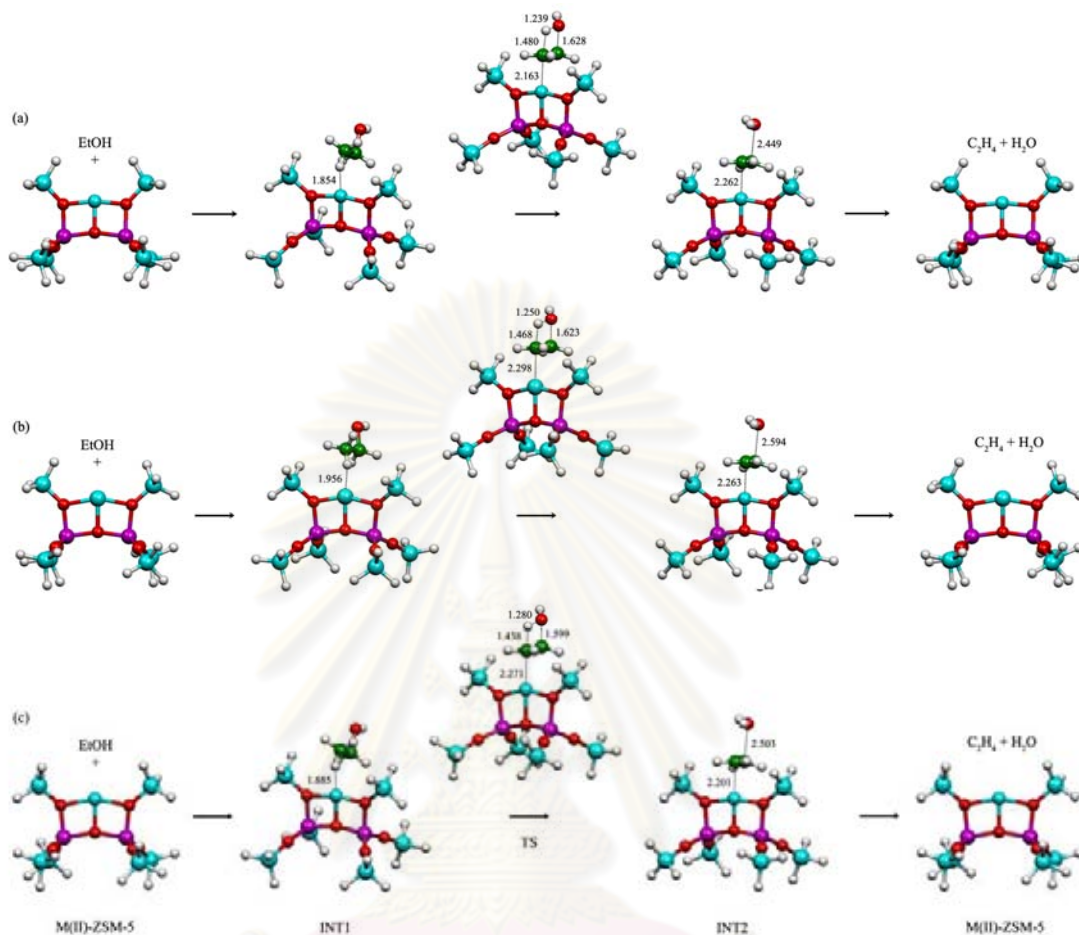
Figure 4.8 Reactions for the ethanol conversion to ethylene on (a) Ni–ZSM–5, (b) Pd–ZSM–5 and (c) Pt–ZSM–5 catalysts as 8T–cluster model. Bond distances are in Å.
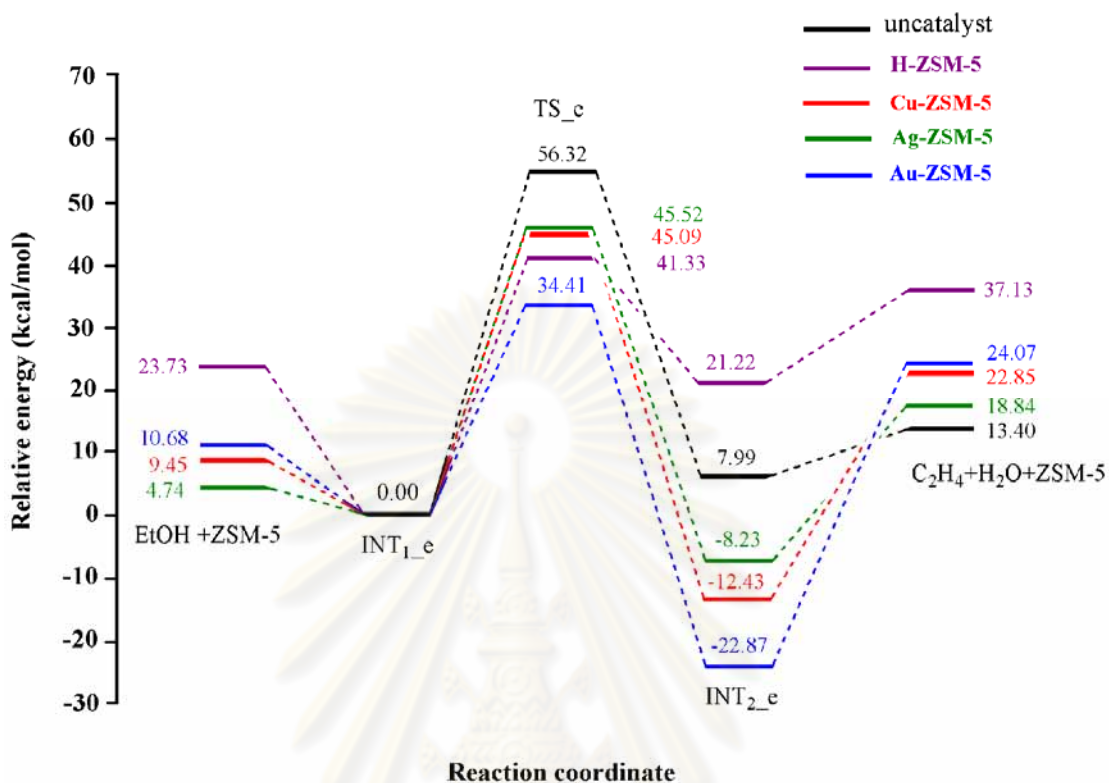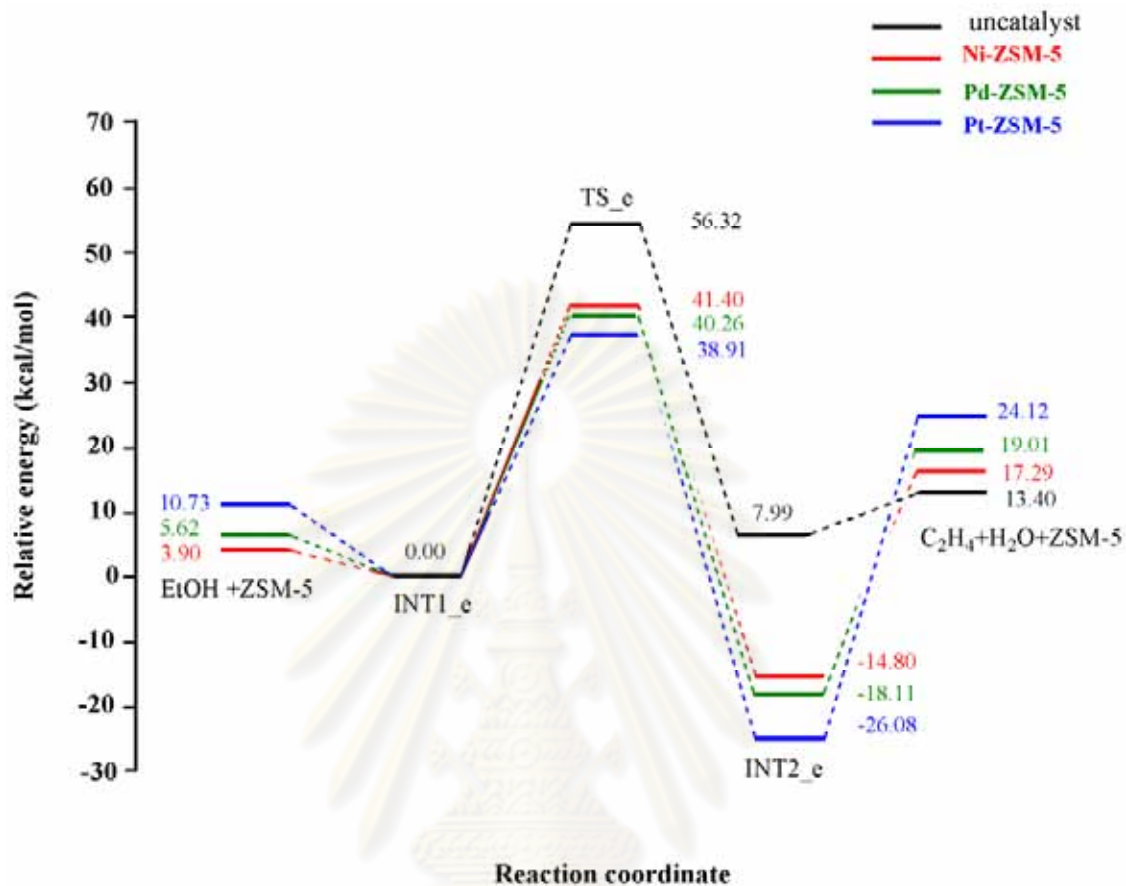
Figure 4.9 Potential energy profiles for the ethanol conversion to ethylene on the Ni–ZSM–5, Pd–ZSM–5 and Pt–ZSM–5 catalysts of 8T–cluster model compared to non–catalytic reaction.

Table 4.2 Energetics, thermodynamic properties, rate constants and equilibrium constants for conversion reactions of ethanol to ethylene by M(II)–ZSM–5 catalysts as strategic model II compared to non–catalytic system

Catalysts/Reactions [a]	$\Delta^{\ddagger}E$ [a,b]	$\Delta^{\ddagger}G$ [a,b]	k_{298} [c]	ΔE [a]	ΔH_{298} [a]	ΔG_{298} [a]	K_{298}
Non–catalytic :							
EtOH → TS_e → INT1	56.59	56.32	3.21×10^{-29}	12.28	14.28	7.99	1.39×10^{-6}
INT1 → C_2H_4 + H_2O	–	–	–	1.12	0.68	–3.22	2.29×10^{2}
Ni–ZSM–5:							
EtOH + NiZ → INT1$_{Ni}$_e	–	–	–	–3.90	–3.11	–6.62	1.39×10^{-5}
INT1$_{Ni}$_e → TS$_{Ni}$_e → INT2$_{Ni}$_e	41.40	42.22	6.98×10^{-19}	–14.80	–15.65	–10.93	1.03×10^{8}
INT2$_{Ni}$_e → NiZ + C_2H_4 + H_2O	–	–	–	32.09	33.71	9.07	2.24×10^{-7}
Pd–ZSM–5:							
EtOH + PdZ → INT1$_{Pd}$_e	–	–	–	–5.62	–5.83	–7.63	2.56×10^{-6}
INT1$_{Pd}$_e → TS$_{Pd}$_e → INT2$_{Pd}$_e	40.26	41.08	7.47×10^{-17}	–18.11	–16.83	–18.87	6.87×10^{13}
INT2$_{Pd}$_e → PdZ + C_2H_4 + H_2O	–	–	–	10.33	10.70	0.80	2.58×10^{-1}
Pt–ZSM–5:							
EtOH + PtZ → INT1$_{Pt}$_e	–	–	–	–10.73	–9.56	–0.15	1.28×10^{0}
INT1$_{Pt}$_e → TS$_{Pt}$_e → INT2$_{Pt}$_e	38.91	38.25	5.69×10^{-16}	–26.08	–26.25	–23.99	3.86×10^{17}
INT2$_{Pt}$_e → PtZ + C_2H_4 + H_2O	–	–	–	50.20	50.77	28.90	6.51×10^{-22}

[a] For 8T cluster models of ZSM–5, computed at B3LYP/LanL2DZ level of theory.
[b] Activation state.
[c] In s^{-1}.

The first steps are the adsorption of ethanol on catalysts which are the spontaneous reaction. The second step (RDS) of the reaction catalyzed by M(II)–ZSM–5 catalysts, the activation energy of these steps via TS$_{Ni}$_e, TS$_{Pd}$_e and TS$_{Pt}$_e are 41.40, 40.26 and 38.9 kcal/mol, respectively. It was found that activation energy of ethanol conversion of to ethylene were obviously reduced by the Ni^{2+}, Pd^{2+} and Pt^{2+} metal–ion– exchanged H–ZSM–5 catalyst rather than non–catalytic system. Reaction rates for conversion of ethanol to ethylene on different catalysts are in order: Pt–ZSM–5 (5.69×10^{-16} s^{-1}) > Pd–ZSM–5 (7.47×10^{-17} s^{-1}) > Ni–ZSM–5 (6.98×10^{-19} s^{-1}). Magnitudes of equilibrium constants of the ethanol conversion to ethylene are in order: Pt–ZSM–5 (3.86×10^{17}) > Pd–ZSM–5 (6.87×10^{13}) > Ni–ZSM–5 (1.03×10^{8}). The third steps for the

reactions either catalyzed by Ni–ZSM–5 or Pd–ZSM–5 or Pt–ZSM–5 are the endothermic reaction.

4.2.5 The comparison of efficiencies of catalysts on the ethanol conversion to ethylene

Due to the catalytic efficiencies of the H–ZSM–5 and M–ZSM–5–type catalysts for the ethanol conversion to ethylene, rate constants in terms of –log k of the reactions catalyzed by ZSM–5–type catalysts plotted against cationic sizes are shown in Figure 4.10.
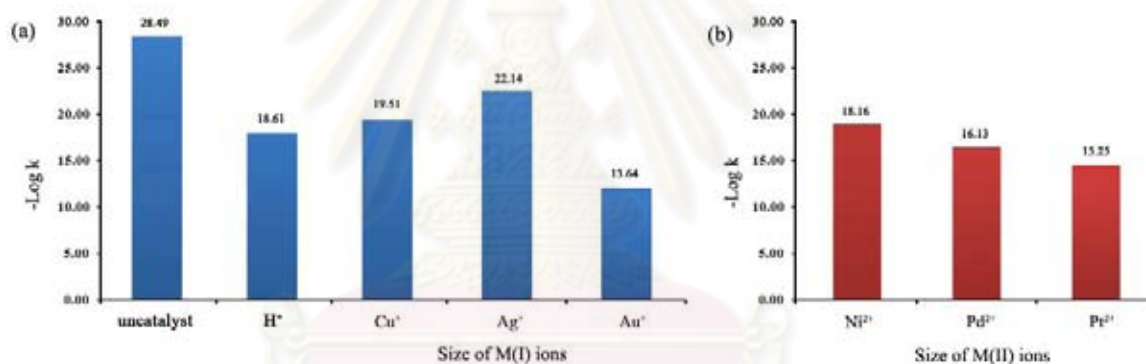
Figure 4.10 Plots of –log k against cationic size of (a) H–ZSM–5 and M(I)–ZSM–5 and (b) M(II)–ZSM–5 catalysts as 5T and 8T–cluster models.

The Au–ZSM–5 and Pt–ZSM–5 catalysts are found to be the most efficient catalyst for the monovalent and divalent metal ions, respectively. The catalytic efficiencies of the M(I)–ZSM–5–type catalysts of the reaction are in unexpected order as mentioned above. The novel metal–ion–exchanged ZSM–5 such as Ag–ZSM–5 is expected to be more efficient than the Cu–ZSM–5.

4.3 Reaction mechanism of ethanol conversion to ethylene over the 28T/ZSM–5–type catalyst

4.3.1 Ethanol conversion to ethylene catalyzed by H–ZSM–5–type catalyst

The potential energy profile for the ethanol conversion to ethylene on the the H–ZSM–5 catalyst is shown in Figure 4.11. The energetics, thermodynamic properties, rate constant and equilibrium constant for the conversion of ethanol to ethylene on the H–ZSM–5 catalyst are shown in Table 4.3. All parameters for calculations of the rate constant of the reaction catalyzed by H–ZSM–5–type catalysts are listed in Table A–5. The transition–states TS(H), for the ethanol conversion to ethylene in the H–ZSM–5 catalytic systems were approved by the intrinsic reaction coordinate (IRC) curves as shown in Figure A–6.

Figure 4.11 Potential energy profile for the ethanol conversion to ethylene on the H–ZSM–5 catalyst as 28T–cluster model.

Table 4.3 Energetics, thermodynamic properties, rate constants and equilibrium constants for conversion reactions of ethanol to ethylene as strategic model III by H–ZSM–5 and M(I)–ZSM–5 catalysts compared to non–catalytic system

Catalysts/Reactions [a]	$\Delta^{\ddagger}E$ [a,b]	$\Delta^{\ddagger}G$ [a,b]	k_{298} [c]	ΔE [a]	ΔH_{298} [a]	ΔG_{298} [a]	K_{298}
Non–catalytic :							
EtOH → TS_e → INT1	56.59	56.32	3.21×10^{-29}	12.28	14.28	7.99	1.39×10^{-6}
INT1 → C_2H_4 + H_2O	–	–	–	1.12	0.68	–3.22	2.29×10^{2}
H–ZSM–5:							
EtOH + HZ → INT(H)	–	–	–	–7.98	–7.61	3.73	1.84×10^{-3}
INT(H) → TS(H) → INT(H)'	42.69	43.86	4.36×10^{-20}	2.28	3.11	1.93	3.82×10^{-2}
INT(H)'→ ZH + C_2H_4 + H_2O	–	–	–	19.09	19.46	–0.90	4.57×10^{0}
Cu–ZSM–5:							
EtOH + CuZ→ INT(Cu)	–	–	–	–34.92	–34.19	–24.97	2.01×10^{18}
INT(Cu) → TS(Cu) → INT(Cu)'	52.33	52.75	1.33×10^{-26}	–4.73	–4.34	–4.26	1.34×10^{3}
INT(Cu)'→ CuZ+ C_2H_4 + H_2O	–	–	–	53.04	53.49	34.00	1.20×10^{-25}
Ag–ZSM–5:							
EtOH + AgZ → INT(Ag)	–	–	–	–0.72	–0.51	11.14	6.68×10^{-9}
INT(Ag) → TS(Ag) → INT(Ag)'	40.45	40.51	1.25×10^{-17}	–1.73	–2.28	–0.54	2.50×10^{0}
INT(Ag)'→ AgZ+ C_2H_4 + H_2O	–	–	–	15.85	17.76	–5.86	1.98×10^{4}
Au–ZSM–5:							
EtOH + AuZ → INT(Au)	–	–	–	–6.08	–6.27	–6.55	1.59×10^{-5}
INT(Au) → TS(Au) → INT(Au)'	34.57	36.29	1.56×10^{-14}	–29.71	–28.75	–30.81	3.85×10^{22}
INT(Au)'→ AuZ+ C_2H_4 + H_2O	–	–	–	49.18	49.98	29.03	5.27×10^{-22}

[a] Computed at B3LYP/LanL2DZ level of theory.
[b] Activation state.
[c] In s^{-1}.

The process of ethanol conversion of to ethylene over 28T cluster models as H–ZSM–5 and M–ZSM–5 catalysts is similar to the conversion of ethanol to ethylene discussed above. The second step (RDS) is conversion of reactant intermediate to product intermediate via transition state TS_{H}_e and the rate constant of 4.36×10^{-20} s^{-1} was obtained. The activation energy for this transition state is 42.69 kcal/mol. The last step is the isolation of product intermediate to obtain the final product and the endothermic reaction.

4.3.2 Ethanol conversion to ethylene catalyzed by M(I)–ZSM–5–type catalyst

Reactions for the ethanol conversion to ethylene on the Cu–ZSM–5, Ag–ZSM–5 and Au–ZSM–5 catalysts are shown in Figure 4.12. The potential energy profiles for the ethanol conversion to ethylene on M(I)–ZSM–5−type catalysts are shown in Figure 4.13. The energetics, thermodynamic properties, rate constant and equilibrium constant for the conversion of ethanol to ethylene on the M(I)–ZSM–5–type catalysts are shown in Table 4.3. All parameters for calculations of the rate constant of the reaction catalyzed by M(I)–ZSM–5–type catalysts are listed in Table A–5. The transition–states of the reaction on the M(I)–ZSM–5 catalytic systems were approved by the intrinsic reaction coordinate (IRC) curves as shown in Figures A–7, A–8 and A–9, respectively.
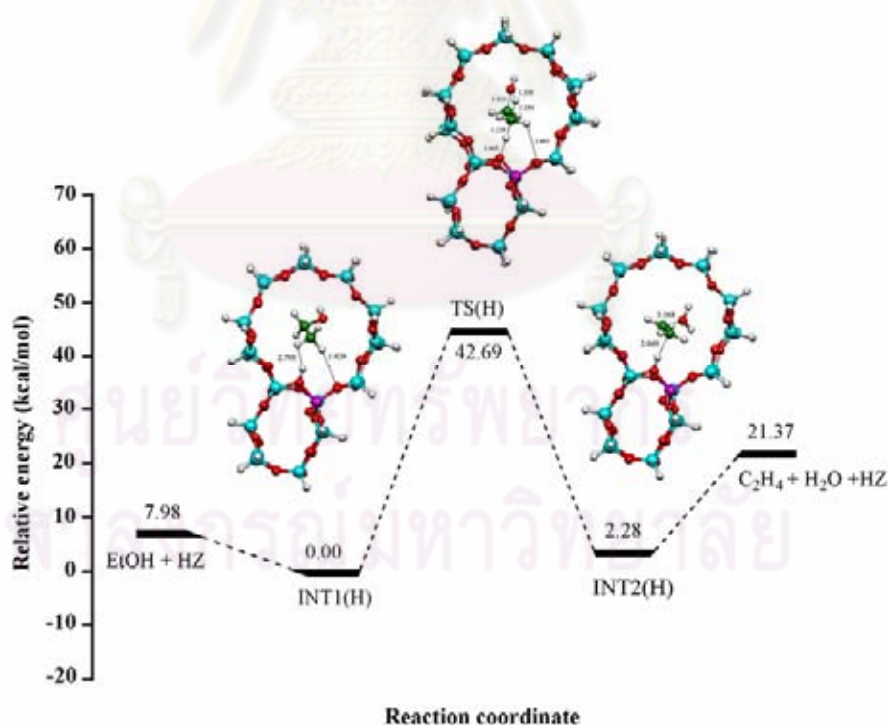
Figure 4.12 Reactions for the ethanol conversion to ethylene on (a) Cu–ZSM–5, (b) Ag– ZSM–5 and (c) Au–ZSM–5 catalysts as 28T–cluster model. Bond distances are in Å.

Figure 4.13 Potential energy profiles for the ethanol conversion to ethylene on the H–ZSM–5, Cu–ZSM–5, Ag–ZSM–5 and Au–ZSM–5 catalysts of 28T–cluster model compared to non–catalytic reaction.

The reaction steps for the conversion of ethanol to ethylene over the 28T–M(I)–ZSM–5–type catalysts are composed of three step namely the adsorption, conversion and desorption steps. The first step is the adsorption of ethanol in the cavity of Cu–ZSM–5, Ag–ZSM–5 and Au–ZSM–5 catalysts. At the transition state due to the RDS step, activation energies for the conversion of ethanol to ethylene on the Cu–ZSM–5, Ag–ZSM–5 and Au–ZSM–5 catalysts are 52.33, 40.45 and 34.57 kcal/mol, respectively. Rate constants for conversion of ethanol to ethylene on different M(I)–ZSM–5 catalysts are in order: Au–ZSM–5 ($1.56 \times 10^{-14}\,\mathrm{s}^{-1}$) > Ag–ZSM–5 ($1.25 \times 10^{-17}\,\mathrm{s}^{-1}$) > Cu–ZSM–5 ($1.33 \times 10^{-26}\,\mathrm{s}^{-1}$). Magnitudes of equilibrium constants of the ethanol conversion to ethylene are in order: Au–ZSM–5 (3.85×10^{22}) > Cu–ZSM–5 (1.34×10^{3}) > Ag–ZSM–5

(2.50 x 10^0). The third steps for the reactions either catalyzed by Cu–ZSM–5 or Ag–ZSM–5 or Au–ZSM–5 are the endothermic reaction.

4.3.3 Ethanol conversion to ethylene catalyzed by M(II)–ZSM–5–type catalyst

The reaction steps for the conversion of ethanol to ethylene over 28T–cluster–modeled on the Ni–ZSM–5, Pd–ZSM–5 and Pt–ZSM–5 catalysts are shown in Figure 4.14. The potential energy profiles for the ethanol conversion to ethylene on the Ni–ZSM–5, Pd–ZSM–5 and Pt–ZSM–5 are shown in Figure 4.15. The energetics, thermodynamic properties, rate constant and equilibrium constant for conversion reactions of ethanol to ethylene on the M(II)–ZSM–5 are shown in Table 4.4. All parameters for calculations of the rate constant of the reaction catalyzed by M(II)–ZSM–5–type catalysts are listed in Table A–10. The transition–states for the ethanol conversion to ethylene in the Ni–ZSM–5, Pd–ZSM–5 and Pt–ZSM–5 catalytic systems were approved by the intrinsic reaction coordinate (IRC) curves as shown in Figures A–11, A–12 and A–13, respectively.
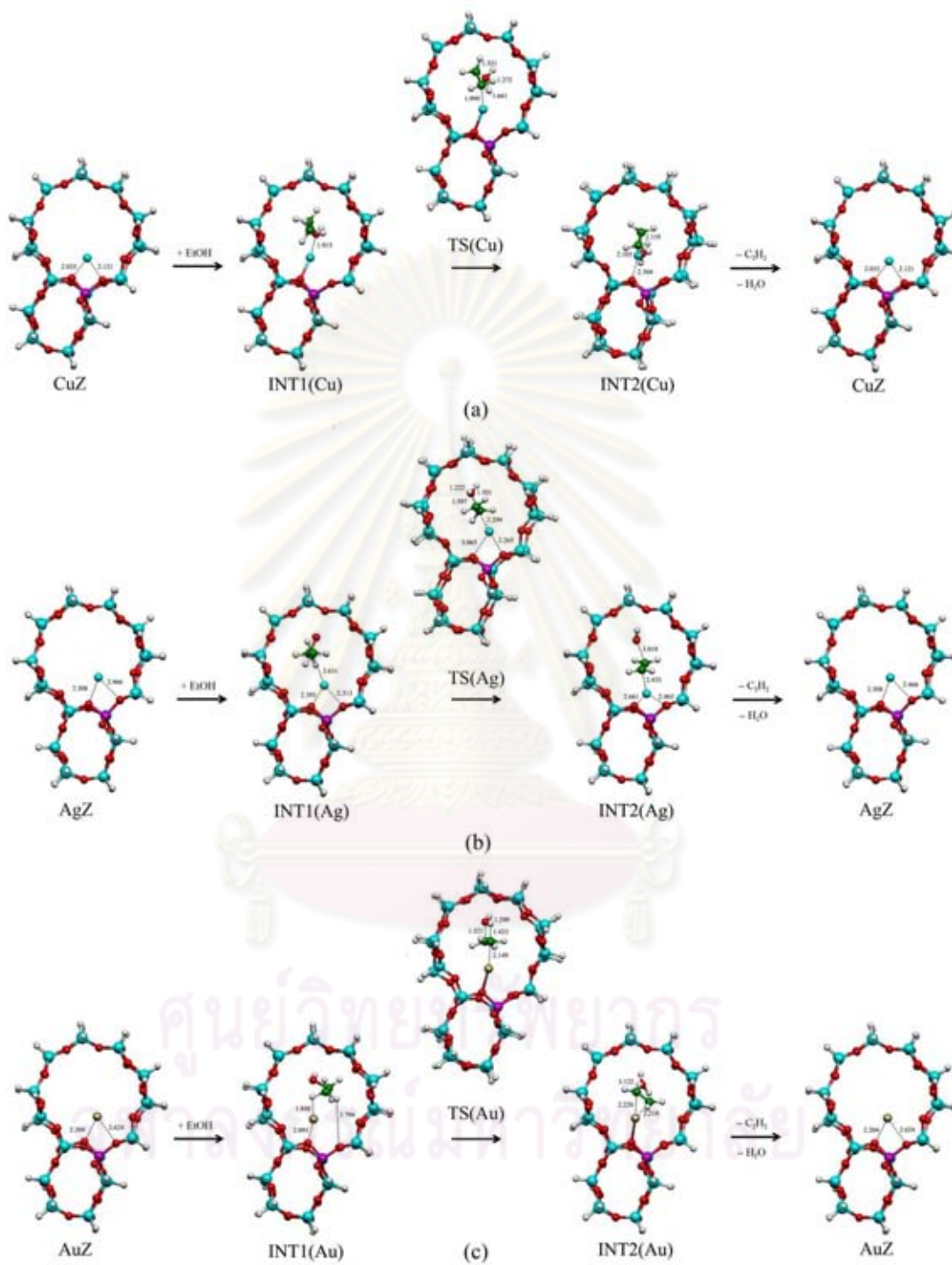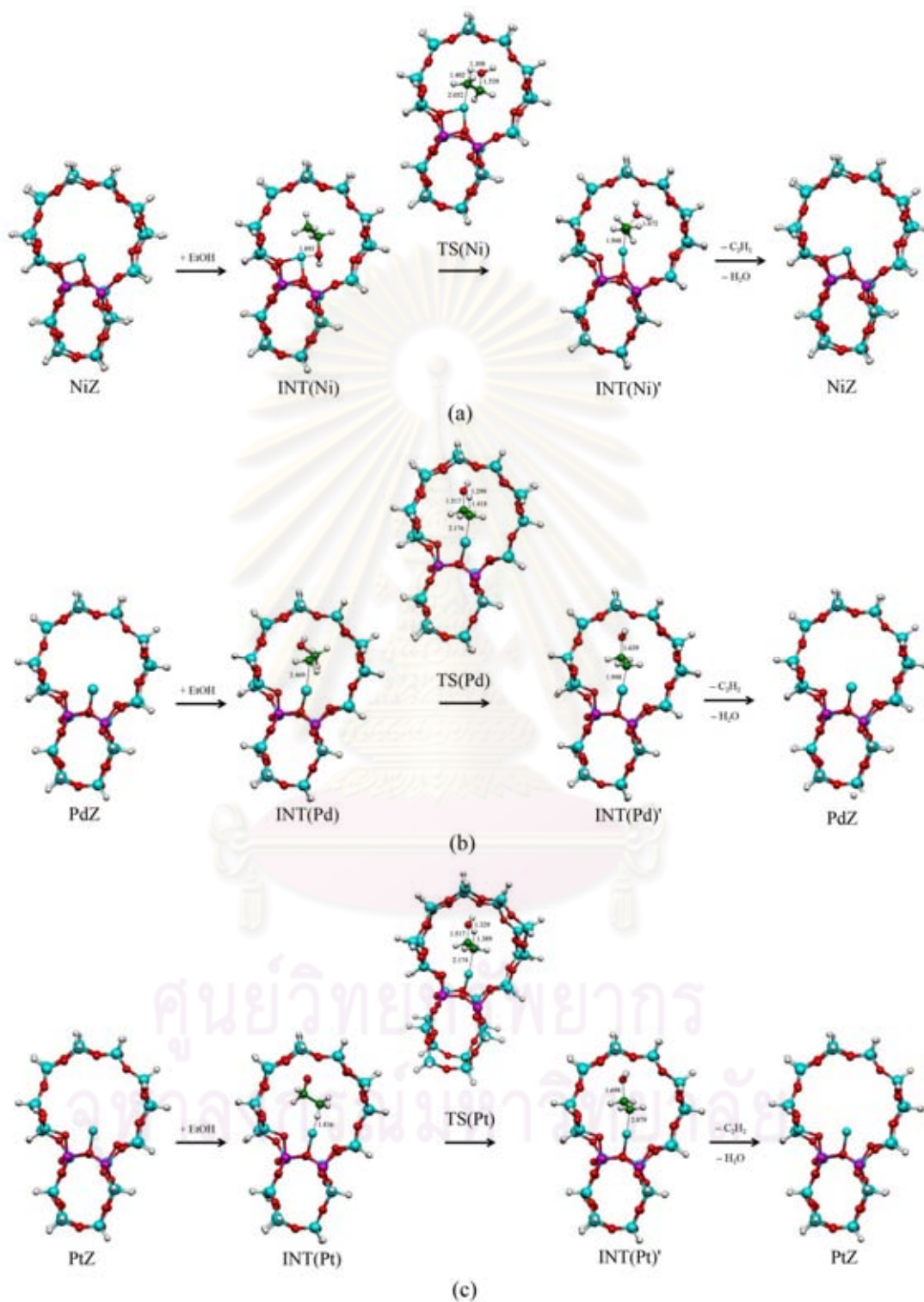
Figure 4.14 Reactions for the ethanol conversion to ethylene on (a) Ni–ZSM–5, (b) Pd–ZSM–5 and (c) Pt–ZSM–5 catalysts as 28T–cluster model. Bond distances are in Å.
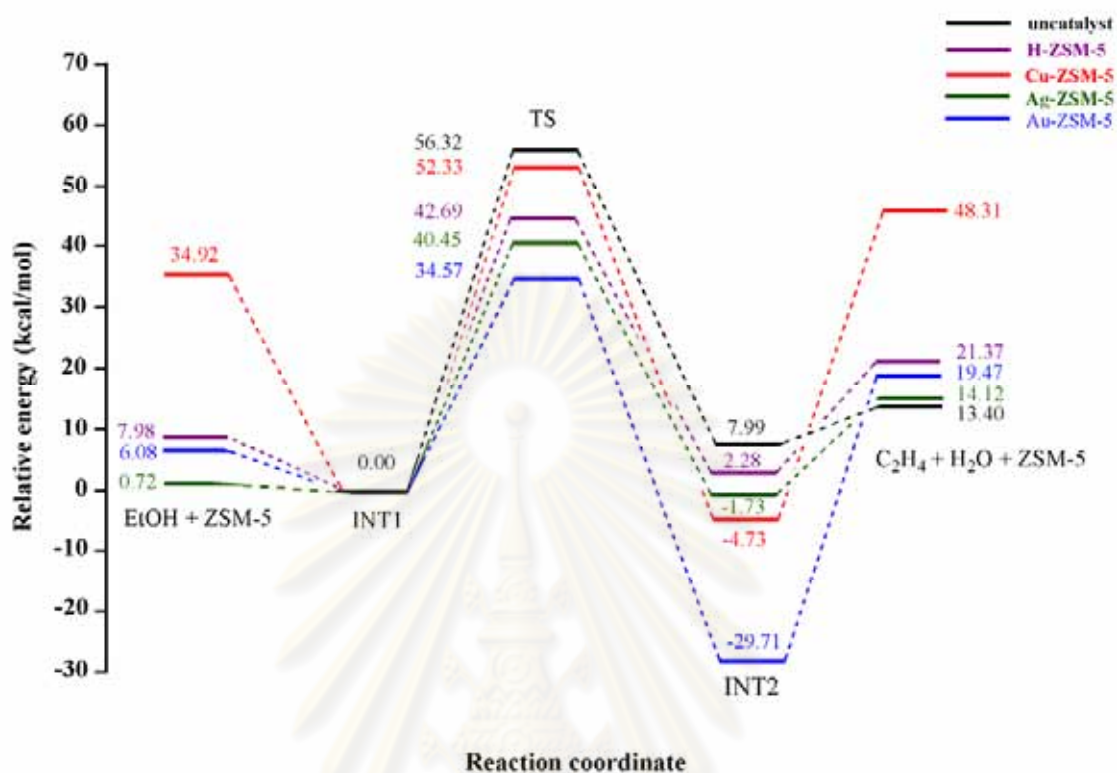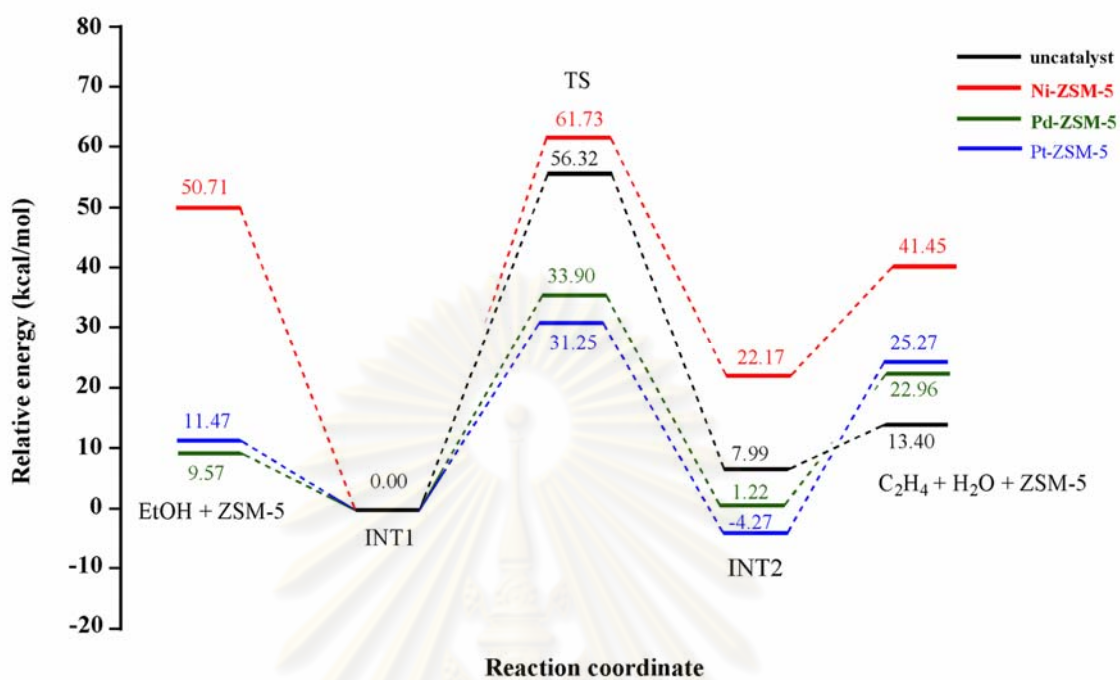
Figure 4.15 Potential energy profiles for ethanol conversion to ethylene on the Ni–ZSM–5, Pd–ZSM–5 and Pt–ZSM–5 catalysts of 28T–cluster model compared to non–catalytic reaction.

Table 4.4 Energetics, thermodynamic properties, rate constants and equilibrium constants for conversion reactions of ethanol to ethylene as strategic model IV by M(II)–ZSM–5 catalysts, compared to non–catalytic system

Catalysts/Reactions [a]	$\Delta^{\ddagger}E$ [a,b]	$\Delta^{\ddagger}G$ [a,b]	k_{298} [c]	ΔE [a]	ΔH_{298} [a]	ΔG_{298} [a]	K_{298}
Non–catalytic :							
EtOH → TS_e → INT1	56.59	56.32	3.21×10^{-29}	12.28	14.28	7.99	1.39×10^{-6}
INT1 → C_2H_4 + H_2O	–	–	–	1.12	0.68	–3.22	2.29×10^{2}
Ni–ZSM–5:							
EtOH + NiZ → INT(Ni)	–	–	–	–50.71	–51.30	–36.68	7.79×10^{26}
INT(Ni) → TS(Ni) → INT(Ni)'	61.73	61.71	3.59×10^{-33}	27.17	27.38	26.99	1.62×10^{-20}
INT(Ni)'→ NiZ+ C_2H_4 + H_2O	–	–	–	36.94	38.88	14.45	2.45×10^{-11}
Pd–ZSM–5:							
EtOH +PdZ → INT(Pd)	–	–	–	–9.57	–9.56	2.45	1.61×10^{-2}
INT(Pd) → TS(Pd) → INT(Pd)'	33.90	35.47	6.16×10^{-14}	1.22	0.70	2.83	8.47×10^{-3}
INT(Pd)'→ PdZ+ C_2H_4 + H_2O	–	–	–	21.74	23.83	–0.51	2.36×10^{0}
Pt–ZSM–5:							
EtOH +PtZ → INT(Pt)	–	–	–	–11.88	–12.26	1.47	8.42×10^{-2}
INT(Pt) → TS(Pt) → INT(Pt)'	31.25	31.39	5.11×10^{-11}	–4.27	–4.78	–3.28	2.55×10^{2}
INT(Pt)'→ PtZ+ C_2H_4 + H_2O	–	–	–	29.55	32.00	6.58	1.50×10^{-5}

[a] Computed at B3LYP/LanL2DZ level of theory.
[b] Activation state.
[c] In s^{-1}.

The adsorption step, ethanol molecule diffuses into the cavity of Ni–ZSM–5, Pd–ZSM–5 and Pt–ZSM–5 catalysts. The second step (RDS) of the reaction, the activation energies for the conversion of ethanol to ethylene on the Ni–ZSM–5, Pd–ZSM–5 and Pt–ZSM–5 catalysts are 61.73, 33.90 and 31.25 kcal/mol, respectively. Rate constants for conversion of ethanol to ethylene on different catalysts are in order: Pt–ZSM–5 (5.11×10^{-11} s^{-1}) > Pd–ZSM–5 (6.16×10^{-14} s^{-1}) > Ni–ZSM–5 (3.59×10^{-33} s^{-1}). Magnitudes of equilibrium constants of the ethanol conversion to ethylene are in order: Pt–ZSM–5 (2.55×10^{2}) > Pd–ZSM–5 (8.47×10^{-3}) > Ni–ZSM–5 (1.62×10^{-20}). The third steps for the reactions either catalyzed by Ni–ZSM–5 or Pd–ZSM–5 or Pt–ZSM–5 are the endothermic reaction.

4.3.4 The comparison of efficiencies of catalysts on the ethanol conversion to ethylene

Due to the catalytic efficiencies of the H–ZSM–5 and M–ZSM–5–type catalysts for ethanol conversion to ethylene, the rate constants in terms of –log k of the reactions catalyzed by ZSM–5–type catalysts plotted against cationic sizes of the catalysts are shown in Figure 4.16. The Au–ZSM–5 and Pt–ZSM–5 catalysts modeled as 28T cluster are found to be the most efficient catalyst for the monovalent and divalent metal ions, respectively. However, the different orders of rate constant due to the strategic models I and III should be affected by the different cluster model of the M(I)–ZSM–5ctype catalysts namely cavity effect of the strategic model I has not been included in 8T–cluster model.
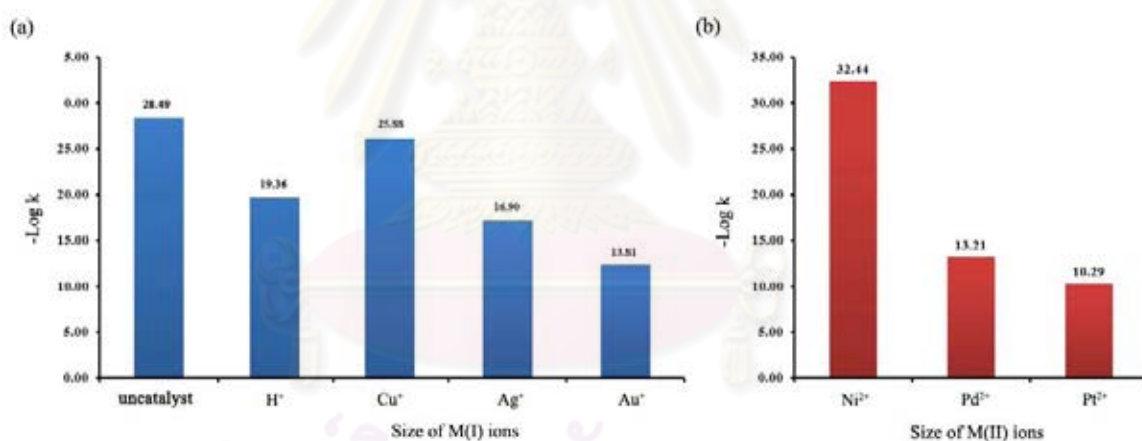
Figure 4.16 Plots of –log k against cationic size of (a) H–ZSM–5 and M(I)–ZSM–5 and (b) M(II)–ZSM–5 catalysts as 28T–cluster model.

As the 28T–cluster model which includes 10T–ring as cavity of the ZSM–5. The DFT–calculations of the 28T–cluster representing for the M–ZSM–5–type catalysts are therefore more accurate than the 8T–cluster model at the same level of the theory. In case of use of Ni–ZSM–5 in the conversion of the ethanol to ethylene, the rate constant computed using the 8T–cluster model of Ni–ZSM–5 is more different value as compared

with the rate constant computed using the 28T–cluster model. The different values of the rate constants of the reaction obtained from different cluster sizes because the transition–state of its rate–determining step obtained in the 28T–Ni–ZSM–5 cluster model is restricted as the shape and size selectivities.

4.4 Reaction mechanism of ethanol conversion to butene

4.4.1 Ethanol conversion to 1–butene in non–catalytic system

The potential energy profile of the conversion of ethanol to 1–butene is shown in Figure 4.17. The energetics, thermodynamic properties, rate constant and equilibrium constant for the reaction calculated at the B3LYP/LanL2DZ level are listed in Table 4.5.

Figure 4.17 Potential energy profile of ethanol and ethylene conversion reaction pathway in non–catalytic system. Bond distances are in Å.

Table 4.5 Energetics, thermodynamic properties, rate constants and equilibrium constants for conversion reactions of ethylene to 1–butene by H–ZSM–5 and M(I)–ZSM–5 catalysts compared to non–catalytic system

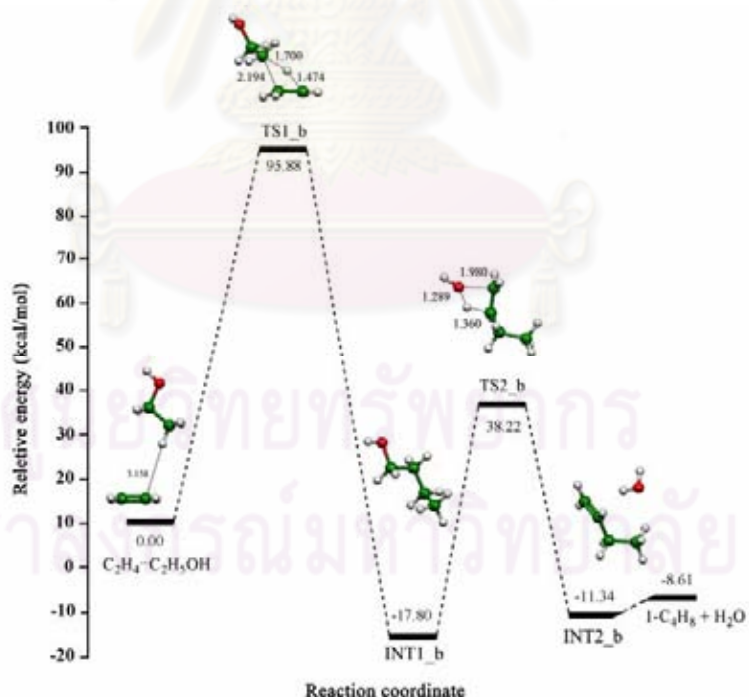| Catalysts/Reactions [a]	$\Delta^{\ddagger}E$ [a,b]	$\Delta^{\ddagger}G$ [a,b]	k_{298} [c]	ΔE [a]	ΔH_{298} [a]	ΔG_{298} [a]	K_{298}
Non–catalytic:							
$C_2H_4 + C_2H_5OH \rightarrow TS1\_b \rightarrow INT1\_b$	95.88	102.37	5.63×10^{-63}	–17.80	–19.68	–10.37	4.02×10^{7}
$INT1\_b \rightarrow TS2\_b \rightarrow INT2\_b$	56.02	55.95	6.01×10^{-29}	6.47	7.82	4.20	8.37×10^{-4}
$INT2\_b \rightarrow 1–C_4H_8 + H_2O$	–	–	–	2.72	2.76	–4.39	1.65×10^{3}
H–ZSM–5							
$C_2H_4 \cdots ZH \rightarrow TS1_H\_b \rightarrow INT1_H\_b$	40.07	42.16	7.71×10^{-19}	–8.11	–9.17	–6.12	3.08×10^{4}
$INT1_H\_b + C_2H_5OH \rightarrow INT2_H\_b$	–	–	–	–0.20	0.62	8.22	9.49×10^{-7}
$INT2_H\_b \rightarrow TS2_H\_b \rightarrow INT3_H\_b$	55.17	59.20	2.50×10^{-31}	–27.88	–28.95	–26.38	2.16×10^{19}
$INT3_H\_b \rightarrow TS3_H\_b \rightarrow INT4_H\_b$	41.47	43.21	1.03×10^{-19}	16.79	17.55	17.24	2.32×10^{-13}
$INT4_H\_b \rightarrow 1–C_4H_8 + H_2O + HZ$	–	–	–	16.66	16.41	–2.48	6.53×10^{1}
Cu–ZSM–5							
$C_2H_4 \cdots CuZ + C_2H_5OH \rightarrow INT1_{Cu}\_b$	–	–	–	0.25	0.69	7.48	3.30×10^{-6}
$INT1_{Cu}\_b \rightarrow TS1_{Cu}\_b \rightarrow INT2_{Cu}\_b$	91.43	92.33	1.28×10^{-55}	2.78	1.90	5.94	4.41×10^{-5}
$INT2_{Cu}\_b \rightarrow TS2_{Cu}\_b \rightarrow INT3_{Cu}\_b$	56.00	53.29	5.37×10^{-27}	6.25	8.54	1.81	4.72×10^{-2}
$INT3_{Cu}\_b \rightarrow CuZ + 1–C_4H_8 + H_2O$	–	–	–	14.02	12.98	–1.91	2.50×10^{1}
Ag–ZSM–5							
$C_2H_4 \cdots AgZ + C_2H_5OH \rightarrow INT1_{Ag}\_b$	–	–	–	0.15	0.69	5.20	1.55×10^{-4}
$INT1_{Ag}\_b \rightarrow TS1_{Ag}\_b \rightarrow INT2_{Ag}\_b$	81.77	87.16	7.90×10^{-52}	–3.49	–4.04	0.04	9.28×10^{-1}
$INT2_{Ag}\_b \rightarrow TS2_{Ag}\_b \rightarrow INT3_{Ag}\_b$	56.04	56.22	3.82×10^{-29}	–10.49	–9.74	–10.83	8.73×10^{7}
$INT3_{Ag}\_b \rightarrow AgZ + 1–C_4H_8 + H_2O$	–	–	–	26.31	26.08	9.14	2.00×10^{-7}
Au–ZSM–5							
$C_2H_4 \cdots AuZ + C_2H_5OH \rightarrow INT1_{Au}\_b$	–	–	–	0.33	1.30	6.04	3.74×10^{-5}
$INT1_{Au}\_b \rightarrow TS1_{Au}\_b \rightarrow INT2_{Au}\_b$	76.83	83.41	4.41×10^{-49}	13.56	12.78	17.38	1.82×10^{-13}
$INT2_{Au}\_b \rightarrow TS2_{Au}\_b \rightarrow INT3_{Au}\_b$	54.94	55.95	6.01×10^{-29}	6.64	8.43	3.67	2.05×10^{-3}
$INT3_{Au}\_b \rightarrow AuZ + 1–C_4H_8 + H_2O$	–	–	–	13.60	12.28	–1.16	7.04×10^{0}

[a] Computed the B3LYP/LanL2DZ level of theory.
[b] Activation state.
[c] In s^{-1}.

The conversions of ethanol to 1–butene are composed of three reaction steps. The first step (RDS) is an association of ethanol and ethylene to afford 1–butanol via transition state TS1_b and the second step is a dehydration of 1–butanol to form 1–butene interacting with water molecule. The third step is an isolation of 1–butene and water

molecule. The first and the last steps are spontaneous processes. The activation energy of the first step is 95.88 kcal/mol and rate constant, $k = 5.63$ x 10^{-63} s^{-1}.

4.4.2 Ethanol conversion to 1–butene catalyzed by H–ZSM–5

The energy profiles for conversion ethanol to 1-butene are shown in Figure 4.18. The energetics, thermodynamic properties, rate constant and equilibrium constant for conversion reactions of the reaction are listed in Table 4.5. All parameters for calculations of the rate constant of the reaction catalyzed by H–ZSM–5–type catalyst are shown in Table A–14.

In the first step, ethylene weakly adsorbs onto the zeolite acid site via π–interaction. The weakly adsorbed ethylene can be protonated by the acidic proton. The protonated ethylene is transformed to a stabilized alkoxide intermediate (INT1$_{H}$_b) by forming a covalent bond to one of the bridging oxygen atoms. The calculated energy profile for ethoxidation step is shown in Figure 4.18 (a). At the transition state TS1$_{H}$_b due to RDS, the zeolite proton is moving toward a carbon atom of the ethylene while C–C double bond is elongated and the other carbon atom is moving toward the adjacent oxygen atom of the zeolite to form covalent bond. The activation energy for this step is 40.07 kcal/mol and rate constant is 7.71 x 10^{-19} s^{-1}.
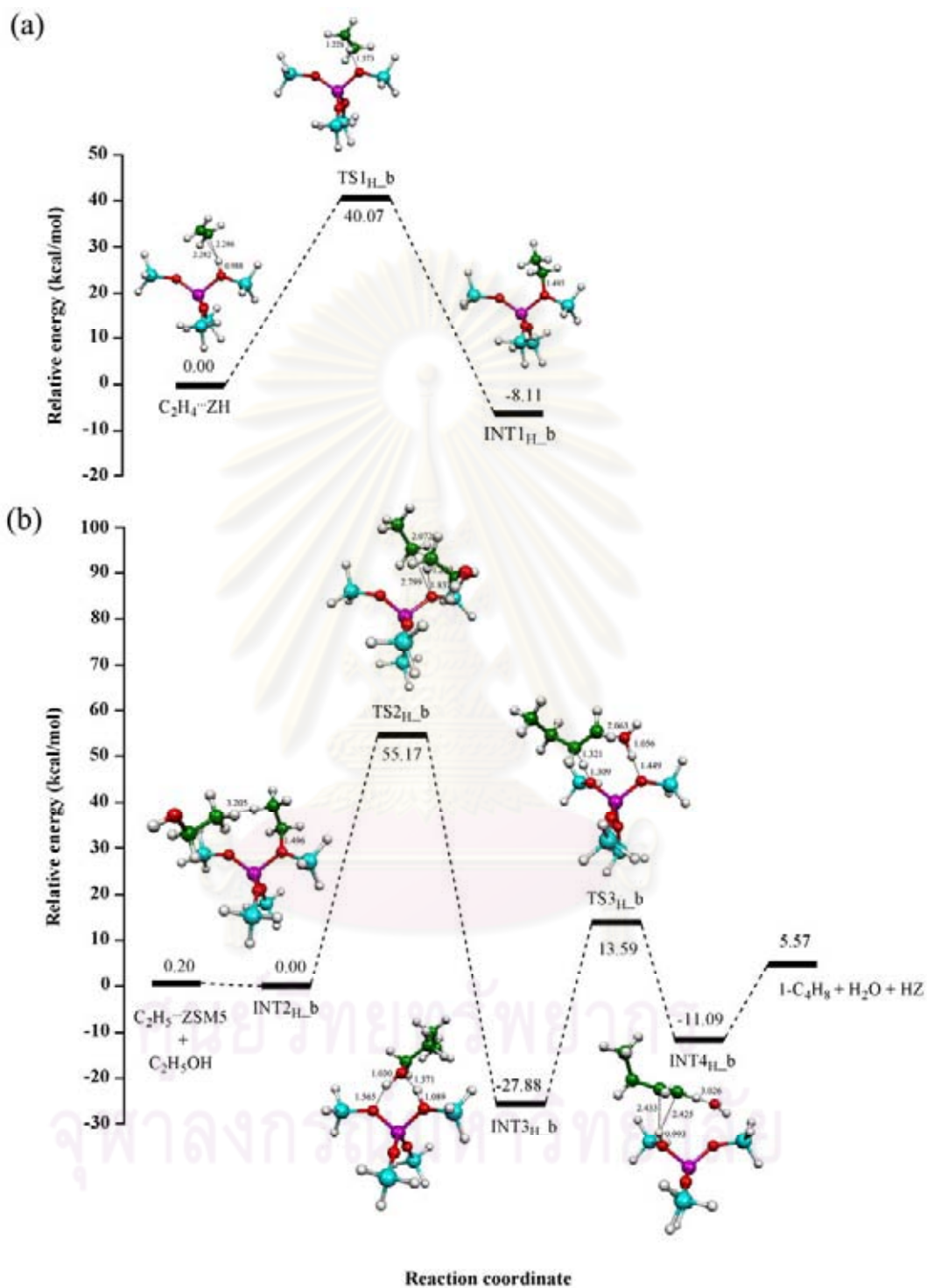
Figure 4.18 Potential energy profiles for (a) ethoxidation step and (b) associative ethanol ethylation pathway. Bond distances are in Å.

Subsequently, the surface ethoxide species acts as ethylating agent. It is assumed that an ethylene diffuses onto the zeolite pore and adsorbs on the reactive ethoxide intermediate to form ethylene–ethoxide adsorption complex (INT2$_{H}$_b), see Figure 4.18 (b). Next, the reaction proceeds via the transition state TS2$_{H}$_b that involves the concerted bond breaking between carbon atom of ethoxide and zeolite oxygen while the formation carbon atom of ethoxide and ethanol carbon atom is formed. The activation energy is 55.17 kcal/mol, and reaction rate is 2.50 x 10^{-31} s^{-1}.

The 1–butanol intermediate INT2$_{H}$_b produced for ethylation of ethanol is formed a strong hydrogen bond between the alcoholic oxygen atom of 1–butanol and OH group of zeolite. Here, its adsorption energy is –27.88 kcal/mol. The H–bond adsorption complex reacts to form 1–butene product via the transition state TS3$_{H}$_b as shown in Figure 4.18 (b). In this transition state, the dehydration of 1–butanol occurs which lead to the formation of a water molecule and 1–butene product. The activation energy for this transition state is 41.47 kcal/mol with rate constant of 1.03 x 10^{-19} s^{-1}.

4.4.3 Ethanol conversion to 1–butene catalyzed by M(I)–ZSM–5–type catalyst

Reactions for the ethanol conversion to 1–butene on the Cu–ZSM–5, Ag–ZSM–5 and Au–ZSM–5 catalysts are shown in Figure 4.19. The potential energy profiles of the reactions on M(I)–ZSM–5−type catalysts are shown in Figure 4.20. The energetics, thermodynamic properties, rate constant and equilibrium constant for the conversion of ethanol to ethylene on the M(I)–ZSM–5–type catalysts are shown in Table 4.5. All parameters for calculations of the rate constant of the reaction catalyzed by M(I)–ZSM–5–type catalysts are listed in Table A–14.

Figure 4.19 Reactions for the formation of 1–butene from ethylene adsorbed with ethanol over (a) Cu–ZSM–5, (b) Ag–ZSM–5 and (c) Au–ZSM–5 catalysts as 5T–cluster model. Bond distances are in Å.

Figure 4.19 continue.

ศูนย์วิทยทรัพยากร

จุฬาลงกรณ์มหาวิทยาลัย

Figure 4.20 Potential energy profiles for the formation of 1–butene from ethylene adsorbed with ethanol on Cu–ZSM–5, Ag–ZSM–5 and Au–ZSM–5 catalysts of 5T–cluster model compared to non–catalytic reaction.

The conversion of ethanol to 1–butene on M(I)– ZSM–5 are composed of four steps. The first step is adsorption of ethanol on the adsorbed ethylene at the acid site of the Cu–ZSM–5, Ag–ZSM–5 and Au–ZSM–5 catalysts. The second step (RDS), proton transfer from ethanol to adsorbed ethylene on the acid site and the C–C bond between the ethanol and ethylene via transition–state TS1Cu_b, TS1$_{Ag}$_b and TS1$_{Au}$_b are formed lead to 1–butanol. The activation energy of RDS via TS1$_{Cu}$_b, TS1$_{Ag}$_b and TS1$_{Au}$_b are

91.43, 81.77 and 76.83 kcal/mol, respectively. The rate constants for conversion of ethanol to 1-butene on different catalysts are in order: Au–ZSM–5 (4.41 x 10^{-49} s^{-1}) > Ag–ZSM–5 (7.90 x 10^{-52} s^{-1}) > Cu–ZSM–5 (1.23×10^{-55} s^{-1}). These values shown the co–adsorption of ethanol on the absorbed ethylene at the acid site should be significantly faster over Au–ZSM–5 than Ag–ZSM–5 and Cu–ZSM–5 catalysts. The third step is the dehydration of 1–butanol intermediate to form product intermediate via transition–state $TS2_{Cu}$_b, $TS2_{Ag}$_b and $TS2_{Au}$_b. The activation energy of this step is 56.00, 56.04 and 54.94 kcal/mol, respectively. The last step is endothermically an isolation of 1–butene and water molecule.

4.4.4 Ethanol conversion to 1–butene catalyzed by M(II)–Z SM–5–type catalyst

Reactions for the ethanol conversion to 1–butene on the Ni–ZSM–5, Pd–ZSM–5 and Pt–ZSM–5 catalysts are shown in Figure 4.21. The potential energy profiles of the reactions on M(I)–ZSM–5−type catalysts are shown in Figure 4.22. The energetics, thermodynamic properties, rate constant and equilibrium constant for the conversion of ethanol to ethylene on the M(II)–ZSM–5–type catalysts are shown in Table 4.6. All parameters for calculations of the rate constant of the reaction catalyzed by M(II)–ZSM–5–type catalysts are listed in Table A–15.
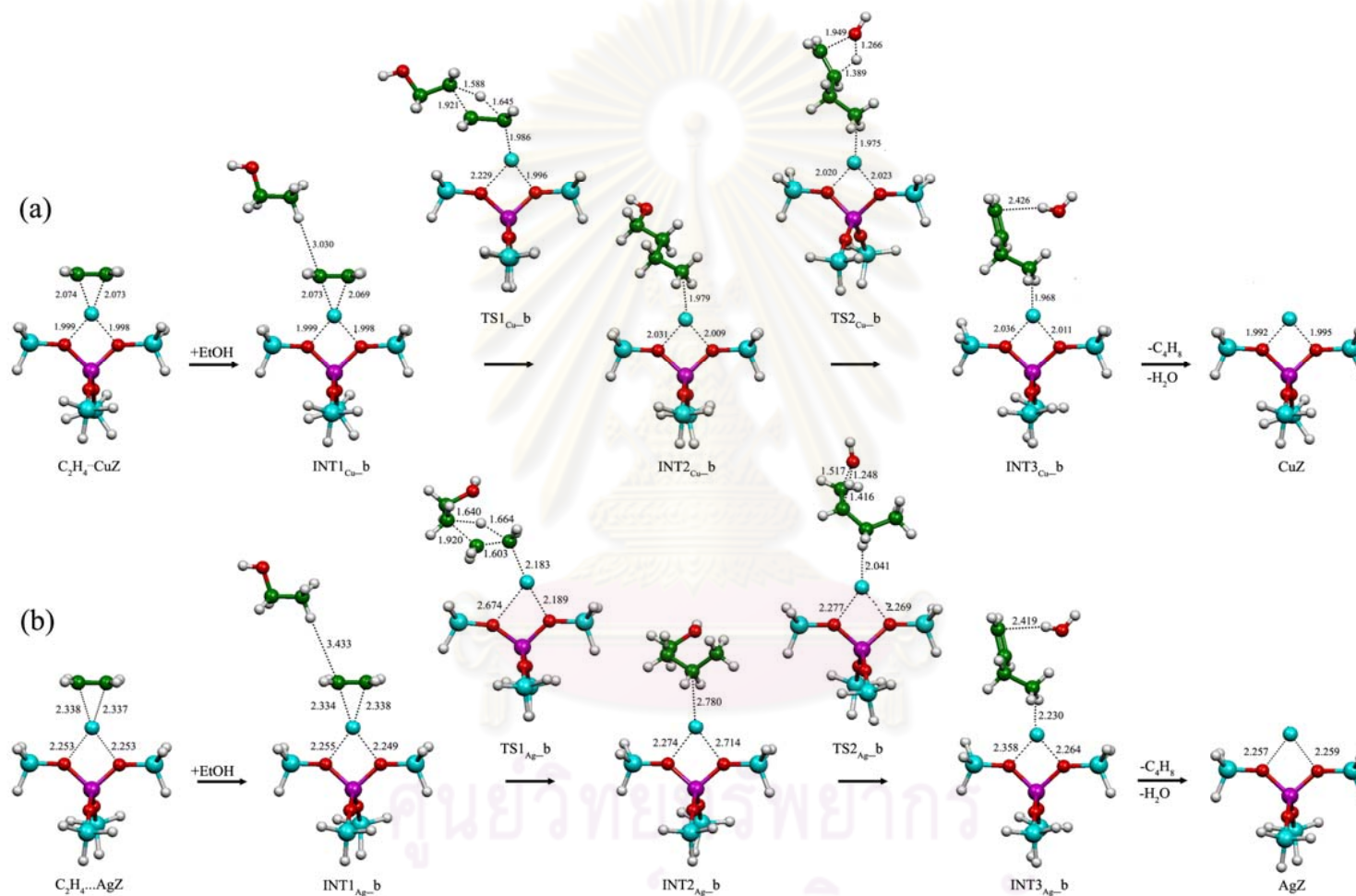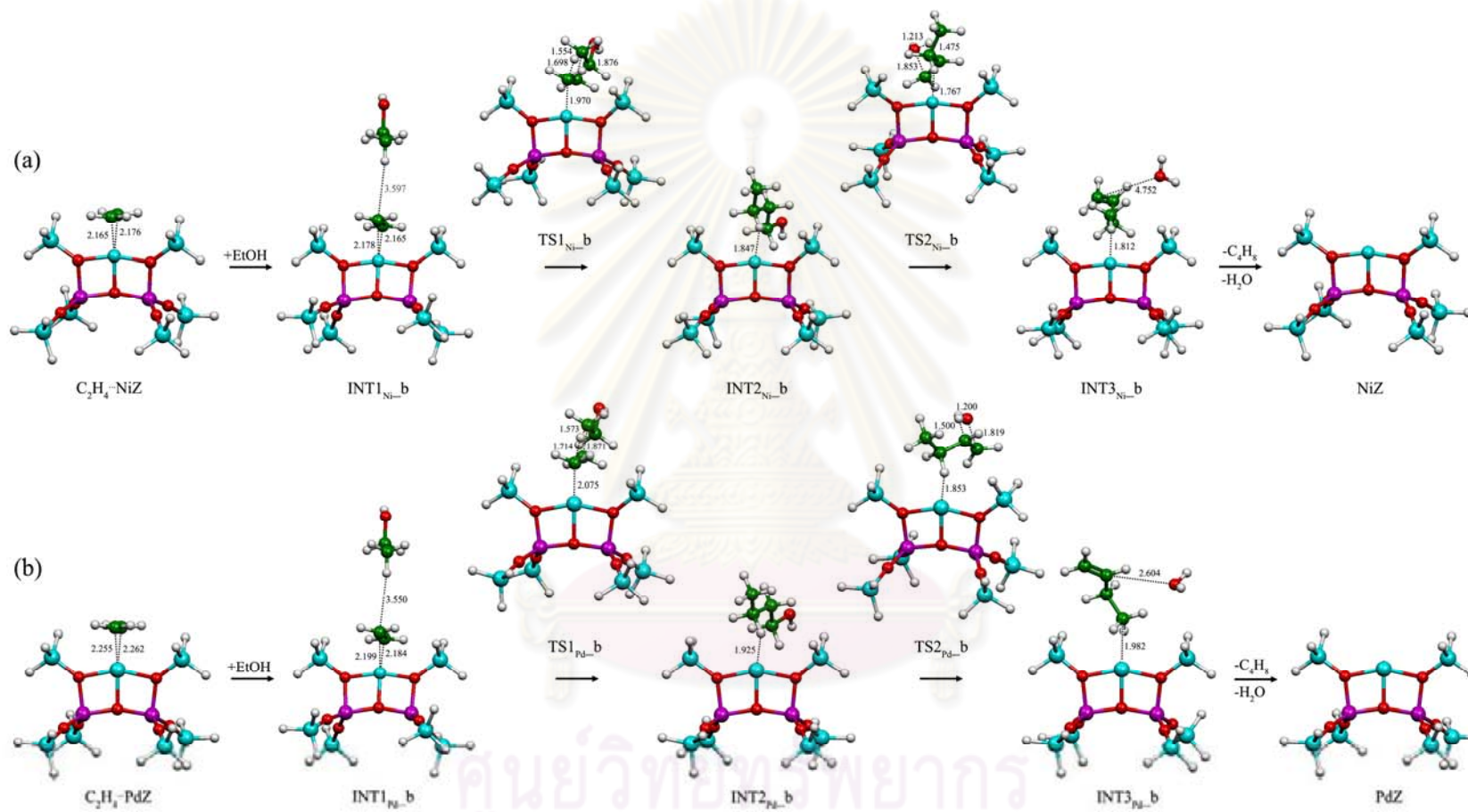
Figure 4.21 Reactions for the formation of 1–butene from ethylene adsorbed with ethanol on (a) Ni–ZSM–5, (b) Pd–ZSM–5 and (c) Pt–ZSM–5 catalysts as 8T–cluster model. Bond distances are in Å.
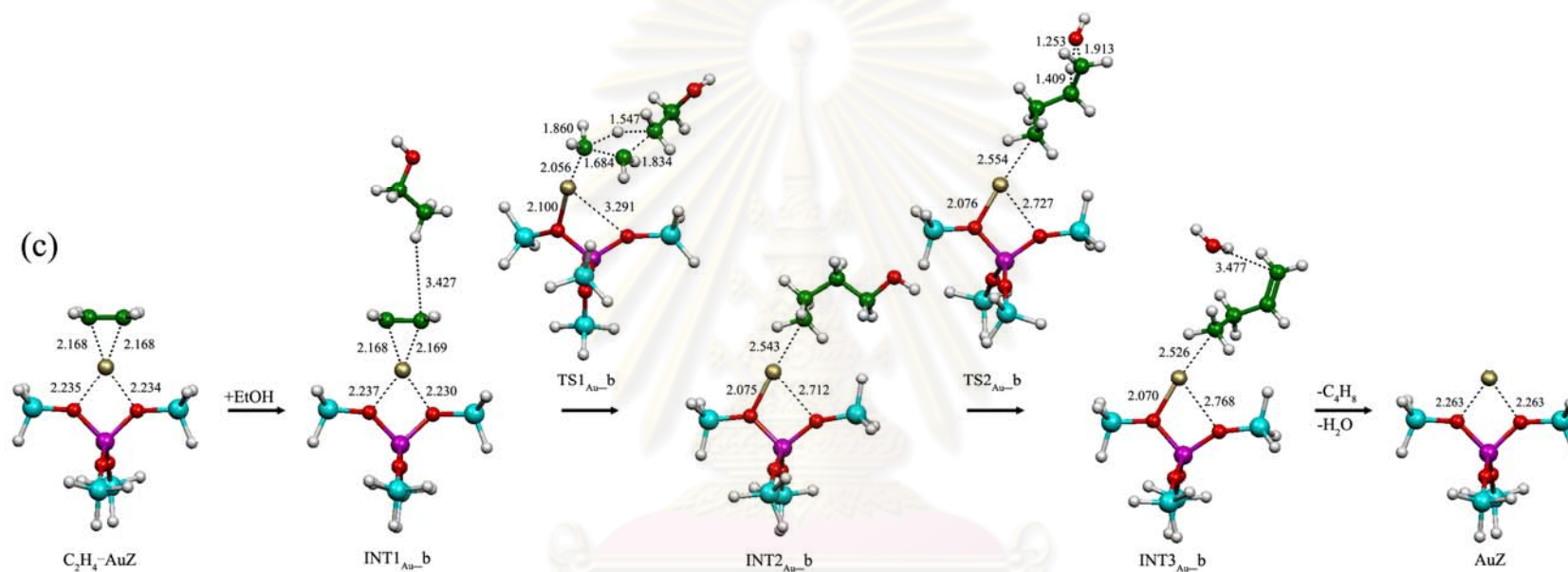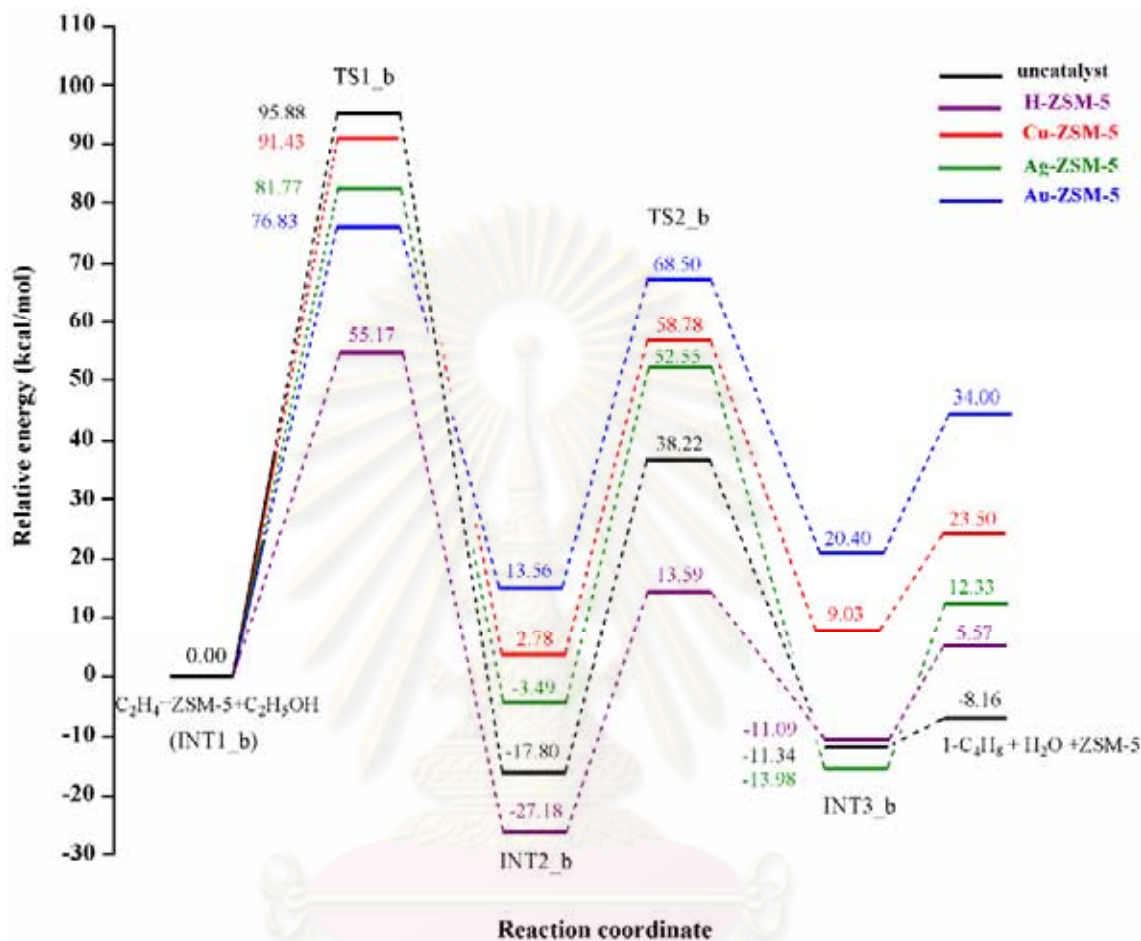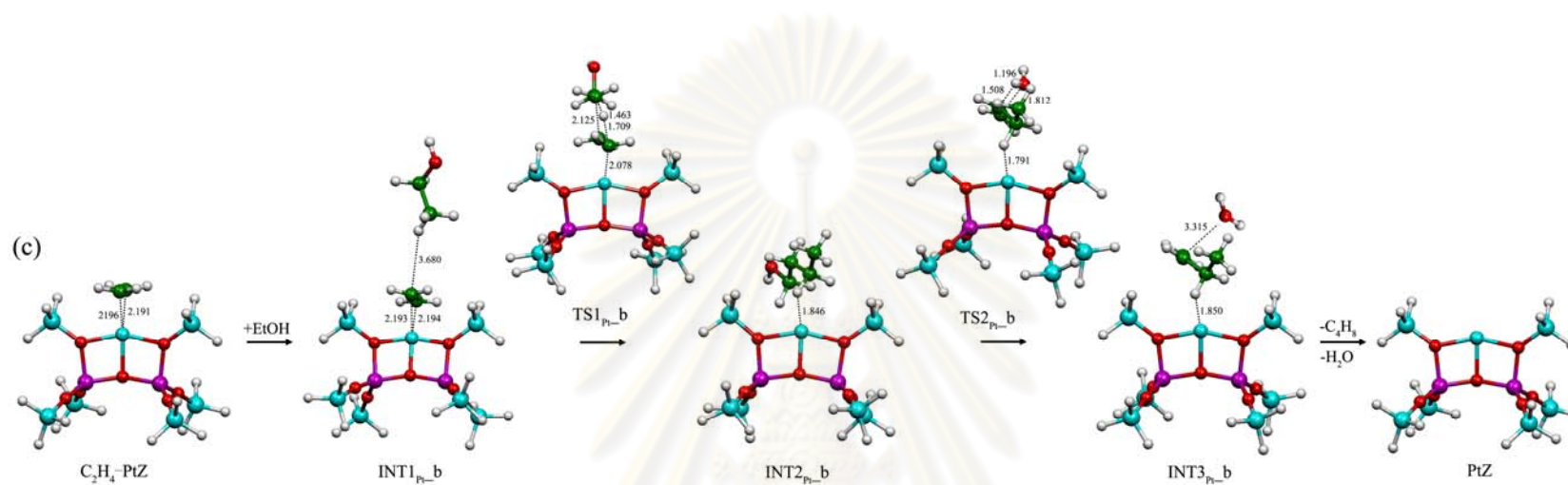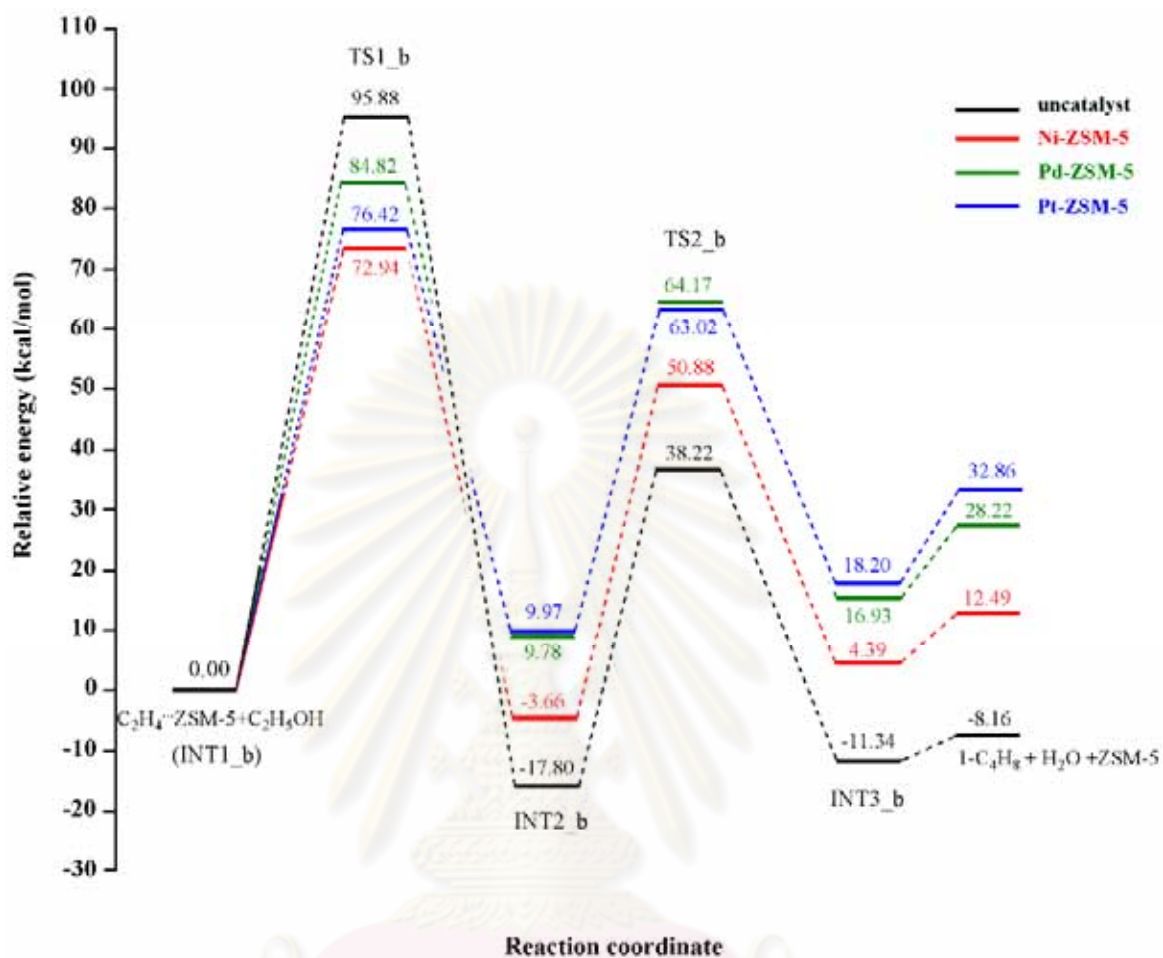
Figure 4.21 continue.

Figure 4.22 Potential energy profiles for the formation of 1–butene from ethylene adsorbed with ethanol on Ni–ZSM–5, Pd–ZSM–5 and Pt–ZSM–5 catalysts of 8T–cluster model compared to non–catalytic reaction.

Table 4.6 Energetics, thermodynamic properties, rate constants and equilibrium constants for conversion reactions of ethylene to 1–butene by M(II)–ZSM–5 catalysts compared to non–catalytic system

Catalysts/Reactions [a]	$\Delta^{\ddagger}E$ [a,b]	$\Delta^{\ddagger}G$ [a,b]	k_{298} [c]	ΔE [a]	ΔH_{298} [a]	ΔG_{298} [a]	K_{298}
Non–catalytic:							
$C_2H_4 + C_2H_5OH \rightarrow TS1\_b \rightarrow INT1\_b$	95.88	102.37	5.63×10^{-63}	–17.80	–19.68	–10.37	4.02×10^{7}
$INT1\_b \rightarrow TS2\_b \rightarrow INT2\_b$	56.02	55.95	6.01×10^{-29}	6.47	7.82	4.20	8.37×10^{-4}
$INT2\_b \rightarrow 1–C_4H_8 + H_2O$	–	–	–	2.72	2.76	–4.39	1.65×10^{3}
Ni–ZSM–5							
$C_2H_4 \cdots NiZ + C_2H_5OH \rightarrow INT1_{Ni}\_b$	–	–	–	1.07	–0.51	9.70	7.69×10^{-8}
$INT1_{Ni}\_b \rightarrow TS1_{Ni}\_b \rightarrow INT2_{Ni}\_b$	72.94	75.95	1.31×10^{-43}	–3.66	–3.39	–1.38	1.02×10^{1}
$INT2_{Ni}\_b \rightarrow TS2_{Ni}\_b \rightarrow INT3_{Ni}\_b$	54.23	54.65	5.38×10^{-28}	8.04	9.49	4.81	2.95×10^{-4}
$INT3_{Ni}\_b \rightarrow NiZ + 1–C_4H_8 + H_2O$	–	–	–	8.11	7.59	–10.47	4.71×10^{7}
Pd–ZSM–5							
$C_2H_4 \cdots PdZ + C_2H_5OH \rightarrow INT1_{Pd}\_b$	–	–	–	–9.55	–9.56	2.84	8.25×10^{-3}
$INT1_{Pd}\_b \rightarrow TS1_{Pd}\_b \rightarrow INT2_{Pd}\_b$	84.82	80.59	5.02×10^{-47}	9.78	8.78	11.12	7.08×10^{-9}
$INT2_{Pd}\_b \rightarrow TS2_{Pd}\_b \rightarrow INT3_{Pd}\_b$	54.39	50.27	8.77×10^{-25}	7.15	10.19	0.74	2.98×10^{-1}
$INT3_{Pd}\_b \rightarrow PdZ + 1–C_4H_8 + H_2O$	–	–	–	11.29	9.77	–6.30	4.16×10^{4}
Pt–ZSM–5							
$C_2H_4 \cdots PtZ + C_2H_5OH \rightarrow INT1_{Pt}\_b$	–	–	–	0.14	1.71	2.59	1.27×10^{-2}
$INT1_{Pt}\_b \rightarrow TS1_{Pt}\_b \rightarrow INT2_{Pt}\_b$	76.42	82.23	3.23×10^{-48}	9.97	9.53	16.81	4.72×10^{-13}
$INT2_{Pt}\_b \rightarrow TS2_{Pt}\_b \rightarrow INT3_{Pt}\_b$	53.05	52.02	4.58×10^{-26}	8.23	9.57	5.32	1.26×10^{-4}
$INT3_{Pt}\_b \rightarrow PtZ + 1–C_4H_8 + H_2O$	–	–	–	14.66	13.36	–2.72	1.07×10^{2}

[a] Computed the B3LYP/LanL2DZ level of theory.
[b] Activation state.
[c] In s^{-1}.

ศูนย์วิทยทรัพยากร
จุฬาลงกรณ์มหาวิทยาลัย

This reaction proceeds like the adsorption of ethanol on the adsorbed ethylene at the acid site of the Cu–ZSM–5, Ag–ZSM–5 and Au–ZSM–5 catalysts as discussed above. The first step is the adsorption of ethanol on the adsorbed ethylene at the acid site over Ni–ZSM–5, Pd–ZSM–5 and Pt–ZSM–5 catalysts. In the second step (RDS), the proton transfer from ethanol to ethylene via transition state $TS1_{Ni}\_b$, $TS1_{Pd}\_b$ and $TS1_{Pt}\_b$, this leads to 1–butanol and the activation energy barrier for proton transfer was calculated as 72.94, 84.82 and 76.42 kcal/mol for $TS1_{Ni}\_b$, $TS1_{Pd}\_b$ and $TS1_{Pt}\_b$,

respectively. Rate constants for conversion of ethanol to ethylene on different catalysts are in order: Ni–ZSM–5 (1.31×10^{-43} s^{-1}) > Pd–ZSM–5 (5.02×10^{-47} s^{-1}) > Pt–ZSM–5 (3.23×10^{-48} s^{-1}). Magnitudes of equilibrium constants of the ethanol conversion to 1–butanol are in order: Ni–ZSM–5 (1.02×10^{1}) > Pd–ZSM–5 (7.08×10^{-9}) > Pt–ZSM–5 (4.72×10^{-13}). These results show that the adsorption of ethanol on the absorbed ethylene at the acid site should be significantly faster on Ni–ZSM–5 than Pt–ZSM–5 and Pd–ZSM–5 catalysts.

The third step is the dehydration of 1–butanol intermediate to form 1–butene interacting with water molecule via transition–state TS2$_{Ni\_b}$, TS2$_{Pd\_b}$ and TS2$_{Pt\_b}$. The activation energy of this step is 54.23, 54.39 and 53.05 kcal/mol, respectively. The last steps for the reactions either catalyzed by Ni–ZSM–5 or Pt–ZSM–5 or Pd–ZSM–5 are the endothermic reaction.

4.4.5 The comparison efficiencies of catalysts on the ethanol conversion to 1– butene

Due to the catalytic efficiencies of the H–ZSM–5 and M–ZSM–5 catalysts for ethanol conversion to 1–butene, the rate constants in terms of –log k of the reactions to 1–butene catalyzed by ZSM–5 type catalysts plotted against cationic sizes are shown in Figure 4.23. The H–ZSM–5 and Ni–ZSM–5 catalysts are found to be the most efficient catalyst for the monovalent and divalent metal ions, respectively.
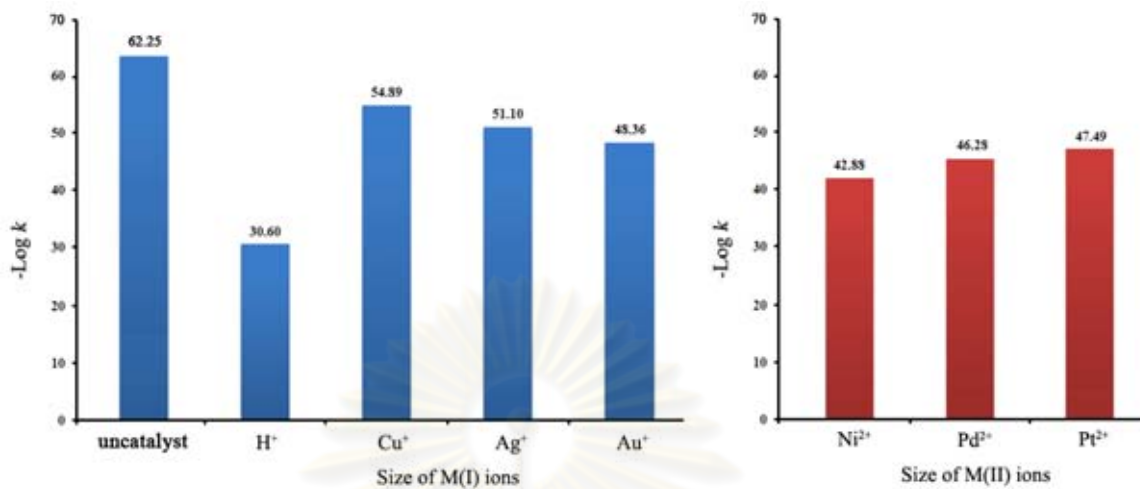
Figure 4.23 Plots of –log k against cationic size of (a) H–ZSM–5 and M(I)–ZSM–5 and (b) M(II)–ZSM–5 catalysts as 5T and 8T–cluster models.

The rate constant of conversion of ethanol to 1–butene catalyzed by the H–ZSM–5 is found to be the highest value compared with the M–ZSM–5–type catalysts. The reason is that the conversion of ethanol to 1–butene prefers to occur on the Brønsted acid catalysts as H–ZSM–5 rather than the Lewis acid catalyst as M–ZSM–5. As the H–ZSM–5 catalysts contains the acid proton, its proton can therefore be transferred and involve with the reaction but in the M–ZSM–5–type catalysts, no acid proton is involved.

CHAPTER V

CONCLUSIONS

In the present theoretical study, the molecular mechanisms of conversion reaction of ethanol to ethylene and to 1–butene using the H–ZSM–5 and M–ZSM–5 catalysts, M=Cu(I), Ag(I), Au(I), Ni(II), Pd(II) and Pt(II) have been theoretically investigated employing the calculations at the B3LYP/LanL2DZ level of theory. All the results can be concluded as follows:

(a) Rate constants based on the rate–determining step of the ethanol conversion to ethylene over the zeolite catalysts as the strategic model I and II are in order: Au–ZSM–5 > Pt–ZSM–5 ≈ Pd–ZSM–5 > Ni–ZSM–5 > H–ZSM–5 > Cu–ZSM–5 > Ag–ZSM–5.

(b) Rate constants based on the rate–determining step of the ethanol conversion to ethylene over the zeolite catalysts as the strategic model III and IV are in order: Pt–ZSM–5 > Pd–ZSM–5 ≈ Au–ZSM–5 > Ag–ZSM–5 > H–ZSM–5 > Cu–ZSM–5 >> Ni–ZSM–5.

(c) Rates constants for the ethanol conversion to 1–butene over the M–ZSM–5– type catalysts are in decreasing order: H–ZSM–5 >> Ni–ZSM–5 > Pd–ZSM–5 ≈ Pt–ZSM–5 ≈ Au–ZSM–5 > Ag–ZSM–5 > Cu–ZSM–5.

Suggestion for future work

To get more reliable results of energies and thermodynamic properties for the conversion reaction of ethanol to 1–butene, the 28T cluster models for all zeolite catalysts should be applied.

REFERENCES

[1]   Borges, P., et al. Light ol efin transformation over ZSM-5 zeolites A kine tic model for olefin consumption. Appl. Catal. A: Gen. 324 (2007): 20-29.

[2]   Haw, J.F., Song, W., Marc us, D.M., and Nicholas, J.B. The m echanism of methanol to hydrocarbon catalysis. Acc. Chem. Res. 36 (2003): 317-326.

[3]   Zhang, X., Wang, R., Yang, X., and Zhang F. Com parison of four catalysts in the catalytic dehydratio n of ethanol to ethyle ne. Micropor. Mesopor. Mater. 116 (2008): 210-215.

[4]   Dai, P.S.E. Zeolite catalysis for a better environment. Catal. Today 26 (1995): 3-11.

[5]   Aguayo, A.T., Gayubo, A.G., Atutxa, A., Valle, B., and Bilbao, J. Regeneration of a H–Z SM–5 zeolite catalyst deactivated in the transformation of aqueous ethanol into hy drocarbons. Catal.Today 107-108 (2005): 410-416.

[6]   Zaki, T. Catalytic dehydration of ethanol using tr ansition metal oxide catalysts. J. Colloid Interface Sci. 284 (2005): 606-613.

[7]   Xu, R., Pang, W., Yu , J., Huo, Q., and Chen, J. Chemistry of zeolites and related porous materials: synthesis and structure. Singapore: John Wiley & Sons, 2007.

[8]   Kiricsi, I., Förster, H., Tasi, G., and Nagy, J.B. Generation, characterization, and transformations of unsaturated carbenium ions i n zeolites. Chem . Rev. 99 (1999): 2085-2114.

[9]   Coombs, D.S., et al. R ecommended nomenclature for zeolite minerals. The Canadian Mineralogist. 35 (1997): 1571-1606.

[10]   Bond, G.C. Hetero geneous catalysis: principles and applications. New York: Oxford chemistry series, 1987.

[11]   Breck, D.W. Zeolite molecular sieves. New York John: Wiley and Sons, 1984.

[12]   Machoa, V., Králik, M., Jurecekova, E., Hudecd, J., and J urecek, L. Dehydration of C 4 alkanols conjugated with a positional and skeletal isomerisation of the formed C4 alkenes. Appl.Catal. A: Gen. 214 (2001): 251-257.

[13] Mao, L.V., and Dao, L.H. Ethylene light olefins from ethanol. In U.S. Patent (ed.), 1987.

[14] Talukdar, A.K., Bhattacharyya, K.G., and Sivasanker, S. H–ZSM–5 catalysed conversion of aqueous ethanol to hydrocarbons. Appl.Catal. A: Gen. 148 (1997): 357-371.

[15] Song, Z., Takahashi, A., Mimura, N., and Fujitani, T. Production of Propylene from ethanol over ZSM–5 zeolites. Catal. Lett. 131 (2009): 364-369.

[16] Redondo, A., Hay, P.J., Alvarado-Swaisgood, A. E., and Barr, M.K. Ab initio quantum chemical calculations of aluminum substitution in zeolite ZSM–5. J. Phys. Chem. 95 (1991): 10031-10036.

[17] Redondo, A., and Hay, P.J., Quantum chemical studies of acid sites in zeolite ZSM-5. J. Phys. Chem. 97 (1993): 11754-11761.

[18] Derouanea, E.G., and Fripiat, J.G. Non-empirical quantum chemical study of the siting and pairing of aluminium in the MFI framework. Zeolites 5 (1985): 165-172.

[19] Barone, G., et al. Confined but–2–ene catalytic isomerization inside H–ZSM–5 models: A DFT study. J. Chem. Theo. Comput. 5 (2009): 1274-1283.

[20] Huang, D.S., and Wang, W. Methane activation over Ag-exchanged ZSM–5 zeolites: A theoretical study. Appl. Surf. Sci. 254 (2008): 4944-4948.

[21] Sierraalta, A., Alejosa, P., Ehrm annb, E., Rodriguezc, L.J., and Ferrerc, Y., DFT–ONIOM study of Au/ZSM–5 catalyst: Active sites, thermodynamic and vibrational frequencies. J. Mol. Catal. A: Chem. 301 (2009): 61-66.

[22] Jiang, S., Huang, S., T u, W., and Z hu, J. Infrared spectra and stability of CO and H_2O sorption over Ag-exchanged ZSM–5 zeolite: DFT study. Appl. Surf. Sci. 255 (2009): 5764-5769.

[23] Young, D.C. Com putational chemistry: A practical guide for applying techniques to real world problems. New Y ork: John Wil ey and Sons, 2001.

[24] Grant, G.H., and Ric hards, W.G. Computational chemistry. New Yo rk: Oxford university press, 1995.

[25] Jensen, F. Introduction to computational chemistry. Chichester: John Wile y and Sons, 1999.

[26] Wigner, E., and Hirschfeld er, J.O. Some quantum-mechanical considerations in the theory of reactions involving an activ ation energy. J. Chem. Phys. 7 (1939): 616-628.

[27] Eckart, C. The penetration of a pote ntial barrier by electrons. Phys. Rev. 35 (1930): 1303-1309.

[28] Garrett, B.C., Truhlar, D.G., Grev , R.S., and Magnuson, A.W. Improve d treatment of threshold contributions in vibra tional transition–state theory. J. Phys. Chem. 84 (1980): 1730-1748.

[29] Skodje, R.T., Truhlar, D.G., and Garr ett, B.C. A ge neral small–curvature approximation for transition–state–the ory transmission coefficients. J. Phys. Chem. 85 (1981): 3019-3023.

[30] Cramer, C.J. Essentials of computational chemistry: theories and models. 2nd edition, Singapore John: Wiley & Sons, 2004.

[31] Ochterski, J.W. Thermochemistry in Gaussian. Gaussian Inc., 2000.

[32] Curtiss, L. A., Raghavachari , K., Redfern, P. C., and Pople, J. A. Assessment of Gaussian-2 and density functional theories for the co mputation of enthalpies of formation. Chem. Phys. 106 (1997): 1063 - 1079.

[33] Brand, H.V., Curtiss, L.A., and Iton, L. E. Ab initio m olecular orbital cluster studies of the zeolite ZSM–5. J. Phys. Chem. 97 (1993): 12773- 12782.

[34] Becke, A.D. Density-functional thermochemistry. III. The role of exact exchange. J. Chem. Phys. 98 (1993): 5648-5652.

[35] Lee C., Yang, W., and Parr, R.G. Development of the Colle-Salvetti correlation-energy formula into a functional of the electron density. Phys. Rev. B 37 (1988): 785-789.

[36] Hay, P.J., and Wadt, W.R. Ab initio ef fective core potentials f or molecular calculations: potentials for the transition metal atom Sc to Hg. J. Chem . Phys. 82 (1985): 270-283.

[37] Wadt, W.R., and Hay , P.J. Ab initio ef fective core potentials f or molecular calculations: potentials for main group elements Na to Bi. J. Chem. Phys. 82 (1985): 284-298.

[38] Hay, P.J., and Wadt, W.R. Ab initio ef fective core potentials f or molecular calculations: potentials for K to Au including the outermost core orbitals. J. Chem. Phys. 82 (1985): 299-310.

[39]   Peng, C., Ayala, P .Y., Schlegel, H.B., and F risch, M.J. Using redundant
        internal coordinates to optim ize geometries and transition states. J.
        Comp. Chem. 17 (1996): 49-56.

[40]   Gonzalez, C., and Schlegel, H.B. An   improved algorithm for reaction path
        following. J. Chem. Phys. 90 (1989): 2154-2161.

[41]   Frisch, M.J., et al. Gaussian 03. Re   vision D.02. Gaussian Inc., Wallingf ord
        CT, 2006.

APPENDIX

APPENDIX

Table A-1 Selected geometrical parameters for the 5T–cluster–modeled H–ZSM–5 and M–ZSM–5 and 8T–cluster–modeled catalysts

Catalysts	Bond distances [a]		
	O1–M [b]	O2–M [b]	O3–M [b]
H–ZSM–5	–	0.978	–
M(I)–ZSM–5			
Cu–ZSM–5	1.995	1.992	–
Ag–ZSM–5	2.259	2.257	–
Au–ZSM–5	2.263	2.263	–
M(II)–ZSM–5			
Ni–ZSM–5	1.863	1.838	1.864
Pd–ZSM–5	2.050	1.986	2.049
Pt–ZSM–5	2.059	1.972	2.059

[a] In Å.

[b] M represents the metal ion in M(I)-ZSM-5 and M(II)-ZSM-5 catalysts.

Table A-2 Selected geometrical the 28T–cluster–modeled H–ZSM–5 and M–ZSM–5 catalysts

Catalysts	Bond distances [a]		
	O1–M [b]	O2–M [b]	O3–M [b]
H–ZSM–5	–	0.977	–
M(I)–ZSM–5			
Cu–ZSM–5	2.121	2.033	–
Ag–ZSM–5	2.446	2.208	–
Au–ZSM–5	2.624	2.304	–
M(II)–ZSM–5			
Ni–ZSM–5	3.216	1.761	1.865
Pd–ZSM–5	2.236	1.908	2.248
Pt–ZSM–5	2.196	1.926	2.180

[a] In Å.

[b] M represents the metal ion in M(I)-ZSM-5 and M(II)-ZSM-5 catalysts.

Table A-3 Imaginary frequency, tunneling coefficients, and A factors of ethanol conversion to ethylene by various the 5T–cluster–modeled as H–ZSM–5 and M(I)–ZSM–5 catalysts and non-catalytic system

Reaction	Imaginary frequency, ν_i (cm^{-1})	κ	$Q_{TS}/Q_{Complex}$	A
Non−catalytic :				
EtOH → TS_e → INT1	-1643.19	3.62	1.89×10^0	$1.17E \times 10^{13}$
H-ZSM-5:				
INT1$_H$_e → TS$_H$_e → INT2$_H$_e	-876.60	1.75	5.19×10^{-1}	3.22×10^{12}
Cu-ZSM-5:				
INT1$_{Cu}$_e → TS$_{Cu}$_e → INT2$_{Cu}$_e	-1687.05	3.76	5.44×10^0	3.38×10^{13}
Ag-ZSM-5:				
INT1$_{Ag}$_e → TS$_{Ag}$_e → INT2$_{Ag}$_e	-1634.49	3.59	6.94×10^{-2}	4.31×10^{11}
Au-ZSM-5:				
INT1$_{Au}$_e → TS$_{Au}$_e → INT2$_{Au}$_e	-1551.04	3.33	6.27×10^{-2}	3.90×10^{11}

Table A−4 Imaginary frequency, tunneling coefficients, and A factors of ethanol conversion to ethylene by various the 8T–cluster–modeled as M(II)–ZSM–5 catalysts

Reaction	Imaginary frequency, ν_i (cm^{-1})	κ	$Q_{TS}/Q_{Complex}$	A
Ni-ZSM-5:				
INT1$_{Ni}$_e → TS$_{Ni}$_e → INT2$_{Ni}$_e	-1630.98	3.58	2.48×10^{-1}	1.54×10^{12}
Pd-ZSM-5:				
INT1$_{Pd}$_e → TS$_{Pd}$_e → INT2$_{Pd}$_e	-1627.88	3.57	3.86×10^1	2.40×10^{14}
Pt-ZSM-5:				
INT1$_{Pt}$_e → TS$_{Pt}$_e → INT2$_{Pt}$_e	-1578.00	3.42	2.91×10^0	1.81×10^{13}

Table A−5 Imaginary frequency, tunneling coefficients, and A factors of ethanol conversion to ethylene by various the 28T−cluster–modeled as H–ZSM–5 and M(I)–ZSM–5 catalysts

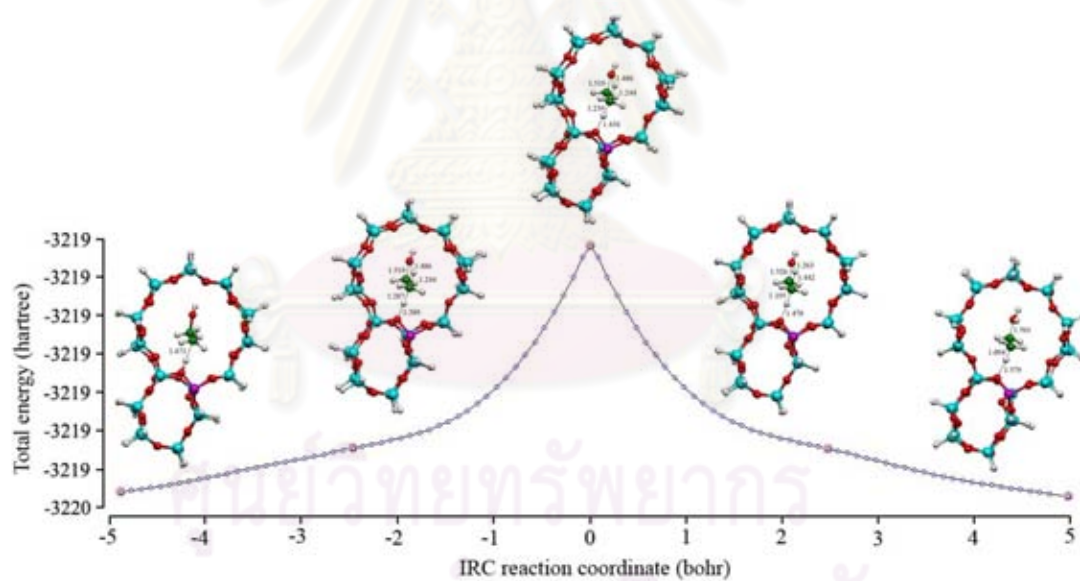| Reaction	Imaginary frequency, ν_i (cm^{-1})	κ	$Q_{TS}/Q_{Complex}$	A
H-ZSM-5:				
INT1(H) → TS(H) → INT2(H)	-1493.29	3.16	1.37 x 10^{-1}	8.50 x 10^{11}
Cu-ZSM-5:				
INT1(Cu) → TS(Cu) → INT2(Cu)	-1144.75	2.27	4.97 x 10^{-1}	3.09 x 10^{12}
Ag-ZSM-5:				
INT1(Ag) → TS(Ag) → INT2(Ag)	-1623.59	3.56	9.07 x 10^{-1}	5.63 x 10^{12}
Au-ZSM-5:				
INT1(Au) → TS(Au) → INT2(Au)	-1609.92	3.51	5.22 x 10^{-2}	3.43 x 10^{12}

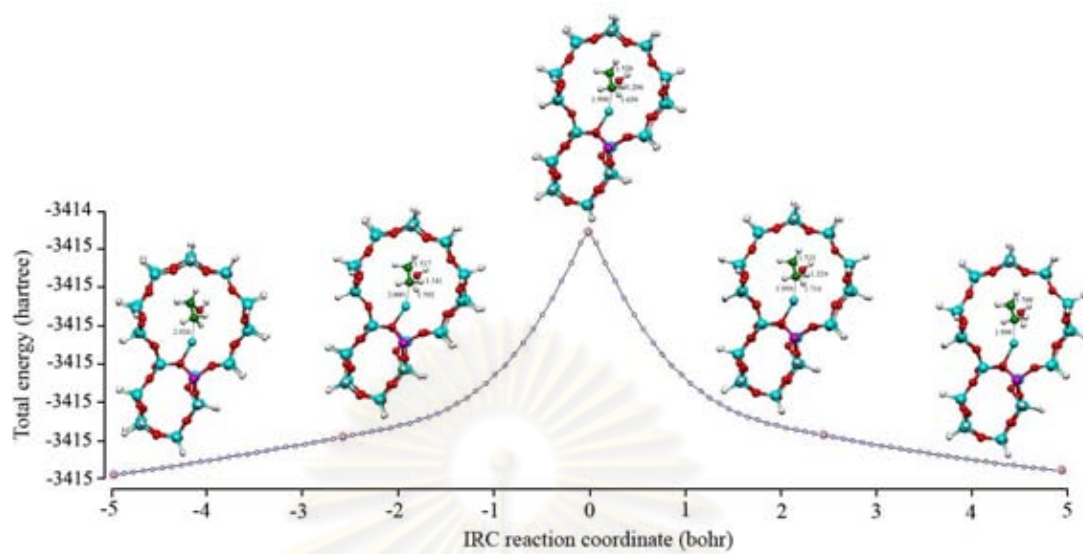**Figure A−6** Intrinsic reaction coordinate for the transition state TS(H).

Figure A−7 Intrinsic reaction coordinate for the transition state TS(Cu).
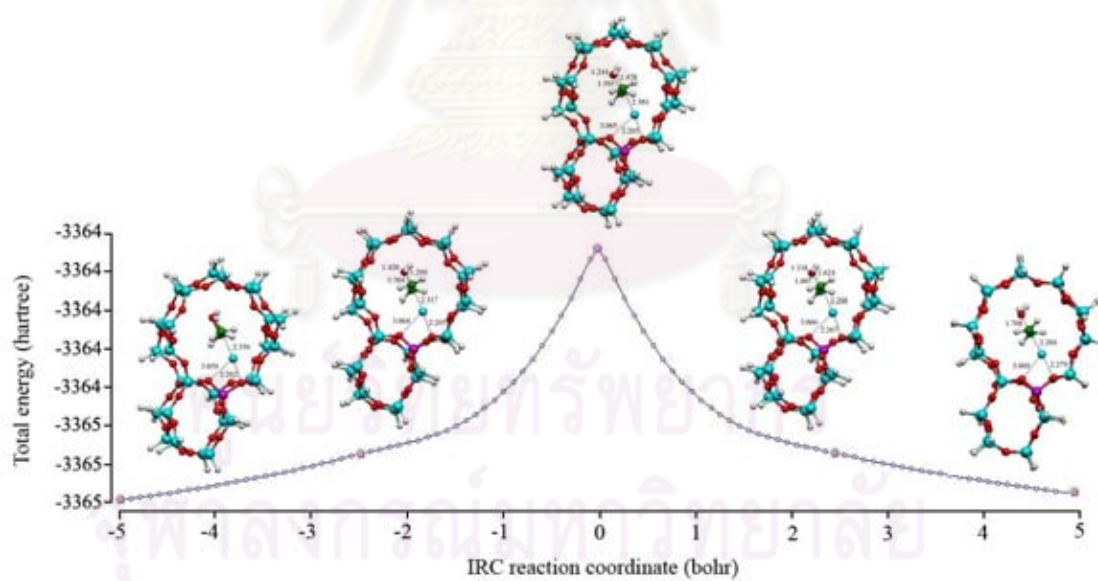

Figure A−8 Intrinsic reaction coordinate for the transition state TS(Ag).
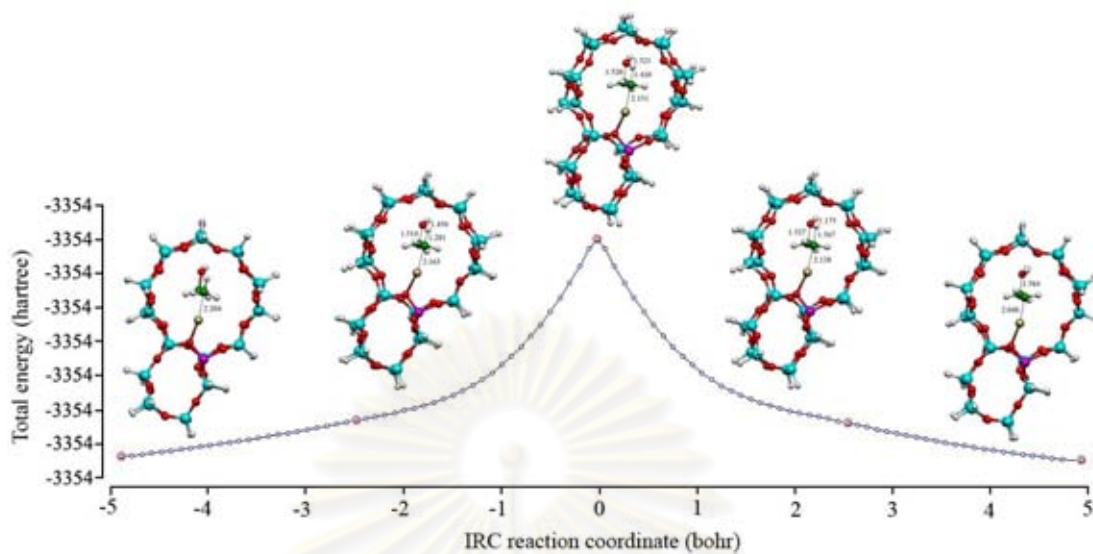
Figure A−9 Intrinsic reaction coordinate for the transition state TS(Au).

Table A-10 Imaginary frequency, tunneling coefficients, and A factors of ethanol conversion to ethylene by various the 28T−cluster–modeled M(II)–ZSM–5 catalysts

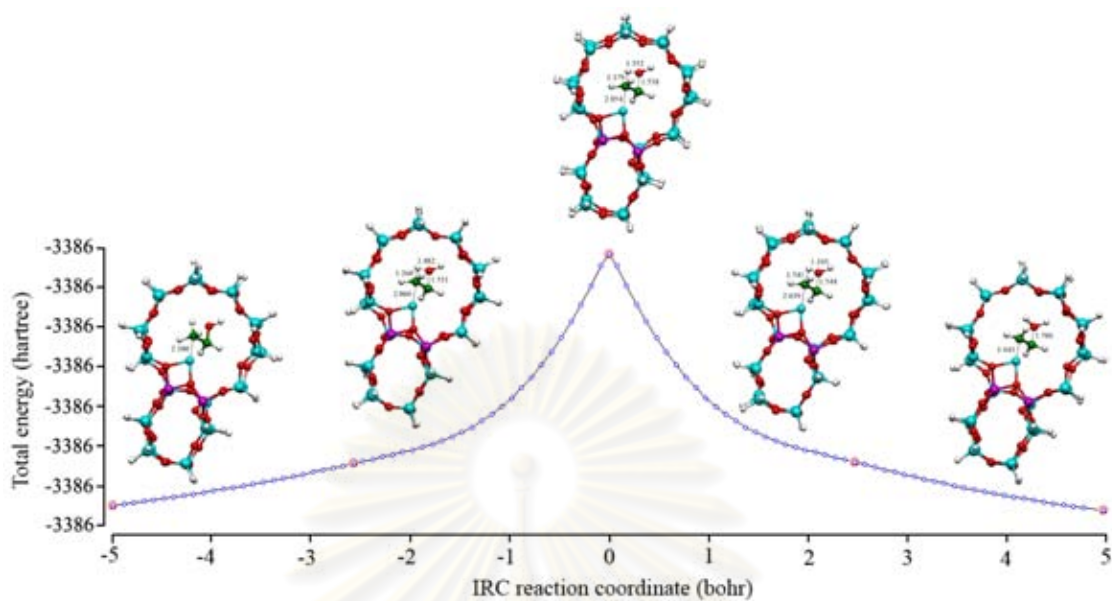| Reaction	Imaginary frequency, v_i (cm^{-1})	κ	$Q_{TS}/Q_{Complex}$	A
Ni-ZSM-5:				
INT1(Ni) → TS(Ni) → INT2(Ni)	-1606.25	3.50	1.04×10^0	6.45×10^{12}
Pd-ZSM-5:				
INT1(Pd) → TS(Pd) → INT2(Pd)	-1642.18	3.62	6.99×10^{-2}	4.34×10^{11}
Pt-ZSM-5:				
INT1(Pt) → TS(Pt) → INT2(Pt)	-1577.09	3.41	6.68×10^{-1}	4.15×10^{12}

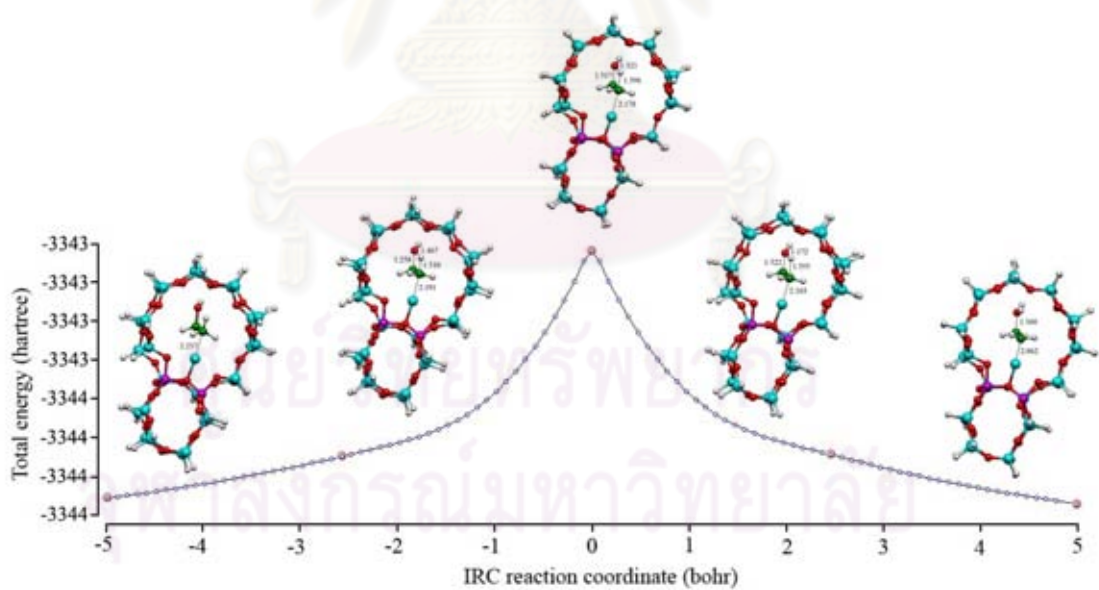**Figure A−11** Intrinsic reaction coordinate for the transition state TS(Ni).

Figure A−12 Intrinsic reaction coordinate for the transition state TS(Pd).
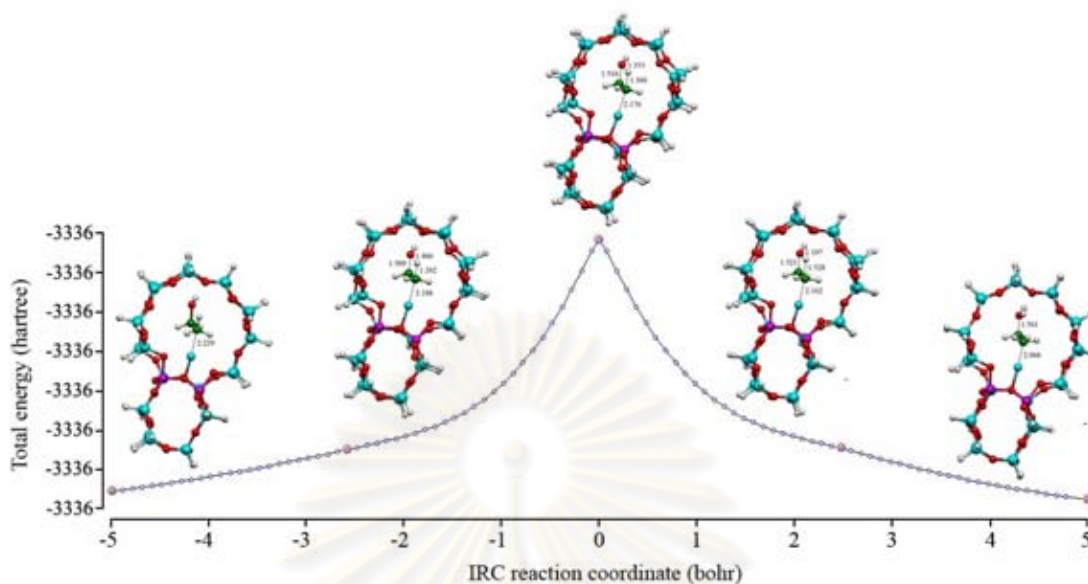
Figure A−13 Intrinsic reaction coordinate for the transition state TS(Pt).

Table A-14 Imaginary frequency, tunneling coefficients, and A factors of ethanol conversion to 1–butene by various the 5T–cluster–modeled as H–ZSM–5 and M(I)–ZSM–5 catalysts

Reaction	Imaginary frequency, ν_i (cm^{-1})	κ	$Q_{TS}/Q_{Complex}$	A
H−ZSM−5				
$C_2H_4 \cdots ZH \rightarrow TS1_{H\_b} \rightarrow INT1_{H\_b}$	-1091.17	2.16	2.73×10^{-2}	1.70×10^{11}
$INT2_{H\_b} \rightarrow TS2_{H\_b} \rightarrow INT3_{H\_b}$	-322.39	1.10	9.73×10^{-4}	6.04×10^{9}
$INT3_{H\_b} \rightarrow TS3_{H\_b} \rightarrow INT4_{H\_b}$	-825.05	1.66	4.35×10^{-2}	2.70×10^{11}
Cu−ZSM−5				
$INT1_{Cu\_b} \rightarrow TS1_{Cu\_b} \rightarrow INT2_{Cu\_b}$	-1126.92	2.23	1.73×10^{-1}	1.08×10^{12}
$INT2_{Cu\_b} \rightarrow TS2_{Cu\_b} \rightarrow INT3_{Cu\_b}$	-1674.77	3.72	2.30×10^{-2}	1.43×10^{11}
Ag−ZSM−5				
$INT1_{Ag\_b} \rightarrow TS1_{Ag\_b} \rightarrow INT2_{Ag\_b}$	-1014.77	2.00	7.96×10^{-5}	4.95×10^{8}
$INT2_{Ag\_b} \rightarrow TS2_{Ag\_b} \rightarrow INT3_{Ag\_b}$	-1727.68	3.90	8.07×10^{-1}	5.02×10^{12}
Au−ZSM−5				
$INT1_{Au\_b} \rightarrow TS1_{Au\_b} \rightarrow INT2_{Au\_b}$	-1004.82	1.98	1.30×10^{-5}	8.10×10^{7}
$INT2_{Au\_b} \rightarrow TS2_{Au\_b} \rightarrow INT3_{Au\_b}$	-1551.62	3.34	1.93×10^{-1}	1.20×10^{12}

Table A-15 Imaginary frequency, tunneling coefficients, and A factors of ethanol conversion to 1-butene by various the 8T–cluster–modeled as M(II)–ZSM–5 catalysts

Reaction	Imaginary frequency, ν_i (cm^{-1})	κ	$Q_{TS}/Q_{Complex}$	A
Ni−ZSM−5				
INT1$_{Ni\_b}$ → TS1$_{Ni\_b}$ → INT2$_{Ni\_b}$	-1005.11	1.98	4.62 x 10^{-3}	2.87 x 10^{10}
INT2$_{Ni\_b}$ → TS2$_{Ni\_b}$ → INT3$_{Ni\_b}$	-1723.32	1.00	4.84 x 10^{-1}	3.01 x 10^{12}
Pd−ZSM−5				
INT1$_{Pd\_b}$ → TS1$_{Pd\_b}$ → INT2$_{Pd\_b}$	-964.93	1.90	1.52 x 10^{-3}	9.45 x 10^{15}
INT2$_{Pd\_b}$ → TS2$_{Pd\_b}$ → INT3$_{Pd\_b}$	-1702.83	3.81	1.08 x 10^{-3}	6.73 x 10^{15}
Pt−ZSM−5				
INT1$_{Pt\_b}$ → TS1$_{Pt\_b}$ → INT2$_{Pt\_b}$	-875.05	1.74	4.42 x 10^{-5}	2.74 x 10^{8}
INT2$_{Pt\_b}$ → TS2$_{Pt\_b}$ → INT3$_{Pt\_b}$	-1676.44	3.73	0.59 x 10^{-1}	3.66 x 10^{13}

VITA

Name:	Miss PARISA DUMRONGSAK
Date of Birth:	March 4, 1986
Place of Birth:	Rayong, Thailand
Address:	2 Sumnuktong, Muang, Rayong 21100, Thailand
Telephone:	080-6382992
E-mail address:	ab_pe@hotmail.com

Educations:

2008-2010   M.Sc. (Petrochemistry and Polymer Science), Chulalongkorn University, Thailand

2004-2007   B.Eng. (Petrochemicals and Polymeric Materials), Silpakorn University, Thailand

1998-2003   Rayongwittayakom High School, Rayong, Thailand

1992-1997   St.Joseph, Rayong, Thailand

Scholarship:

2009-2010   The NCE-PPAM (National Center of Excellence for Petroleum, Petrochemicals and Advanced Materials)

Presentation:

2010   Theoretical Study of Conversion of Ethanol to Ethylene over ZSM-5 Zeolite (Poster Session): The 3rd Silpakorn University Research Fair on Creative Economy Conference, January 19-21 2010 at Silpakorn University (Sanamchandra Palace Campus), Nakhon Pathom, Thailand.

Theoretical Investigation of Conversion of Ethanol to Ethylene over Transition Metal Ions ZSM–5 Catalysts (Poster Session): The 7th International Symposium on Advanced Materials in Asia-Pacific and JAIST International Symposium on Nano Technology September 30- October 1, 2010 at Ishikawa, Japan.